8-21-2008

Flavonoids as Modulators of Amyloid Precursor Protein Metabolism and Alzheimer Disease Pathology

Kavon Rezai-Zadeh
University of South Florida

Flavonoids as Modulators of Amyloid Precursor Protein Metabolism and Alzheimer Disease Pathology

by

Kavon Rezai-Zadeh

A dissertation submitted in partial fulfillment
of the requirements for the degree of
Doctor of Philosophy
Department of Molecular Medicine
College of Medicine
University of South Florida

Co-Major Professor: Jun Tan, Ph.D.
Co-Major Professor: Huntington Potter, Ph.D.
Susan Pross, Ph.D.
Andreas Seyfang, Ph.D.
R. Douglas Shytle, Ph.D.

Date of Approval:
August 21, 2008

Keywords: secretase, app, egcg, luteolin, diosmin

ACKNOWLEDGEMENTS

The completion of a dissertation and doctorate is an accomplishment achieved by the work of not just one individual, but many. For this reason, I would like to acknowledge these many individuals for their part in this accomplishment. First, I would like to thank my family for believing in me and being the kind of people I aspired to make proud. Next, I would like to thank all the members of my laboratory and students with whom I have collaborated over the past 4 years, Jin Zeng, Nan Sun, Kirk Townsend, Lucy Hou, Deborah Jeanniton, Yun Bai, Demian Obregon, Jun Tian, Yuyan Zhu, Brian Giunta, Carla Parker-Athill, Antoinette Bailey, Melissa Runfeldt, William Schleif, and Maren Jensen. I would especially like to thank William V. Nikolic and Jared Ehrhart for being like my brothers in arms throughout graduate school, getting me to the other side of academia in good spirits and relatively unscathed. Finally, I would like to thank those individuals who guided and mentored me as a graduate student, Dr. Takashi Mori, Dr. Dave Morgan, Dr. Gary Arendash, Dr. Andreas Seyfang, Dr. Susan Pross, Dr. Huntington Potter, and Dr. Terrence Town. I would especially like to thank Dr. R. Douglas Shytle and Dr. Jun Tan for inspiring me with their passion for scientific investigation, having confidence in my research abilities, and providing an environment in which I would succeed.

TABLE OF CONTENTS

LIST OF FIGURES

Flavonoinds as Modulators of Amyloid Precursor Protein Metabolism and Alzheimer Disease Pathology

Kavon Rezai-Zadeh

ABSTRACT

Alzheimer disease (AD) is a progressive neurodegenerative disorder pathologically characterized by deposition of β-amyloid (Aβ) peptides as plaques in the brain. Central to this AD pathology is mismetabolism of the amyloid precursor protein (APP). Recent studies suggest that flavonoids, a class of secondary plant metabolites, may be useful for the prevention and treatment of a variety of neurodegenerative diseases. The studies detailed herein, investigate the ability of two such classes of flavonoids, green tea derived catechins and 5,7-dihydroxyflavones, to modulate APP metabolism in "Swedish" mutant APP (APP_{sw}) models of AD. Studies showed that green tea derived (-)-epigallocatechin-3-gallate (EGCG) effectively reduced Aβ generation and resultant amyloidosis both *in vitro* and *in vivo*. In concert with these findings, EGCG markedly promoted non-amyloidogenic APP proteolysis via activation of the putative α-secretase, a-disintegrin-and-metalloprotease-10 (ADAM10). Furthermore, luteolin and various related 5,7-dihydroxyflavones, effectively reduced Aβ generation and resultant amyloidosis both *in vitro* and *in vivo*, as well. Data revealed that luteolin decreased amyloidogenic γ-secretase APP proteolysis via presenilin-1 (PS1) carboxyl-terminal

fragment (CTF) phosphorylation. Elucidation of these flavonoids' cellular/molecular mechanisms also revealed their potential for opposing neurofibrillary tangle (NFT) pathology, another hallmark of AD. These data raise the possibility that flavonoid administration to AD patients may prove to be viable and effective prophylactic strategy.

CHAPTER 1

INTRODUCTION

1.1 Alzheimer disease

As first characterized by Alois Alzheimer in 1906, Alzheimer disease (AD) is a progressive neurodegenerative disorder pathologically distinguished from other forms of dementia by the presence of amyloid plaques and neurofibrilary tangles (NFTs) in the brain. As a result of the atrophy that occurs in both cortical and subcortical regions, patients lose their cognitive and emotional ability to function independently and safely. Although the course of the disease is progressive, there is great variability in the rate of decline of different cognitive abilities and skills, emotional responses, and personal functioning (Eisdorfer et al., 1992; Loewenstein et al., 1995). Accordingly, AD becomes a devastating experience for patients coping with the illness as well as family members, who often suffer depression, health problems, increased mortality, and other negative outcomes because of the strains of caregiving. There is no cure or effective treatment for AD at this time.

AD has emerged as a national and international pandemic. It is the most common form of dementia, affecting an estimated 5.2 million Americans this year alone, and that number is projected to increase to more than 13.2 million persons by 2050 (Herbert et al., 2003; Plassman et al., 2007). There were an estimated 30 million affected individuals in the world in 2000, and that number is also projected to increase to over 85 million. Many risk factors have been implicated by epidemiological study, but age remains the most significant. The occurrence of AD is rare before age 65, affecting less than 1 person per

1000. The prevalence is about 2.5-3% at age 65, and it roughly doubles every five years, until age 85-90, where the prevalence approaches 50% and appears to plateau (Petersen, 2000; Tanzi, 2000). However, prevalence is expected to increase as diagnosis of the disease improves and general medicine prolongs longevity. The public health challenge is significant.

AD is classified into 2 major subcategories, early-onset or familial Alzheimer disease (EOAD/FAD) and late-onset or sporadic Alzheimer disease (LOAD or SAD), with 60 to 65 years as the age cutoff. EOAD/FAD accounts for about 5% of all cases. While EOAD/FAD is considered entirely heritable, genetic factors are also believed to account for 5-10% of LOAD/SAD cases (Rocchi et al., 2003; Tanzi, 2000). Of the genes linked to AD, amyloid precursor protein (APP), presenilin-1 and -2 (PS1 and PS2), and apolipoprotein E (APOE), APP on chromosome 21 was the first identified (Goate et al., 1991; Levy-Lahad et al., 1995; Strittmatter et al., 1993). Interestingly, nearly all individuals with Down syndrome (trisomy 21) who survive into their thirties or longer develop a form of AD (Selkoe et al., 2001; Wisniewski et al., 1985). It is now well known that APP metabolites, 39-43 amino acid β-amyloid (Aβ) peptides, comprise a large component of the amyloid plaques deposited in the brains of AD patients (Glenner and Wong, 1984; Masters et al., 1985; Roher et al., 1993).

1.2 APP metabolism

APP is a 695-770 amino acid transmembrane protein highly expressed in the brain. There are 3 major APP isoforms generated by alternative splicing (APP_{695}, APP_{751}, APP_{770}), with APP_{695} being the predominant isoform in neurons. APP exhibits a

rapid turnover rate (half-life of ~2-4 hours) in neuronal tissue as it is trafficked through secretory and endocytic pathways (LeBlanc et al., 1996). Although its exact endogenous function has yet to be fully established, APP has been implicated as a mediator of synaptic plasticity (Priller et al., 2006; Turner et al., 2003). Interestingly, both APP knock-out and overexpressing transgenic mice exhibit learning impairments (Matsuyama et al., 2007; Phinney et al., 1999). Proteolysis of APP is the fundamental process for the production of the Aβ peptides implicated in AD pathology (Funamoto et al., 2004; Golde et al., 2000; Sambamurti et al., 2002). APP metabolites arise from the coordinated proteolytic action of α, β and γ-secretases (Figure 1). In the amyloidogenic pathway, Aβ peptides are produced by the initial action of β-secretase (BACE) cleavage, which creates an Aβ-containing carboxyl-terminal fragment known as β-CTF, or C99 (Sinha and Lieberburg, 1999; Yan et al., 1999). This proteolysis also generates an amino-terminal, soluble APP-β (sAPP-β) fragment, which is released extracellularly. Intracellularly, β-CTF is then cleaved by a multi-protein γ-secretase complex, that results in generation of the Aβ peptide and a smaller γ-CTF, also known as C57 (De Strooper et al., 1998; Steiner et al., 1999). Conversely, in the non-amyloidogenic pathway, APP is first cleaved at the α-secretase site, which results in release of amino-terminal soluble APP-α (sAPP-α) and the generation of an α-CTF or C83 (Hooper et al., 2002), events that are indicative of α-secretase activity (Hooper et al., 2002). Because of the limiting amount of APP in the cell and the failure to saturate the BACE pathway during APP overexpression, it is believed that the amyloidogenic and non-amyloidogenic pathways compete for substrate in the process of APP proteolysis (Gandhi et al., 2004). Therefore, it is often inferred that

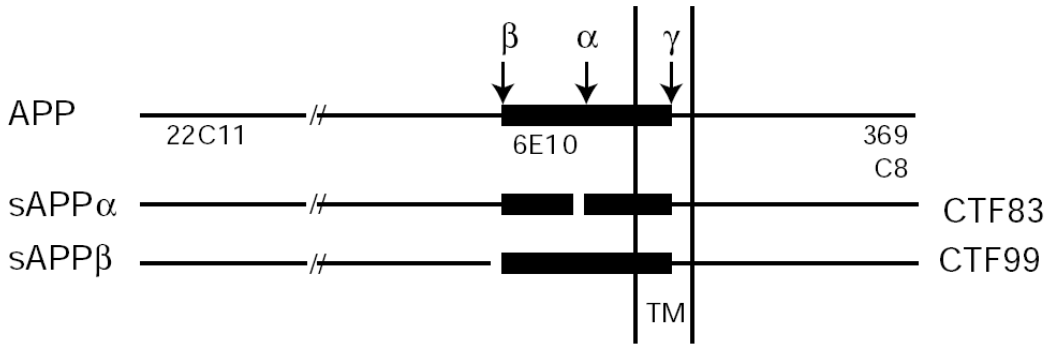

Figure 1

APP metabolism. Antibody binding sites for amino-terminal APP antibody 22C11, carboxyl-terminal APP antibodies 369 and C8, and amino-terminal Aβ antibody 6E10 are as indicated. Adopted from Yan and colleagues (1999).

extracellular elevation of sAPP-α (non-amyloidogenic pathway product) can be taken as indirect evidence of inhibition of BACE and the resulting amyloidogenic pathway.

Aβ metabolism is also quite rapid (half-life of ~2-4 hours) and tightly regulated (Cirrito et al., 2003). In addition, its native physiological role also remains elusive. Moreover, its primary sequence is not well-conserved with APP across species (Zheng and Koo, 2006). Aβ peptides can be degraded by various proteases including, insulin degrading enzyme (IDE) and neprilysin (Iwata et al., 2000; Kurochkin and Goto, 1994). Furthermore, peptides can be shuttled into the endocytic/lysosomal pathway and degraded or exported into the periphery for subsequent degradation via the low density lipoprotein receptor related protein (LRP) (Deane et al., 2004; Kang et al., 2000; Qiu et al., 1999). Interestingly, endosomal abnormalities are among the earliest evidenced pathological dysfunctions in AD (Cataldo et al., 1995; Nixon et al., 2000).

1.3 Amyloid hypothesis

The Aβ peptide has long been the prime suspect in pathogenesis of AD, as aggregated strands of the peptide, called fibrils, are the main constituents of amyloid plaques. As the major amyloidogenic forms of the peptide ($A\beta_{1\text{-}40,42}$) accumulate both inside and outside of neurons, amino acid residues begin to link together, forming oligomers, which subsequently form protofibrils and fibrils rich in β-sheet secondary structures (Harper et al., 1997; Soto et al., 1995; Teplow, 1998). The conformational change driven-insolubility of these stacked sheets eventually causes the oligomers to precipitate out of the cellular milieu. These precipitated oligomers, protofibrils, and

fibrils subsequently combine with other excreted cellular components to form a thick, viscous buildup called an amyloid plaque (Sipe and Cohen, 2000).

From their generation to their deposition as amyloid plaques, Aβ peptides can potentially trigger a toxic cascade that contributes both directly and indirectly toward neuronal dysfunction and death. One of the most widely held theories of the pathogenesis of AD that encapsulates this sentiment is the "amyloid hypothesis." As first proposed by Hardy and Allsop (1991), the hypothesis purported that mismetabolism and deposition of Aβ peptides are the principal etiopathological events in AD. As research has expanded what is known of AD pathophysiology over the past two decades proponents have amended the hypothesis accordingly. A more contemporary view emphasizes the role of soluble oligomeric forms of Aβ as etiological agents of the disease, rather than the deposited fibrils or plaques. Recent research has further elucidated these oligomers' ability to disrupt synaptic functioning both *in vitro* and *in vivo* (Cleary et al., 2005; Klyubin et al., 2005; Shankar et al., 2007). In particular, soluble Aβ oligmers termed "amyloid-derived diffusible ligands" (ADDLs) were detected to be at least an order of magnitude higher in AD patients and may account for the imperfect correlation between amyloid plaques and diagnosis (Gong et al., 2003; Klein, 2002). However, previous research suggesting the potential neurotoxicity of insoluble fibrillar forms of Aβ should not be forgotten (Loo et al., 1993; Lorenzo et al., 1994). In view of this, it may be that both soluble and insoluble forms of Aβ contribute, via discrete mechanisms, to the continuum of AD pathology.

1.4 AD pathology

While the exact cause of neurodegeneration in AD is uncertain, it is has been suggested to involve the interplay of apoptosis, oxidative stress, inflammation, NFT formation, excitotoxcity, and glucose metabolism dysfunction, all of which may be mediated by Aβ-dependent mechanisms. As touched upon in the section above, both oligomeric and fibrillar forms of $A\beta_{1\text{-}42}$ have been extensively reported to induce apoptosis in cultured neurons and neuron-like cells. Apoptosis is a tightly regulated process in which a series of biochemical events promote morphological changes in cellular structures that ultimately result in death of a cell. It has been postulated that Aβ directly interacts with neurons to propagate intracellular signaling, which triggers these biochemical events via activation of a caspase cascade (Awasthi et al., 2005; Harada and Sugimoto, 1999). Aβ-mediated oxidative stress may also induce apoptosis (Butterfield et al., 2002; Shearman et al., 1994). Aβ has been shown to readily react with large metal ions such as, copper (Cu^{2+}), iron (Fe^{3+}), and zinc (Zn^{2+}), and through redox chemistry generate hydrogen peroxide (H_2O_2) (Opazo et al., 2002). This reactive oxygen species (ROS) can damage cells by both oxidation of lipoproteins of cellular membranes and mitochondrial and nuclear DNA. In addition, H_2O_2 has been shown to directly mediate apoptosis by modulation of the regulatory proteins Bax and Bcl-2 and activation of caspase-3 (Jiang et al., 2003; Milton, 2004). Another source of ROS, while secondary, is believed to come from microglial activation during inflammation.

An abundance of post-mortem and basic research studies have confirmed that inflammatory processes play a role in the pathology of AD. Microglial and astroglial activation in close proximity to amyloid plaques are two of the most consistently

evidenced markers of inflammation. For this reason, many current research efforts focus on the complex cascade of potentially deleterious inflammatory events, especially activation of microglia, the resident immune cells of the central nervous system (CNS), to identify and clarify the neurodegenerative effects caused by the immune response to Aβ. Chronic activation of microglia is believed to trigger and maintain an inflammatory response, which may ultimately lead to neuronal cell death such as that observed in AD. In fact, this chronic activation may expose the CNS to elevated levels of a wide array of potentially neurotoxic molecules including pro-inflammatory cytokines, complement proteins, proteinases, excitotoxins, and (as mentioned above) ROS . Conversely, an alternative view suggests that dysregulation of microglial activation may prevent appropriate inflammatory responses necessary to respond to neuroinsults such as accumulation of Aβ. Accordingly, the debate over whether this inflammatory component of AD is intrinsically beneficially of harmful continues (Akiyama et al., 2000; Streit, 2005).

Another major pathologically contributing process in AD is the formation of NFTs inside neurons. While generation and deposition of Aβ peptides as amyloid plaques typically occurs before NFT formation, the latter follows closely with, but supposedly independently of cerebral amyloidosis. However, a growing number of reports have suggested that these two pathologies may be linked, as Aβ generation and deposition may promote NFT formation (Alvarez et al., 1999; Busciglio et al., 1995; Calhoun et al., 1998; Greenberg and Kosik, 1995). The main protein constituent of the NFTs is the microtubule associated protein (MAP) tau. The tau protein forms an essential part of the neuron cytoskeleton, aiding with the support of the shape of the cell and

facilitating intercellular transport. In the case of AD and various other tauopathies, tau has been found to be abnormally phosphorylated/dephosphorylated at specific residues by several possible neuronal kinases/phosphatases both *in vitro* and *in vivo*, which is hypothesized to ultimately lead to conformational abnormality, dysfunction, and aggregation (Arendt et al., 1998; Lee et al., 2000; Wang et al., 1998; Yamamoto et al., 2002). Unfortunately, once NFTs have formed anti-Aβ therapeutic strategies may prove to be ineffective against their underlying pathological mechanisms and removal.

Overstimulation of excitatory N-methyl-D-aspartate receptors (NMDA-Rs) has also been implicated in the pathology of AD (Doraiswamy, 2003; Mattson and Chan, 2003). This process, termed excitotoxicity, progresses as NMDA-Rs begin to indirectly mediate calcium (Ca^{2+}) transport into neurons. This influx is routinely used to trigger the release of neurotransmitters from synaptic vessicles. However, as Ca^{2+} accumulates within the neuron, Ca^{2+}-dependent calpains and endonucleases may begin to degrade essential proteins and DNA, respectively in line with apoptotic mechanisms. Ca^{2+}-related mitochondrial dysfunction may also generate significant amounts of ROS within neurons (Rego and Oliveira, 2003). While glutamate typically functions as the excitatory ligand, De Felice and colleagues (2007) recently reported that ADDLs may bind to or in close proximity to NMDA-Rs to propagate excitotoxic effects.

Multiple lines of evidence from both clinical and basic research studies have also suggested that neuronal glucose metabolism is impaired in AD. The brain almost exclusively utilizes glucose as its source of energy. In view of this, it is becoming increasingly evident that neuronal glucose metabolism is essential for maintaining synaptic plasticity required for memory formation and retrieval. Positron emission

tomography (PET) employing (^{18}F)fluoro-2-deoxyglucose (FDG) has confirmed glucose hypometabolism in cortical regions of AD patients' brains, although it remains unclear whether neuronal populations are specifically affected (Friedland et al., 1983; Minoshima et al., 1997; Swerdlow et al., 1994). Remarkably, Aβ may also be linked to processes that govern this metabolism. Previous *in vitro* studies suggest that $A\beta_{1\text{-}40,42}$ may inhibit glucose metabolism by competitively binding to insulin receptors and preventing their signaling (Xie et al., 2002). Conversely, other studies have suggested that Aβ promotes glucose metabolism via activation of hypoxia-inducible factor-1 (HIF-1) (Soucek et al., 2003). However, this metabolic activation may still ultimately result in neuronal death through glucose starvation (Schubert, 2005).

Whether one specific process confers more neurotoxicity than the other will continue to be an area on controversy. Yet, just as the impact of genetic and environmental risk factors may vary in each individual, so may the relative effects of each specific pathological process. Only through continued research will effective therapies capable of preventing, halting, or reversing these pathological processes be identified.

1.5 Flavonoids

The intense search for small-molecular compounds that may modulate AD pathology has advanced the analysis of specific dietary derived substances, which epidemiological studies suggest are beneficial against disease-related neurodegeneration and aging processes (Bastianetto, 2002; Dai et al., 2006; Genkinger et al., 2004; Laurin et al., 2004; Sun et al., 2002). Recent research has focused on the analysis of flavonoids, a

group of phenolic phytochemicals common in vascular plants and abundant in particular spices, vegetables, and fruits. Similar to alkaloids, but less toxic, flavonoids are secondary metabolites and as such do not directly contribute to plant development, growth, or reproduction. The function or importance of these secondary metabolites is usually of an ecological nature. Both flavonoids and alkaloids can be used as defenses against predators, parasites and diseases, or even for interspecies competition. For these reasons, many flavonoids possess intrinsic anti-microbial and anti-fungal properties (Nijveldt et al., 2001). Flavonoids are also considered important constituents in the human diet, although their daily intake varies with dietary habits (Nielsen et al., 1999; Sampson et al., 2002). Numerous medicinal properties have been ascribed to flavonoids, notably for their anti-oxidant (Saija et al., 1995; van Acker et al., 1996), anti-carcinogenic (Kanadaswami et al., 2005; Ren et al., 2003), and anti-inflammatory activity (Pelzer et al., 1998; Middleton, 1998). While the molecular basis for these properties has not been fully established, a growing number of studies have begun to dissect out the disease modifying mechanisms of these compounds.

Over the past decade, intense focus has been given to investigating the processes of APP and Aβ metabolism as possible targets for AD therapy (Hardy and Selkoe, 2002). In this regard, few flavonoids have been analyzed for their efficacy in the modulation of these pathological events. In particular, the naturally occurring compounds curcumin, from the spice turmeric, and resveratrol, from red wine, have been reported to alter APP and Aβ metabolism in models of AD (Marambaud et al., 2005; Yang et al., 2005). Other naturally occurring compounds achieving worldwide popularity for their therapeutic application are from green tea. Green tea contains a unique subset of flavonoids,

catechins, which are believed to be the active components accounting for the therapeutic properties of green tea. Arguably one of the most promising green tea compounds being analyzed is (-)-epigallocatechin-3-gallate (EGCG), which has been extensively studied due largely to its reported anti-carcinogenic effects (Lin and Liang, 2000; Moyers and Kumar, 2004). Interestingly, EGCG has been found to modulate protein kinase C (PKC) activity and consequently increase secreted levels of sAPP-α, which suggests a potential underlying APP metabolic mechanism (Levites et al., 2002, 2003). Multiple *in vitro* studies have also evidenced EGCG's ability to act as a free radical scavenger. Additionally, EGCG has been shown to inhibit various activities of pro-inflammatory cytokines (Ahmed et al., 2002; Han, 2003; Li et al., 2004). Accordingly, signal transducer and activator of transcription 1 (STAT1) and nuclear factor κB (NFκB) responses are inhibited by EGCG (Aktas et al., 2004; Han, 2003). Studies investigating glutamate-induced Ca^{2+} influx have shown that EGCG may be an effective regulator of this process as well (Bae et al., 2002; Lee et al., 2004). EGCG has also been reported to promote glucose metabolism by increasing insulin sensitivity (Lin et al., 2008; Potenza et al., 2007). Elucidation of these molecular actions of EGCG substantiates the compound as a versatile modulator of cellular responses that may contribute to AD pathogenesis.

Importantly, the studies mentioned above provide a criterion for selecting future flavonoids to screen for their efficacies as modulators of APP metabolism and ultimately potential therapeutics for AD. For instance, the flavonoid luteolin, largely found in parsley, peppers, and celery, has been reported to be a free radical scavenger (Horvathova et al., 2004; Reddy et al., 2005), an anti-inflammatory agent (Odontuya et al., 2005; Ueda et al., 2002), a regulator of Ca^{2+}influx (Kimata et al., 2000), and potential promoter of

glucose metabolism (Zarzuelo et al., 1996). If luteolin should also prove to be a potent modulator of APP metabolism, it may be an ideal candidate compound for opposing AD pathogenesis. In the chapters to come the anti-amyloidogenic properties of EGCG and luteolin are established and their underlying mechanisms fully explored in "Swedish" mutant APP (APP_{sw}; Mullan et al., 1992) models of AD.

CHAPTER 2

MATERIALS AND METHODS

2.1 Cell culture

2.1.1 Immortalized murine cell lines

Both parental murine neuroblastoma (N2a) and N2a cell lines stably transfected with the "Swedish" mutant form of APP (SweAPP N2a cells; APP_{695}), a well established in vitro model of AD, were kind gifts from S. Gandy (Thomas Jefferson University, Philadelphia, PA, USA). SweAPP N2a cells were maintained in Dulbecco's modified Eagle's medium (DMEM), 10% fetal calf serum (FCS), and 200 μg/ml G418. Prior to treatment N2a cells were differentiated in serum-free Neurobasal medium supplemented with 300 μM dibutyryl-cAMP for 4 hours. N9 microglial cell lines, originally generated from myc-immortalized mice, were a kind gift from Dr. P. Ricciardi-Castagnoli (Universita Degli Studi di Milano-Bicocca, Milan, Italy). N9 microglial cells were maintained in DMEM, 5% FCS and 2 mM glutamine. All cultures were incubated in serum-free medium at 37° C with 10% CO2 during treatment.

2.1.2 Murine-derived primary cell lines

Murine primary neuronal cells were prepared as previously described (Tan et al., 2000). Briefly, cerebral cortices were isolated from mouse embryos, between 15 and 17 days in utero, and were mechanically dissociated in trypsin (0.25%) individually after

incubation for 15 minutes at 37 °C. Cells were collected after centrifugation at 1,200 x *g*, resuspended in DMEM supplemented with 10% fetal calf serum, 10% horse serum, uridine (33.6 µg/mL; Sigma, St. Louis, MO, USA), and fluorodeoxyuridine (13.6 µg/mL; Sigma), and seeded in 24-well poly-D-lysine coated culture plates at 2.5 x 10^5 cells per well. When neuronal cells were isolated from transgenic APP_{sw} (Tg mice APP_{sw}), to verify the presence of the transgene, PCR genotype analysis was performed as previously described (Tan et al., 2002). Murine primary microglial cells also isolated as previously described (Tan et al., 2000). Briefly, cerebral cortices from newborn mice (1-2 day-old) were isolated under sterile conditions and were kept at 4°C before mechanical dissociation in trypsin (0.25%). The resulting cultures were plated in 75 cm^2 poly-D-lysine coated flasks and grown in RPMI 1640 medium supplemented with 5% fetal calf serum, 2 mM glutamine, 100 units/ml penicillin, 0.1 µg/mL streptomycin, and 0.05 mM 2-mercaptoethanol. Primary cultures were kept for 14 days so that only glial cells remained and microglial cells were isolated by shaking flasks at 200 rpm in a Lab-Line incubator-shaker. Following isolation, glial cells were seeded in 24-well poly-D-lysine coated culture plates at 2.5 x 10^5 cells per well. To verify their glial status, cells were subsequently stained for the microglial marker Mac-1 (CD11b/CD18; Boehringer Mannheim, Indianapolis, IN, USA). All cultures were incubated in their respective complete medium at 37° C with 10% CO2 during treatment.

2.1.3 Lysate preparation

All cultured cells were lysed in ice-cold lysis buffer (20 mM Tris, pH 7.5, 150 mM NaCl, 1 mM EDTA, 1 mM EGTA, 1% v/v Triton X-100, 2.5 mM sodium

pyrophosphate, 1 mM β-glycerolphosphate, 1 mM Na3VO4, 1 μg/mL leupeptin, 1 mM PMSF) for 5 minutes followed by scraping. Lysates were collected and centrifuged at 14,000 x *g* for 15 minutes at 4°C. Protein levels in cell lysate supernatants were determined and normalized by bicinchoninic acid assay (BCA; Pierce Biotechnology, Rockford, IL, USA) in accordance with the manufacturer's instruction.

2.2 Mice

2.2.1 Housing and maintanence

Tg APP_{sw} mice of a hybrid B6/SJL background (line 2576; Hsiao et al., 1996) were purchased from Taconic (Germantown, NY, USA). Both non transgenic (NT) and Tg APP_{sw} mice with a mixed background of 56.25% C57, 12.5% B6, 18.75% SJL, and 12.5% Swiss-Webster were kindly provided by G. Arendash (Johnnie B. Byrd Sr. Alzheimer's Center and Research Institute, Tampa, FL, USA). Transgene expression in each of the transgenic mice was confirmed by genotyping as previously described (Arendash et al., 2006; Tan et al., 2002). All animals were given ad libitum access to water and chow and maintained on a 12 hour light/dark cycle. All animals were housed in the College of Medicine Animal Facility at the University of South Florida (USF) and all experiments were in compliance with protocols approved by the USF Institutional Animal Care and Use Committee.

2.2.2 Stereotactic intracerebroventricular injection

Mice were anesthetized using isoflurane via chamber induction at 4-5% with intubation and maintenance at 1-2%. Reflexes were checked to ensure that all animals were unconscious. Mice were positioned on a stereotaxic frame with ear-bars plugged and jaws fixed to a biting plate. Under a surgical microscope, a small incision was made to expose the skull, generally 1 cm above and below bregma. Using a Dremel™ tool fitted with a small burr bit, a small hole was made in the skull (0.6 mm posterior and 1.2 mm left lateral to the bregma). Injections were made in the left lateral ventricle from delimited coordinates relative to bregma (– 0.6 mm anterior/posterior, + 1.2 mm medial/lateral, and – 3.0 mm dorsal/ventral) using stereotaxic device (Stoelting Lab Standard, Wood Dale, IL, USA) and an attached probe holder. Treatment volumes of 5μL were administered at the rate of 1 μL/min using a Hamilton syringe (Sigma). Correctness of the injection was confirmed by trypan blue dye administration and histological examination.

2.2.3 Brain homogenate and tissue section preparation

Mice were anesthetized with isofluorane and transcardially perfused with ice-cold physiological phosphate buffered saline (PBS) containing heparin (10 U/mL). Brains were rapidly isolated and quartered using a mouse brain slicer (Muromachi Kikai, Tokyo, Japan). First and second anterior quarters were homogenized for western blot and ELISA analysis. Briefly, brain quarters were homogenized in ice-cold lysis buffer by sonication for 3 minutes. The resulting homogenates were allowed to stand for 15 minutes at 4°C and were subsequently centrifuged at 14,000 *g* for 15 minutes at 4°C. Protein levels in cell lysate supernatants were determined and normalized by BCA assay in accordance

with the manufacturer's instruction. Third and fourth posterior quarters were used for microtome or cryostat sectioning. Briefly, brain quarters were fixed in 4% paraformaldehyde in PBS at 4°C overnight and routinely processed in paraffin at the core facility of Department of Pathology in the College of Medicine at USF. Following embedment in appropriate medium, five coronal sections from each brain quarter (5 and 25μm thickness for paraffin and cryostat) were cut with a 150 μm interval.

2.3 ELISA

2.3.1 $A\beta_{1-40}$ and $A\beta_{1-42}$

$A\beta_{1-40}$ and $A\beta_{1-42}$ species were quantified in samples using $A\beta_{1-40}$ and $A\beta_{1-42}$ ELISA kits (IBL-American, Minneapolis, MN, USA) in accordance with the manufacturer's instruction, except that standards include 5 M guanidine buffer. Soluble Aβ species were detected in brain homogenates prepared with lysis buffer described above following a 1:10 dilution in lysis buffer. Insoluble Aβ species were detected by acid extraction of brain homogenates in 5 M guanidine buffer (Johnson-Wood et al., 1997), followed by a 1:10 dilution in lysis buffer. ELISA values were reported as % control or pg of $A\beta_{1-x}$/mg of total protein, as determined by BCA assay.

2.3.2 Total Aβ

Total $A\beta_{1\text{-}40,42}$ species were quantified in samples as previously described (Tan et al., 2002). Briefly, 96-well immunoassay plates were coated with monoclonal anti-$A\beta_{1\text{-}17}$ antibody (6E10; 2 μg/mL in PBS; Signet Laboratories, Dedham, MA, USA) overnight at 4 °C. Plates were washed with 0.05% Tween 20 in PBS 5 times and incubated with blocking buffer (PBS with 1% bovine serum albumin (BSA), 5% horse serum) for 2 hours at room temperature. Conditioned media, brain homogenates, or standards were added to the plates, following appropriate dilutions above, and incubated overnight at 4 °C. Following 3 washes, biotinylated anti-$A\beta_{17\text{–}26}$ monoclonal antibody (4G8; 0.5 μg/mL in PBS with 1% BSA; Signet Laboratories), was added to the plates and incubated for 2 hours at room temperature. After 5 washes, streptavidin-horseradish peroxidase (HRP) (1:200 diluted in PBS with 1% BSA) was added to the 96-well plates for 30 minutes at room temperature. Tetramethylbenzidine (TMB) substrate was added to the plates and incubated for 15 minutes at room temperature. Stop solution (2N H_2SO_4) was added to stop the colorimetric reaction and optical density was determined immediately by a microplate reader at 450 nm. ELISA values from were reported as % control or pg of $A\beta_{1\text{-}x}$/mg of total protein, as determined by BCA assay.

2.3.3 sAPP-α

sAPP-α was quantified as previously described by Olsson and colleagues (2003) with minor changes. Briefly, 96-well immunoassay plates were coated with monoclonal amino-terminal APP antibody (22C11; Roche, Basel, Switzerland) overnight at 4°C. Plates were washed with 0.05% Tween 20 in PBS 5 times and incubated with blocking

buffer (PBS with 1% BSA, 5% horse serum) for 2 hours at room temperature. Conditioned media, brain homogenates, or standards were added to the plates, following appropriate dilutions above, and incubated overnight at 4 °C. Following 3 washes, biotinylated 6E10 (Signet) was added to the plates and incubated for 2 hours at room temperature. After 5 washes, streptavidin-HRP (1:200 diluted in PBS with 1% BSA) was added to the 96-well plates for 30 minutes at room temperature. TMB substrate was added to the plates and incubated for 15 minutes at room temperature. Stop solution (2N H_2SO_4) was added to stop the colorimetric reaction and optical density was determined immediately by a microplate reader at 450 nm. ELISA values were reported as % control or μg of sAPP-α/mg of total protein, as determined by BCA assay.

2.4 Western blot

Aliquots from lysates, precipitates, and homogenates corresponding to 50 μg of total protein were electrophoretically separated using 10% Tris/Glycine or 16.5% Tris/Tricine SDS-Polyacrylamide gels. Electrophoresed proteins were then transferred to PVDF or nitrocellulose membranes (Bio-Rad, Hercules, CA, USA), which were subsequently washed in distilled de-ionized water (ddH_2O) and blocked for 1 hour at room temperature in Tris buffered saline (TBS) containing 5% (w/v) non-fat dry milk. After blocking, membranes were hybridized with various primary antibodies for 4 hours at room temperature or overnight at 4°C. Membranes were then washed 3 times for 5 minutes each in ddH_2O and incubated for 1 hour at ambient temperature with the appropriate HRP-conjugated secondary antibody (1:1,000, Pierce). All antibodies were

diluted in TBS containing 5% (w/v) non-fat dry milk in accordance with the manufacturer's suggestions. Blots were washed 3 times for 5 minutes each in ddH_2O prior to being developed using a chemiluminescence luminol reagent (Pierce).

2.4.1 APP metabolite profiling

CTFs of APP were detected by carboxyl-terminal APP antibody (369; a kind gift from S. Gandy and H. Steiner, Ludwig-Maximilians-University, Munich, Germany). Briefly, blots were first hybridized with 369 to characterize APP CTFs. Following development, blots were put in stripping solution (62.5 mM Tris-HCl, pH 6.8, 2% SDS, and 100 mM 2-mercaptoethanol) and incubated at room temperature for 30 minutes. After stripping, blots were rinsed with TBST (TBS, 0.1% Tween 20) and re-blocked with TBSTM (TBST, 5% (w/v) non-fat dry milk), and then re-probed with 6E10. Alternatively, membranes with identical samples were probed either with antibody 369 or with antibody 6E10. An ~11 kDa band was positively detected with both 369 and 6E10 antibodies, thereby distinguishing between α-CTFs and β-CTFs. For sAPP-α, cultured media was collected following treatment according to a modified protocol from Chen and Fernandez (2004). sAPP-α was extracted using 3K Nanosep centrifugal filters (Pall Life Sciences, Ann Arbor, MI, USA) and protein concentrate was subjected to western blot analysis with 6E10 antibody as described above.

2.5 Immunoprecipitation

Aliquots from lysates and homogenates corresponding to 200 μg total protein were pre-cleared by incubating with 10 μL of a protein A-Sepharose bead slurry (50% in

PBS, Sigma) for 1 hour with gentle rocking at 4°C. Samples were centrifuged at 14,000 *g* for 5 minutes, pellets were discarded, and the resulting supernatants were incubated with various primary antibodies overnight with gentle rocking at 4°C. 50 μL of the protein A-Sepharose bead slurry was then added to the samples prior to gentle rocking for 4 hours at 4°C. Samples were centrifuged at 14,000 *g* for 5 minutes, supernatants were either discarded or retained for immunodepletion experiments, and the resulting pellets were washed 3 times PBS. Following washing, precipitated samples were subjected to western blot as described above.

2.5.1 Secreted APP metabolite profiling

sAPP-α, sAPP-β, and Aβ was detected by incubating pre-cleared cultured media with various sequential combinations of 6E10 (1:100) and/or 22C11 (1:100) antibodies overnight with gentle rocking at 4°C. 100 μL of the protein A-Sepharose bead slurry was then added to the samples prior to gentle rocking for 4 hours at 4°C. Samples were centrifuged at 14,000 *g* for 5 minutes, supernatants were either discarded or retained for immunodepletion experiments, and the resulting pellets were washed 3 times lysis buffer. Following washing, precipitated samples were subjected to western blot as described above.

2.6 Secretase activity assay

Secretase activity was quantified in cell lysates using R&D Systems kits (Minneapolis, MN, USA) based on secretase-specific substrates conjugated to

fluorogenic reporter molecules (EDANS/DABCYL) in accordance with the manufacturer's instructions. Briefly, appropriate amounts of lysates or homogenates, reaction buffer, and flurogenic substrate were added to 96-well assay plates and incubated at 37ºC for various periods of time. Following incubation, fluorescence was monitored (excitation at 335 nm and emission at 495 nm) at room temperature with a fluorescence microplate reader. Fluorescence was adjusted using appropriate controls (no lysate or homogenate and no fluorogenic substrate).

2.7 RT-PCR

Analysis of murine ADAM10 was conducted according to previously published methods (Park et al., 2001; Ehrhart et al., 2005). Briefly, total RNA was isolated from SweAPP N2a cells and subjected to reverse transcription utilizing a commercially available kit (cDNA Cycle kit; Invitrogen, Carlsbad, CA, USA) according to the manufacturer's instructions on a Bio-Rad iCycler thermocycler. The same machine was used to amplify murine cDNA by PCR using ADAM10 sense (5'-GCCAGCCTATCTGTGGAAACGGG-3') and antisense (5'-TTAGCGTCGCATGTGTCCCATTTG-3') primers or γ-actin sense (5'-TTGAGACCTTCAACACCC-3') and antisense (5'-GCAGCTCATAGCTCTTCT-3') primers (0.5 µg/25 µl final reaction volume) using a commercially available kit (HotStarTaq Master Mix; Qiagen, Valencia, CA, USA) according to the manufacturer's instructions. Thermocycler conditions consisted of an initial denaturing step at 95 °C for 15 minutes, followed by 35 cycles of 94 °C for 30 seconds, 50 °C for 1 minute, and 72 °C for 1 minute, and a final extension step at 72 °C for 10 minutes. Resolution and analysis

of PCR product (murine ADAM10: 881 bp, murine γ-actin: 357 bp) band densities were conducted by ethidium bromide-stained agarose gel electrophoresis and identified using UV transillumination by comparisons with molecular weight markers (Invitrogen). Samples that were not subjected to reverse transcription were run in parallel as negative controls to rule out DNA contamination as a template for PCR products (data not shown). A no template control was also included for each primer set as a further negative control (data not shown). Amplification of γ-actin was used to normalize for input cDNA.

2.8 RNAi

SweAPP N2a cells were transfected with siRNA pre-designed to knockdown murine ADAM9, -10, or -17 and GSK-3α or GSK-3β mRNA (Dharmacon Inc., Lafayette, CO, USA). SweAPP N2a cells seeded in 24-well poly-D-lysine coated culture plates at 1 x 10^5 cells per well and cultured until they reached 70% confluence. The cells were then transfected with 50–200 nM concentrations of target siRNA or anti-green fluorescent protein (non-target control; Dharmacon) using Code-Breaker transfection reagent (Promega, Madison, WI, USA) and cultured for an additional 18 hours in serum-free DMEM. Transfection efficiency was determined to be greater than 70% (data not shown) using no-RISC siGLOW (fluorescently labeled non-functional siRNA; Dharmacon). The cells were allowed to recover for 24 hous in complete medium before treatment. Resulting lysates were also subjected to western blot as described above for analysis of expression of target proteins.

2.9 Cytotoxicity assay

Cell death was measured from lactate dehydrogenase (LDH) release detected directly in cultured media using a CytoTox 96 Non-Radioactive Cytotoxicity Assay kit (Promega) in accordance with the manufacturer's instructions. Briefly, appropriate amounts of cultured media, reaction buffer, and colorimetric substrate were added to 96-well assay plates and incubated at 37ºC for various periods of time. Following incubation, optical density was monitored at 490 nm at room temperature with a microplate reader. Cytotoxicity values were determined using appropriate controls (reaction buffer alone and lysis buffer treated cell cultured media).

2.10 Tissue staining

2.10.1 Immunohistochemical

Sections were routinely mounted on slides and air dried or deparaffinized and hydrated in a graded series of ethanol before preblocking for 30 minutes at room temperature with serum-free protein block (Dako Cytomation, Carpinteria, CA, USA). Staining was performed for amyloid pathology using 4G8 antibody (1:100; Signet Laboratories) and GSK-3 activity using anti-phospho-GSK3α/β ($pTyr^{279/216}$) antibody (1:50; Sigma) in conjunction with the VectaStain Elite ABC kit (Vector Laboratories, Burlingame, CA, USA) coupled with diaminobenzidine (DAB) substrate. Stained sections were rinsed through three rapid changes of 100% ethanol, cleared through three changes of xylene, then coverslipped with permount. Sections were visualized under bright-field using an Olympus BX-51 microscope (Tokyo, Japan).

2.10.2 Thioflavin S

Sections were routinely mounted on slides and air dried or deparaffinized and hydrated in a graded series of ethanol before staining with fresh-filtered 1% (w/v) thioflavin S diluted in 70% ethanol for 5 minutes. These sections were then rinsed 3 times for 5 minutes each in 70% ethanol, hydrated for 5 minutes in PBS, and mounted in Vectashield fluorescence mounting media (Vector Laboratories). Thioflavin S-positive β-amyloid plaques were visualized under dark field using an Olympus BX-51 microscope.

2.10.3 Congo red

Sections were routinely mounted on slides and air dried or deparaffinized and hydrated in a graded series of ethanol before staining. Hydrated sections were then incubated in an alkaline alcoholic saturated sodium chloride solution (2.5 mM NaOH in 80% alcohol, freshly prepared) for 20 minutes. Following incubation, sections were stained with a 0.2% Congo red in alkaline alcoholic saturated sodium chloride solution (freshly prepared and filtered) for 30 minutes. Stained sections were rinsed through three rapid changes of 100% ethanol, cleared through three changes of xylene, then coverslipped with permount. Congo red-positive β-amyloid plaques were visualized under bright-field and polarized light (to confirm green bifringence) using an Olympus BX-51 microscope.

2.11 Image Analysis

2.11.1 Western Blot

Densitometric analysis was conducted using the Fluor-S MultiImager with Quantity One software (Bio-Rad) or ImageJ software (NIH). Images were obtained from film using a scanner. Protein bands were captured, and a threshold optical density was obtained that discriminated bands from background. Densitometric values were reported as area of positive pixels in reference to an internal control.

2.11.2 Tissue sections

Quantitative image analysis (conventional "Aβ plaque burden" analysis) was performed for 4G8 immunohistochemical, thioflavin S, and Congo red stained sections. Images were obtained using an Olympus BX-51 microscope and digitized using an attached MagnaFire imaging system (Olympus). Briefly, images of five 5 or 25 μm sections (150 μm apart) through each anatomic region of interest (hippocampus or cortical areas) were captured, and a threshold optical density was obtained that discriminated staining from background. Manual editing of each field was used to eliminate artifacts. Data are reported as a percentage of stained area captured (positive pixels) divided by the full area captured (total pixels). Quantitative image analysis was performed by a single examiner blinded to sample identities.

2.12 HPLC

HPLC measurements were carried out using a BioLogic HPLC system (Bio-Rad) equipped with a Duo Flow pump, BioFrac fraction collector, and a Quadtec UV/Vis detector set to 280 nm. Briefly, samples were injected onto a reverse-phase column (Agilent, SB-C8 80A 5μm, length 150 mm, i.d. 4.6 mm) through an injection valve with

a 50 µl sample loop. The mobile phase consisted of an isocratic flow of water:acetonitrile:trifluoroacetic acid (87/13/.1) pumped at a rate of 1.00 mL/min at 25°C for 40 minutes. Standard samples of EGCG (Sigma) dissolved in water were run before and after the experimental samples. Remote control of the HPLC system, data acquisition and calculation of peak areas will be performed via computer-based data system (Bio-Rad EZLogic).

2.13 Tau analysis

Pellets from brain homogenates were re-homogenized in 10 volumes of 10% sucrose lysis buffer solution (10 mM Tris, pH 7.5, 0.8 M NaCl, 1 mM EDTA, 1 mM EGTA, 2.5 mM sodium pyropgosphate, 1 mM β-glycerolphosphate, 1 mM Na_3VO_4, 1 µg/mL leupeptin, 1 mM PMSF) and centrifuged at 14,000 x g for 15 minutes. The resulting supernatants were treated with 1% (wt/v) *N*-laurylsarcosine (sarkosyl) to obtain soluble and insoluble fractions for Western blot as previously described (Greenberg and Davies, 1990). Aliquots corresponding to 100 µg of total protein were subjected to western blot as described above.

2.14 Radial arm water maze (RAWM)

This water-based task of working memory, which is very sensitive to brain Aβ levels, was employed as previously described (Arendash et al., 2004; Arendash et al., 2006). Briefly, the RAWM maze contained 6 swim paths (arms) radiating out of an open central area, with a hidden escape platform located at the end of one of the arms. Spatial cues for the maze were provided on the walls surrounding the RAWM task throughout

testing. In each trial, mice were allowed to swim in the arms for up to 60 seconds to find the escape platform, which was randomly assigned to an arm each day. During this time, if mice chose a wrong arm they were gently guided back to the start arm to renew navigating the maze and an error was recorded. Upon finding the correct arm, mice were permitted to remain on the platform for 30 seconds prior to the next trial. RAWM testing consisted of four acquisition trials and one memory retention trial (e.g. five trials, with each trial starting from a different arm and the remaining arm containing the submerged platform for that day). For each trial, mice were placed in the water at the entrance of a start arm of the maze for that day, facing the central swimming area. This start arm was never the same arm that contained the submerged escape platform, and a different start arm sequence was randomly selected each day. RAWM testing was conducted over 15 successive days, which were broken into 3 day blocks. The last trial of the four successive trials (trial 4, T4) and a 30-minute delayed retention trial (trial 5, T5) of the last 3 blocks were considered as measures of working memory.

2.15 Statistical analysis

All data were normally distributed; therefore, in instances of single mean comparisons, Levene's test for equality of variances followed by a *t* test for independent samples was used to assess significance. In instances of multiple mean comparisons, analysis of variance ANOVA was used, followed by *post hoc* comparison using Bonferonni's method. α-levels were set at 0.05 for all analyses. The statistical package for the social sciences release 10.0.5 (SPSS Inc., Chicago, IL, USA) or Statistica (StatSoft Inc., Tulsa, OK, USA) was used for all data analysis.

CHAPTER 3

ANTI-AMYLOIDOGENIC PROPERTIES OF GREEN TEA EPIGALLOCATECHIN-3-GALLATE (EGCG)

3.1 α-Secretase activation

Therapies that oppose cleavage of APP into Aβ peptides and resultant cerebral amyloidosis have become a primary focus in the recent years. The main targets have been β- and γ-secretase, the two proteases that cleave APP at the amino and carboxyl-terminus of the Aβ peptide, respectively, and hence are directly responsible for Aβ peptide generation (De Strooper et al., 1998; Sinha and Lieberburg, 1999; Steiner et al., 1999; Yan et al., 1999). An alternative strategy, namely the activation of α-secretase, has scarcely been investigated for its therapeutic potential. α-secretase cleaves its APP substrate within the Aβ peptide domain and precludes peptide generation, thereby promoting the non-amyloidogenic pathway of APP proteolysis (Hooper and Turner, 2002). α-secretase activation may even have the added advantage of, not only preventing neurotoxic Aβ peptide formation, but also generating the putatively neuroprotective sAPP-α (Furukawa et al., 1996; Mattson et al., 1997, 1999, Stein et al., 2004).

3.1.1 a-disintegrin-and-metalloprotease (ADAM) proteins

A number of reports have implicated members of the a-disintegrin-and-metalloprotease (ADAM) family, a group of zinc metalloproteases including ADAM9,

10, and 17, as putative α-secretase candidates (Hooper and Turner, 2002; Allinson et al., 2003; Asai et al., 2003). Lammich and colleagues (1999) first described the ability of ADAM10 to act as an α-secretase. Furthermore, a report by Lopez-Perez and colleagues (2001) implicates ADAM10 as a contributor to constitutive sAPP-α production, while others have described it as acting in more of a regulative capacity (Skovronsky et al., 2000). Interestingly, in cerebrospinal fluid from AD patients, ADAM10 and corresponding sAPP-α/α-CTFs are decreased, suggesting that non-amyloidogenic/α-secretase APP proteolysis is impaired in AD patients (Lannfelt et al., 1995; Sennvik et al., 2000; Colciaghi et al., 2004). ADAM10 activity is also decreased in AD and Down's syndrome brains (Bernstein et al., 2003). Moreover, a recent study shows that a moderate neuronal overexpression of ADAM10 in mice transgenic for human APP([V717I]) increased the secretion of the neurotrophic soluble sAPP-α, reduced the formation of Aβ peptides, and prevented their deposition as plaques (Postina et al., 2004). Previous studies have also shown that enhanced ADAM10 activity prevented cognitive impairment in a mouse model of AD. Although the individual contributions of the putative α-secretases to the AD process still remain unclear, the above mentioned studies raise the possibility that a strategy of increasing α-secretase activity may provide a promising therapeutic target for AD.

3.1.2 Proprotein convertases (PC)

Conversion of N-glycosylated zymogen/pro-form of ADAM10 into its mature form by proprotein convertases (PCs) is required for its activation and protease activity in α-secretase APP cleavage (Anders et al., 2001; Camden et al., 2005; Anders et al., 2006).

In a recent study by Hwang and colleagues (2006), the PC furin was identified as a key regulator of ADAM10 mediated α-secretase APP cleavage. Other previous reports not only suggest the role of furin, but also that of prohormone convertase-7 (PC7) in ADAM10 activation (Anders et al., 2001; Lopez-Perez et al., 2001). While the identity of the PC responsible for ADAM10 maturation is uncertain, there also remains a debate over the cellular location of its activation between the trans-Golgi network (TGN) and the plasma membrane. In view of this, it may be important to clarify the degree of surface or TGN ADAM10 maturation and its signaling mechanism.

3.1.3 Phosphoinositide-3 kinase (PI3K)

Several intracellular signaling pathways have been implicated in the actions of EGCG. In particular, the phosphoinositide-3 kinase (PI3K)/AKT signaling pathway have been reported to play a role in the action of EGCG. PI3K consists of a heterodimer, with separate regulatory and catalytic subunits. The most common regulatory subunit is p85 (Terauchi et al., 1999). Following phosphorylation of src-homology (SH) domains on target proteins, p85 docks the PI3K dimer to propagate the signaling cascade (Shepherd et al., 1998). PI3K signaling in EGCG-mediated mechanisms has largely been explored in non-neuronal tissue. For instance, topical EGCG induces proliferation of normal human keratinocytes via ERK1/2 and AKT (Chung et al., 2003). A rapid activation of endothelial nitric oxide synthase involving PI3K, PKA and AKT after EGCG treatment has also been demonstrated (Lorenz et. al, 2004). However, in a study by Petanceska and Gandy (1999) PI3K was implicated for its role in regulating the release of sAPP-α from

SweAPP N2a cells, mainly by affecting vesicular trafficking. Accordingly, PI3K may yet play another role in APP metabolism.

3.2 Materials and methods

3.2.1 Reagents

Green tea-derived flavonoids (>95% purity by HPLC), including EGCG, (-)-epicatechin [(-) EC], (+)-epicatechin [(+) EC], (-)-gallocatechin (GC), and (-)-catechin (C) were purchased from Sigma (St. Louis, MO, USA). TNF-α protease inhibitor-1 (TAPI-1) and wortmannin were obtained from Calbiochem (San Diego, CA, USA). Green tea extract (75% polyphenols) was obtained from the Vitamin Shoppe (North Bergen, NJ, USA). carboxyl-terminal antibody APP 369 (1:1000; kindly provided by S. Gandy and H. Steiner), carboxyl-terminal APP antibody (1:500; Calbiochem, Temecula, CA, USA), amino-terminal APP antibody (1:1000, 22C11; Roche, Basel, Switzerland), amino-terminal Aβ antibodies BAM-10 (1:1000; Sigma) and 6E10 (1:1000; Signet Laboratories, Dedham, MA, USA), ADAM9 antibody (1:1000; Sigma), ADAM10 antibodies (1:1000; Calbiochem and Chemicon), TNF-α converting enzyme (TACE)/ADAM17 antibodies (1:1000; Calbiochem and Sigma), phospho-Tyr p85 PI3K binding motif antibody (1:1000; Cell Signaling Technology, Danvers, MA, USA), Furin antibody (1:1000; Biomol International, Plymouth Meeting, PA, USA), PC7 antibody (1:1000; Abcam, Cambridge, MA, USA), tau antibodies (AT270 and AT8, 1:1000; Innogenetics, Alpharetta, GA, USA) or actin antibody (1:1500; as an internal reference control; Roche) were employed for western blot analysis as described in section 2.4.

3.2.2 Mice

For intraperitoneal administration of EGCG, a total of 10 female APP_{sw} mice from a mixed background of 56.25% C57, 12.5% B6, 18.75% SJL, and 12.5% Swiss-Webster were used. Beginning at 12 months of age, these mice were intraperitoneally injected with EGCG (20 mg/kg; $n = 5$) or PBS vehicle ($n = 5$) daily for 60 days. Similarly-aged non-transgenic (NT) mice ($n = 5$) were concurrently given daily intraperitoneal injections of PBS as well. All mice were then sacrificed at 14 months of age for analyses of Aβ levels and plaque burdens according to methods described in sections 2.3 and 2.10. For intracerebroventricular injection of EGCG, a total of 6 female APP_{sw} mice from a B6/SJL background were used. At 12 months of age these mice were intracerebroventricularlly injected with EGCG (0.5 mg/kg; $n = 3$) or PBS vehicle ($n = 3$) once as described in section 2.2. 24 hours after injection, these mice were sacrificed for analysis of cerebral Aβ levels as described in section 2.3 and 2.10. For oral administration (water bottle) of EGCG, a total of 20 female APP_{sw} mice from a B6/SJL background were used. Beginning at 8 months of age, these mice were administered EGCG (50 mg/kg) in H_2O daily for 6 months ($n = 10$) or H_2O alone ($n = 10$). Similarly-aged NT mice ($n = 8$) also received H_2O alone. All mice were then sacrificed at 14 months of age for analyses of Aβ levels and plaque burdens as described in section 2.3 and 2.10. All behavioral testing for intraperitoneal and oral studies occurred during the final weeks proceeding sacrifice, with treatment being continued, as described in section 2.14.

3.3 Results

3.3.1 EGCG inhibits $A\beta_{1-40,42}$ generation from SweAPP N2a cells and Tg APP_{sw} mouse-derived primary neuronal cells

HPLC analysis of green tea shows that EGCG is the main polyphenolic constituent, although other compounds, including (-) EC, (+) EC, GC, and C, are present in relatively lesser quantities (Moyers and Kumar, 2004). To examine the effects of the polyphenolic constituents of green tea on APP metabolism, SweAPP N2a cells and primary neuronal cells derived from Tg APP_{sw} mice were first treated with a wide concentration range of each of these compounds for 12 hours and cultured media was subjected to ELISA analysis. As shown in Figure 3.1a and b, EGCG significantly reduced $A\beta_{1-40,42}$ generation in both SweAPP N2a cells and primary Tg APP_{sw}-derived neuronal cells in a concentration dependent manner. Importantly, EGCG (20 μM) reduced Aβ generation by 61% and 38% in SweAPP N2a cells and primary Tg APP_{sw}-derived neuronal cells by 38%, respectively (Figure 3.1a,b). It should be noted that both enantiomeric species of another green tea component, EC, inhibited Aβ generation by nearly 20–30% in both cell types, albeit at relatively high doses (Figure 3.1a,b). However, two other components of green tea, GC and C, modestly promoted Aβ production by ~20–30% and 10–15% in SweAPP N2a cells and primary Tg APP_{sw}-derived neuronal cells, respectively, at relatively high (80 μM) concentrations. To determine whether GC and/or C could oppose the inhibition of Aβ generation mediated by EGCG, SweAPP N2a cells were co-treated with EGCG (20 μM) and GC (80 μM), C (80 μM), or both for 12 hours and cultured media was subjected to ELISA analysis. As

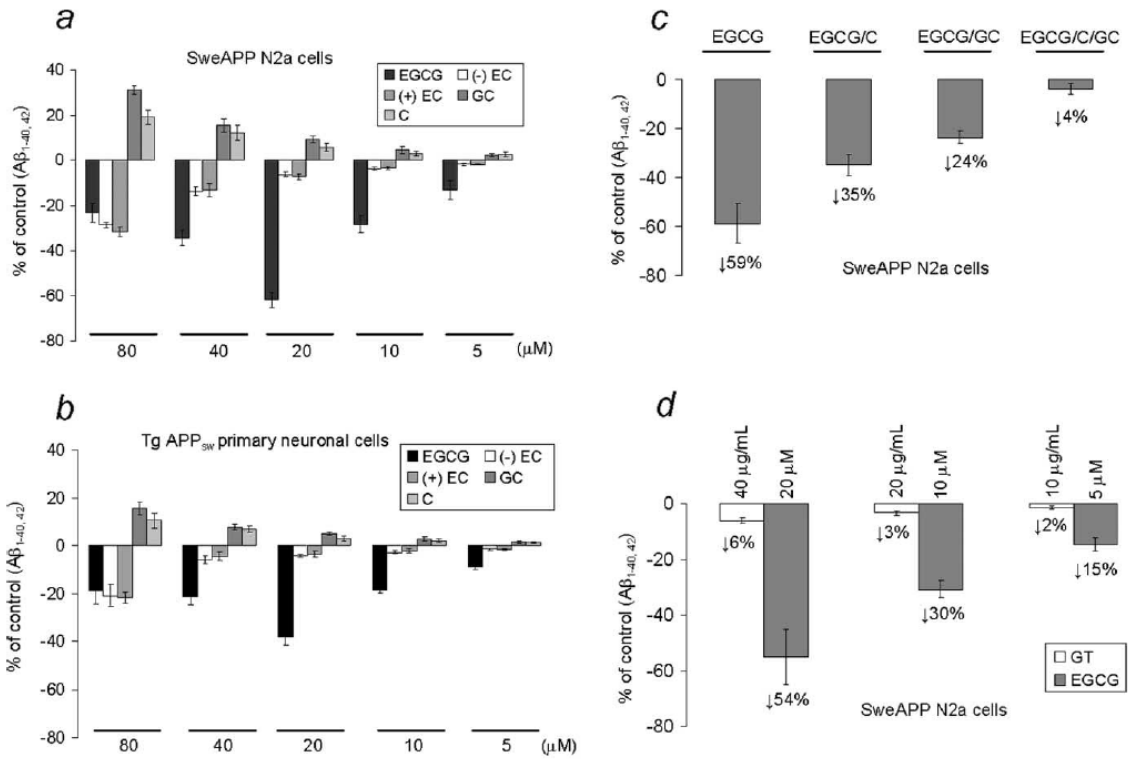

Figure 3.1

EGCG treatment inhibts Aβ generation in cultured neuronal cells. $A\beta_{1–40,42}$ peptides were analyzed in cultured media from SweAPP N2a cells (a, c, d) or $TgAPP_{sw}$ mouse-derived primary neuronal cells (b) by ELISA ($n = 3$ for each condition). Data are represented as a percentage of $A\beta_{1–40,42}$ peptides secreted 12 hours after EGCG treatment relative to control (untreated). a, b, One-way ANOVA followed by *post hoc* comparison revealed significant differences between EGCG and the other compounds at 40, 20, 10, and 5 μM treatment concentrations ($p < 0.001$). c, When comparing EGCG (20 μM) treatment with cotreatment of SweAPP N2a cells with EGCG (20 μM) plus GC (80 μM), C (80 μM), or GC/C, a significant difference was noted for each comparison ($p < 0.001$). d, SweAPP N2a cells were treated with EGCG at a comparable concentration with that found in GT (GT contains 30% EGCG), and a significant difference was noted between GT and EGCG treatments (40 μg/ml vs 20 μM; 20 μg/ml vs 10 μM; 10 μg/ml vs 5 μM) on inhibition of Aβ generation ($p < 0.001$ for each comparison). Reduction for each treatment condition is indicated for c and d.

expected, data show that the presence of GC or C, and particularly the combination of both, markedly inhibited the ability of EGCG to reduce Aβ generation from SweAPP N2a cells (Figure 3.1c). Thus, these data suggest that a purified preparation of EGCG may be more capable of reducing Aβ generation *in vitro* than when it is present in a mixture of whole green tea extract (GT). To further address this hypothesis, SweAPP N2a cells were incubated with various concentrations of EGCG alone and equivalent concentrations of EGCG that were contained in a mixture of GT in parallel. As shown in Figure 3.1d, data indicate that the various concentrations of EGCG alone elicited more profound effects on Aβ generation versus that contained in GT. Accordingly, the ability of the purified EGCG alone to inhibit Aβ generation appears to be much greater than that of GT.

3.3.2 EGCG activates non-amyloidogenic proteolysis of APP in SweAPP N2a cells

To elucidate the potential mechanism whereby green tea components modulate APP metabolism, SweAPP N2a cells were treated with a wide concentration range of EGCG, EC, GC, and C for 12 hours. Following western blot and immunoprecipitation analysis, lysates of EGCG treated cells evidenced significantly increased α-CTF generation and augmented α-CTF to β-CTF band density ratios (Figure 3.2a). In addition, these effects were appeared to be both time and concentration dependent (Figure 3.2c,d). In concert with these findings, sAPP-α, but not sAPP-β, was elevated in cultured media from EGCG treated (20 μM) SweAPP N2a cells (Figure 3.2b). Additionally, as shown in Figure 3.2e (-) EC treatment only increased α-CTF

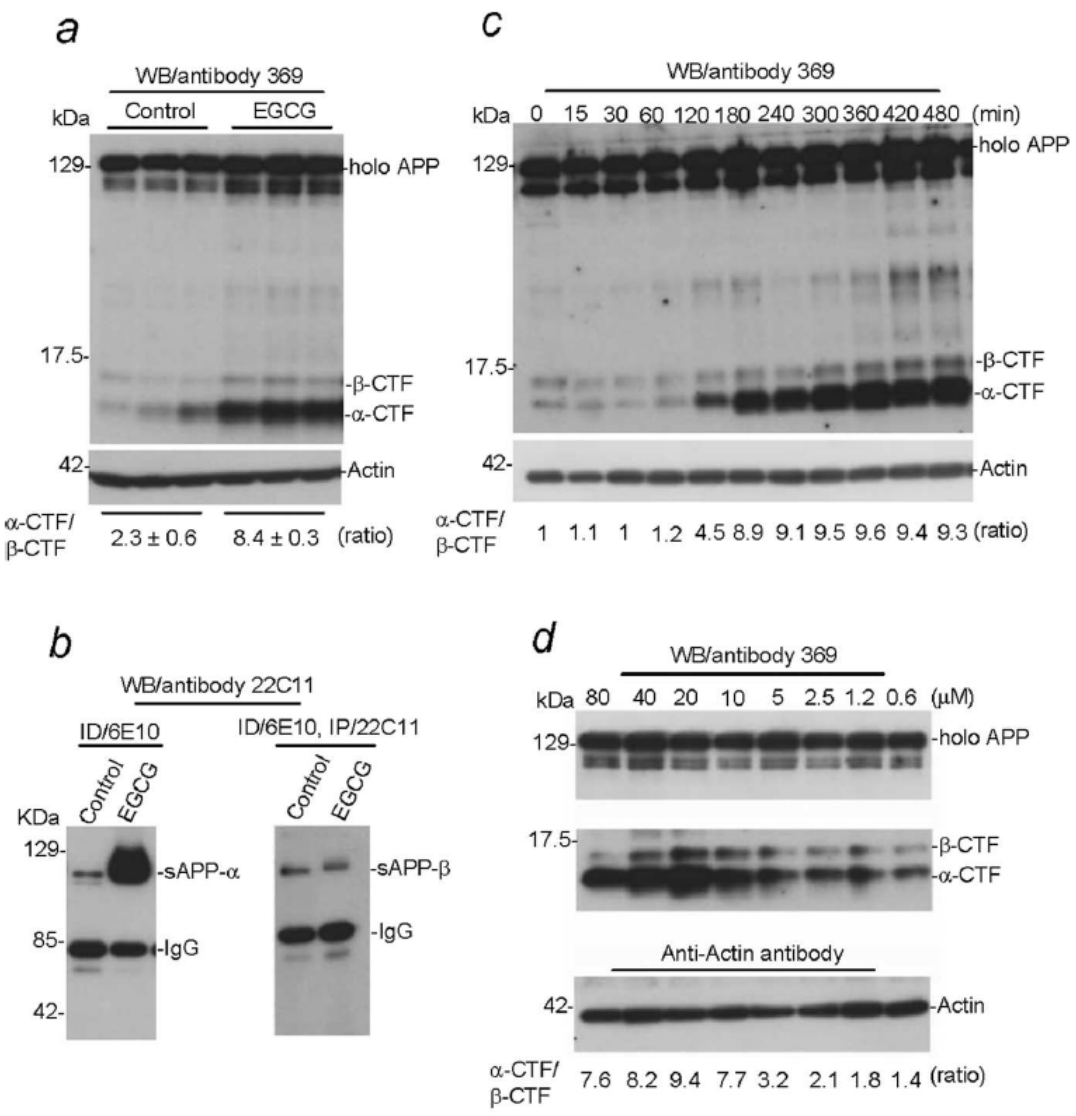

Figure 3.2a-d

EGCG treatment modulates APP metabolism *in vitro*. a, b, SweAPP N2 a cells were treated with EGCG at 20 μM or PBS (control) for 12 hours. a, Cell lysates were prepared and subjected to western blot (WB) analysis of APP CTFs, and b, cultured media were collected for immunoprecipitation (IP)/WB. c, d, Cell lysates were prepared from SweAPP N2a cells treated with EGCG at 20μM for times indicated (c) or concentrations indicated for 12 hours (d) and subjected to WB for APP CTFs. b, WB analysis using antibody 22C11 against the amino-terminus of APP shows sAPP-α (IP with antibody 6E10) and sAPP-β [following immunodepletion (ID) with 6E10 and subsequent IP with 22C11]. a, c, d, Densitometric analysis of the ratio of α-CTF to β-CTF are indicated below the figures. a, A *t* test revealed a significant difference between EGCG treatment and control ($n = 3$ for each condition; $p < 0.001$).

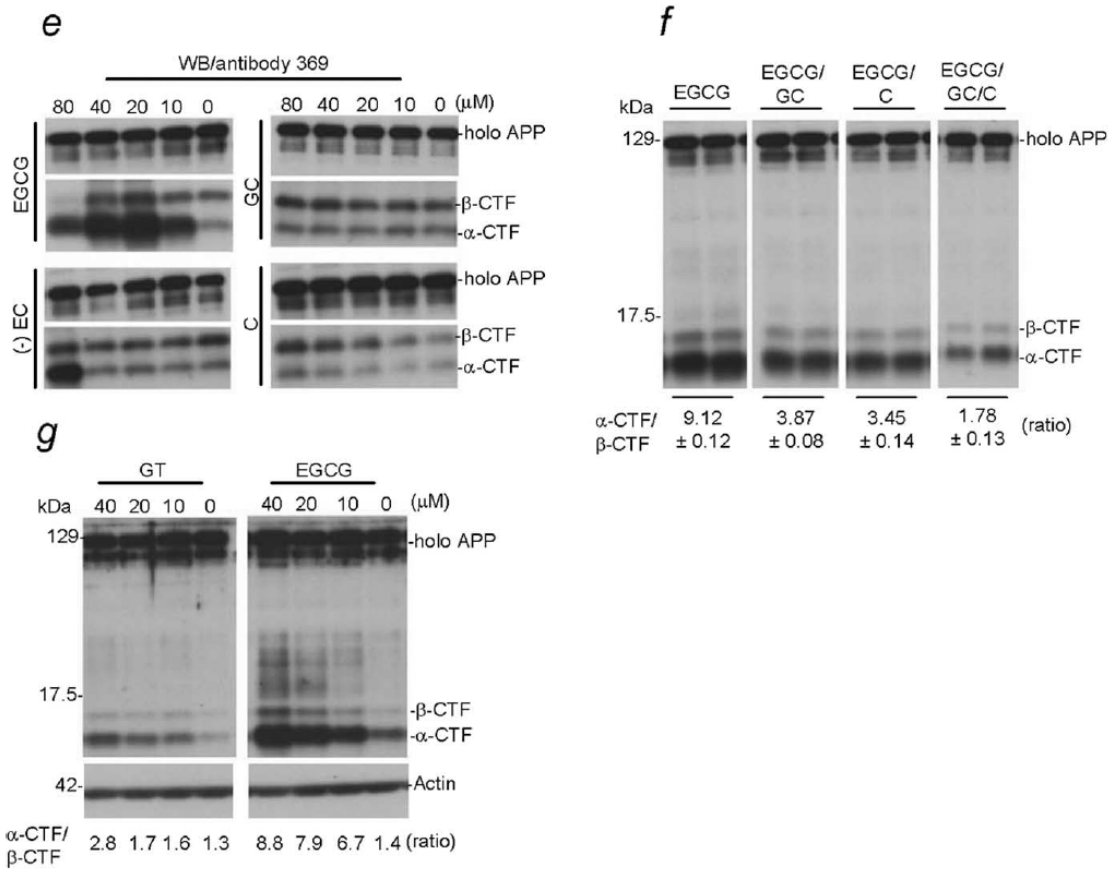

Figure 3.2e-g

Green tea flavonoids modulate APP metabolism *in vitro*. e, g, SweAPP N2a cells were treated with EGCG (-) EC, (+) EC, GC, C, or GT at concentrations indicated for 12 hours. f, SweAPP N2a cells were co-treated with EGCG (20 μM) and GC, C, or GC/C at 80 μM for 12 hours. e, f, g, Lysates were subjected to western blot (WB) analysis of APP CTFs. f, g, Densitometric analysis of the ratio of α-CTF to β-CTF are indicated below the figures. f, One-way ANOVA followed by *post hoc* comparison revealed significant between-groups differences ($p < 0.01$) with $n = 4$ for each condition, and *t* test revealed a significant difference between EGCG and EGCG/GC/C treatments ($p < 0.001$).

generation at a concentration of 80 μM (similar results were obtained with (+) EC; data not shown). Conversely, both GC and C treatment resulted in decreased α-CTF to β-CTF ratios at 80μM concentrations (Figure 3.2e). Interestingly, at this concentration, GC, C, or a GC/C combination significantly opposed the effect of EGCG (20 μM) on α-CTF generation (Figure 3.2f). In agreement with Aβ ELISA data as shown in Figure 3.1d, purified EGCG demonstrated a markedly superior effect on α-CTF generation versus equivalent amounts present in GT (Figure 2g). Taking into consideration the lack of any observable changes in full length holo APP expression after treatment, it is apparent that EGCG promoted α-CTF generation and sAPP-α release at the post-translational level, events which are indicative of non-amyloidogenic APP proteolysis.

3.3.3 EGCG promotes α-secretase activity in SweAPP N2a cells

As illustrated in Figure 3.2c, western blot analysis clearly shows a time dependent increase in α-CTF generation in EGCG-treated SweAPP N2a cells. Notably, α-CTF generation increased at ~3–4 hours through 8 hours after EGCG treatment. To confirm that the observed alterations in APP metabolism were attributable to enhanced α-secretase activity, the expression of TACE/ADAM17, an α-secretase candidate (Skovronsky et al., 2001; Allinson et al., 2003), was examined in SweAPP N2a cells following EGCG treatment. Western blot analysis of lysates revealed significant increases in TACE/ADAM17 expression ~2–4 hours after EGCG treatment, which was then rapidly degraded through 8 hours (Figure 3.3a). To evaluate whether this EGCG-mediated alteration in TACE expression correlated with α-secretase activity, we evaluated α, β, and γ-secretase activity in cell lysates prepared from EGCG treated SweAPP N2a cells

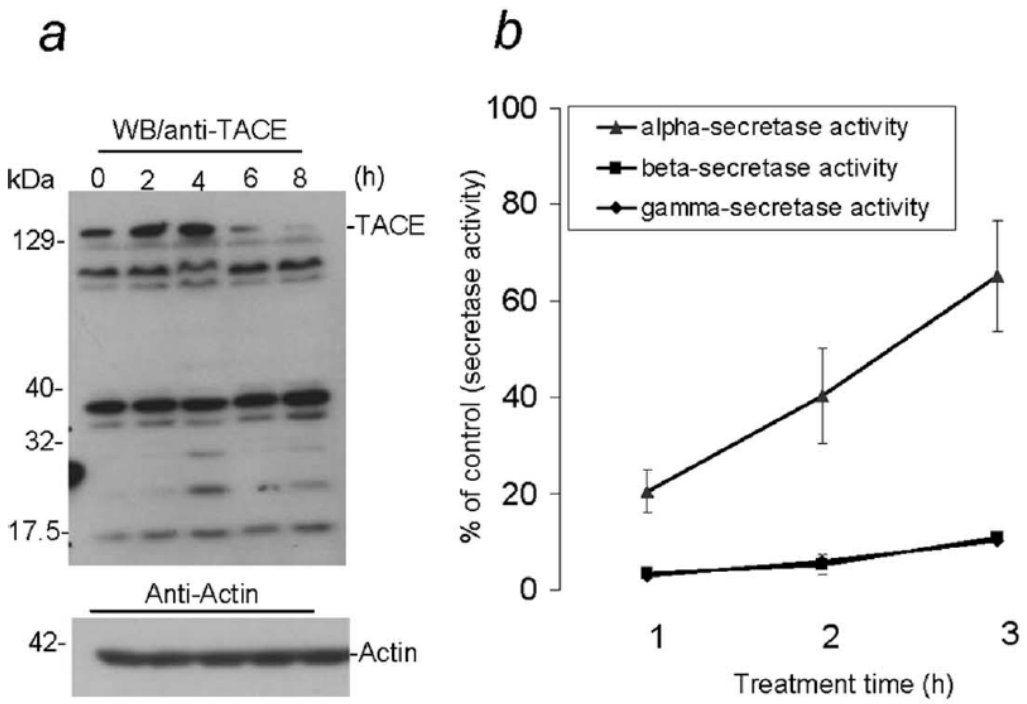

Figure 3.3a and b

EGCG treatment promotes α-secretase activity *in vitro*. a, b, Cell lysates were prepared from SweAPP N2a cells treated with EGCG (20μM) for different time points as indicated. a, Western blot analysis by anti-TACE antibody shows TACE/ADAM17 and cleaved fragments. b, α-, β -, and γ-secretase activities were analyzed in cell lysates using secretase activity assay. Data are presented as a percentage of fluorescence units/milligrams protein activated 1, 2, or 3 hours after EGCG treatment relative to control (PBS). A *t* test revealed a significant difference between α-secretase and either β- or γ-secretase cleavage activity at 1, 2, and 3 hours after EGCG treatment ($p < 0.001$) with $n = 3$ for each condition.

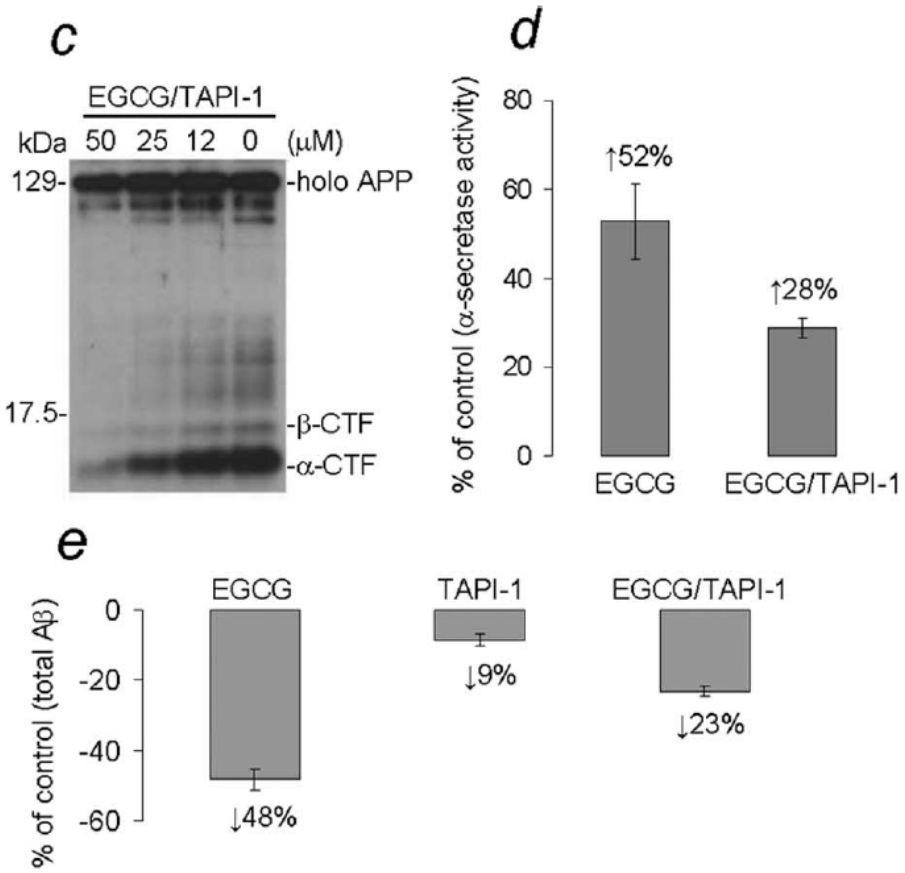

Figure 3.3c-e

EGCG effects are attenuated by an inhibitor of a putative α-secretase *in vitro*. c–e, SweAPP N2a cells were treated with EGCG (20 μM) or PBS (control) in the presence or absence of TAPI-1 at various concentrations (c) or at 25 μM (d, e) for 4 hours. Cell cultured supernatants were collected, and cell lysates were prepared from cultured cells. c, Lysates were subjected to western blot analysis of APP CTFs. d, Data are represented as percentage of α-secretase activity calculated in terms of fluorescence units/milligrams protein. A *t* test revealed a significant difference between EGCG treatment and co-treatment with EGCG and TAPI-1 ($p < 0.001$); increased levels of activity are indicated. e, Data are presented as percentage of Aβ secretion relative to PBS control 4 hours after EGCG treatment in the presence or absence of TAPI-1. A *t* test revealed a significant difference between EGCG and EGCG/TAPI-1 treatment ($p < 0.001$); reduction for each treatment condition ($n = 3$) is indicated.

by fluorometic assay. As indicated by Figure 3.3b, only α-secretase activity was significantly elevated during the first 3 hours following EGCG treatment of SweAPP N2a cells. To further confirm this putative α-secretase role in this mechanism, SweAPP N2a cells were co-treated with EGCG and the TACE/ADAM17 inhibitor TAPI-1 (Slack et al., 2001) for 4 hours. Following western blot and ELISA analysis, lysates and media from TAPI-1 co-treated cells evidenced both significantly diminished α-secretase activity and α-CTF generation (Figure 3.3c,d). Consistent with these findings, EGCG-mediated reductions of soluble Aβ were also decreased by half (Figure 3.3e). Together, these data suggest that elevation of TACE/ADAM17 activation in response to EGCG treatment may be partly responsible for increased α-secretase activity in SweAPP N2a cells.

3.3.4 EGCG treatment enhances ADAM10 activation in cultured CNS cells

To determine whether EGCG invariably modulates the expression of all of the potential candidate α-secretases (ADAM9, -10, or -17), SweAPP N2a cells were treated with various concentrations of EGCG for 8 hours and lysates were subjected to western blot analysis. Interestingly, mature ADAM10 (~60 kDa isoform), but not ADAM9 or TACE/ADAM17, concentration dependently increased in response to EGCG treatment (Figure 3.4a). To investigate if EGCG treatment may affect mRNA expression of ADAM10 across the time frame examined above, total RNA from cells treated in parallel was isolated for RT-PCR analysis. However, no significant differences in ADAM10 mRNA levels between EGCG concentrations were detectable (Figure 3.4b). Temporal

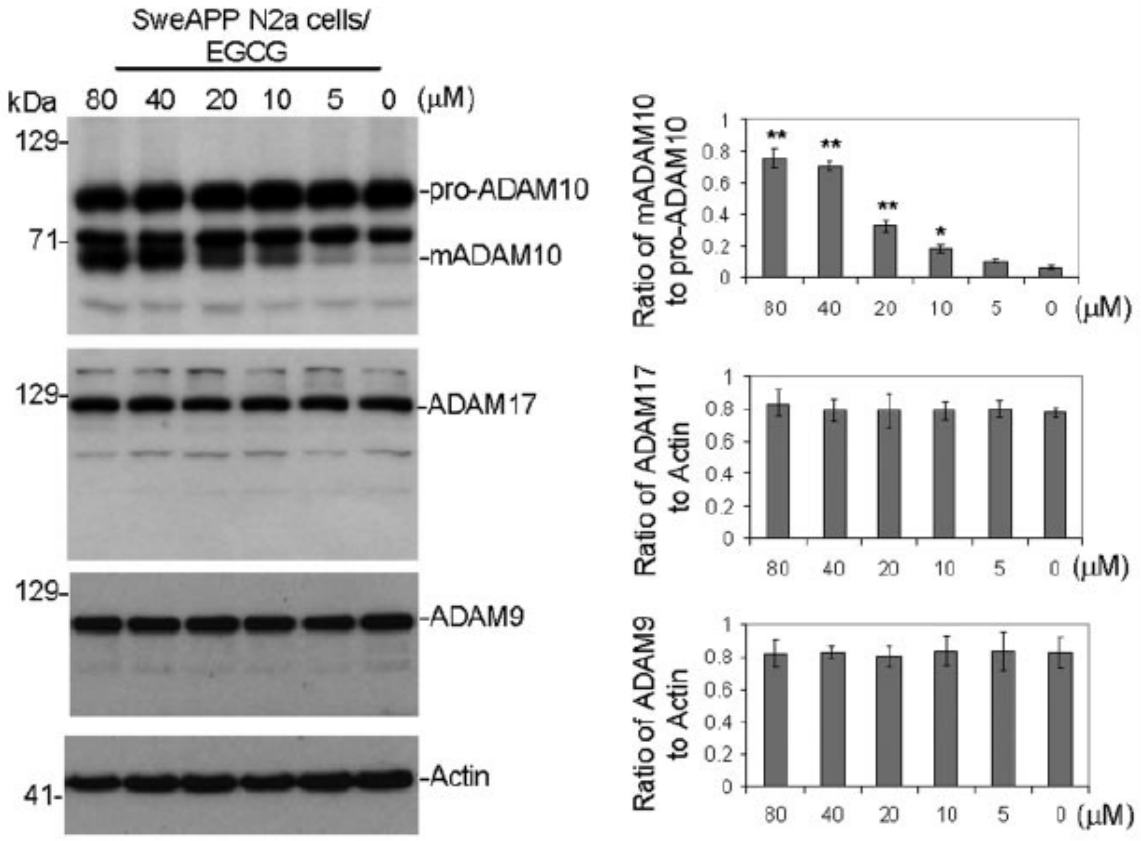

Figure 3.4a

EGCG enhances ADAM10 activation in SweAPP N2a cells. Expression of ADAM9, -10, and -17 was analyzed in cell lysates from SweAPP N2a cells treated with EGCG at the various concentrations indicated for 8 hours by western blot. Densitometric analysis reveals the band density ratio of the mature (mADAM10) to the pro (pro-ADAM10) form of ADAM10 or the band density ratio of ADAM9 or -17 to actin as indicated in panels to the right. One-way ANOVA revealed significant differences between EGCG-treated cells and control cultures on the ratio of mADAM10 to pro-ADAM10 (**, $p < 0.001$; *, $p < 0.05$), but no significant differences were noted for the ratios of ADAM9 or -17 to Actin ($p > 0.05$) with $n = 3$ for each condition.

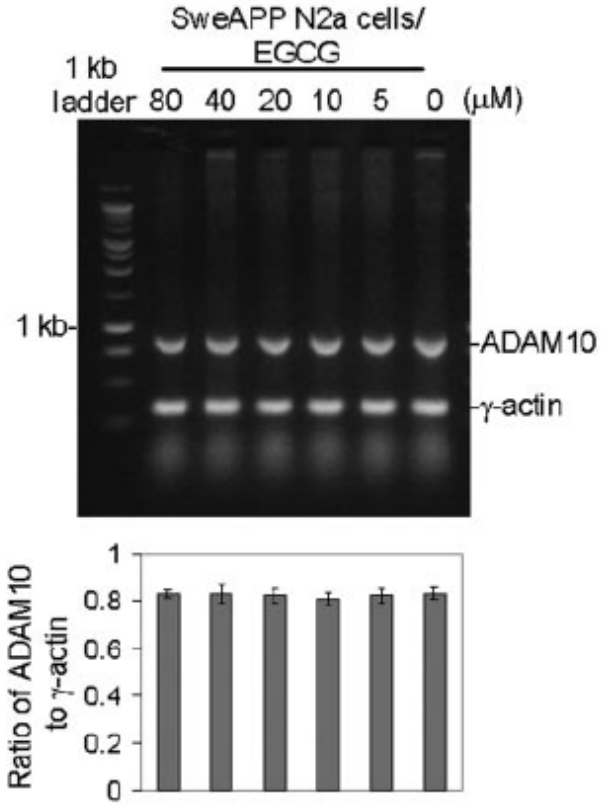

Figure 3.4b

EGCG does not alter ADAM10 mRNA levels in SweAPP N2a cells. ADAM10 mRNA level was analyzed in SweAPP N2a cells treated with EGCG at the various doses indicated for 8 hours by RT-PCR. Densitometric analysis reveals the band density ratio of ADAM10 to γ-actin as indicated below. One-way ANOVA revealed no significant differences between EGCG treated cells and control cultures on the ratio of ADAM10 to γ-actin ($p > 0.05$) with $n = 2$ for each condition.

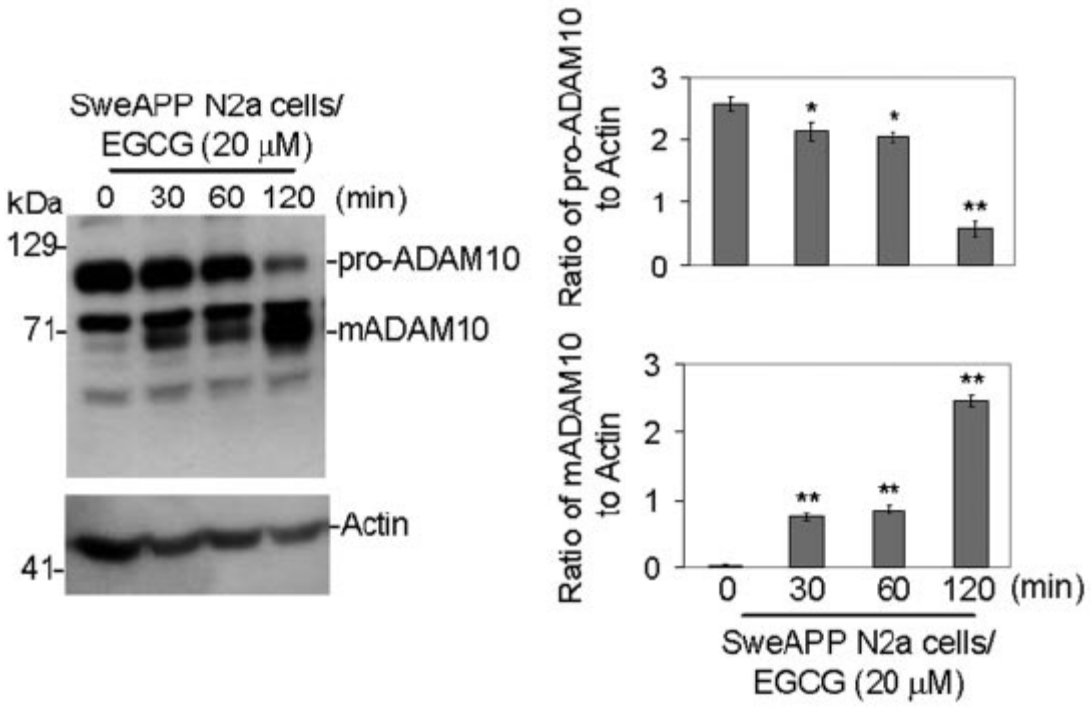

Figure 3.4c

EGCG enhances ADAM10 maturation in SweAPP N2a cells. Cell lysates were prepared from SweAPP N2a cells treated with EGCG (20 μM) for 0, 30, 60, or 120 minutes and subjected to western blot for ADAM10. Densitometric analysis reveals the band density ratios of pro-ADAM10 to actin and mADAM10 to Actin as indicated in the panels to the right. One-way ANOVA revealed significant time point differences (**, $p < 0.001$; *, $p < 0.05$) with $n = 3$ for each condition.

analysis showed significant increases in mature ADAM10 as early as 30 minutes following treatment with EGCG (20 μM) (Figure 3.4c), an effect that continued to increase through to 2 hours after EGCG challenge. However, no such similar significant effects of EGCG treatment on ADAM9 or -17 were noted (data not shown). In addition, EGCG also concentration dependently increased ADAM10 maturation in two separate cell types, parental (non-transfected) N2a cells and N9 microglial cells. Relative to N9 microglia, the neuron-like parental N2a cell line demonstrated increased sensitivity to EGCG treatment (Figure 3.5a). Similar to N2a and N9 cell lines, primary murine neuronal and microglial cultures also displayed concentration dependent increases in mature ADAM10 in response to EGCG treatment (Figure 3.5b), with primary neurons showing increased sensitivity to the lower concentrations (10 and 20 μM) of EGCG.

3.3.5 EGCG-mediated maturation of ADAM10 correlates with α-secretase activity in SweAPP N2a cells

To confirm that EGCG-mediated concentration dependent increases in mature ADAM10 result in modulation of APP metabolism, SweAPP N2a cells were treated with various concentrations of EGCG for 8 hours. APP metabolism and ADAM10 maturation were then analyzed in parallel. Western blot analysis of lysates and cultured media revealed concentration dependent increases in α-CTF generation and sAPP-α release with corresponding increases in mature ADAM10 in response to EGCG treatment (Figure 3.6a-c). In concert with these findings, concentration dependent reductions in $A\beta_{1-40}$ and

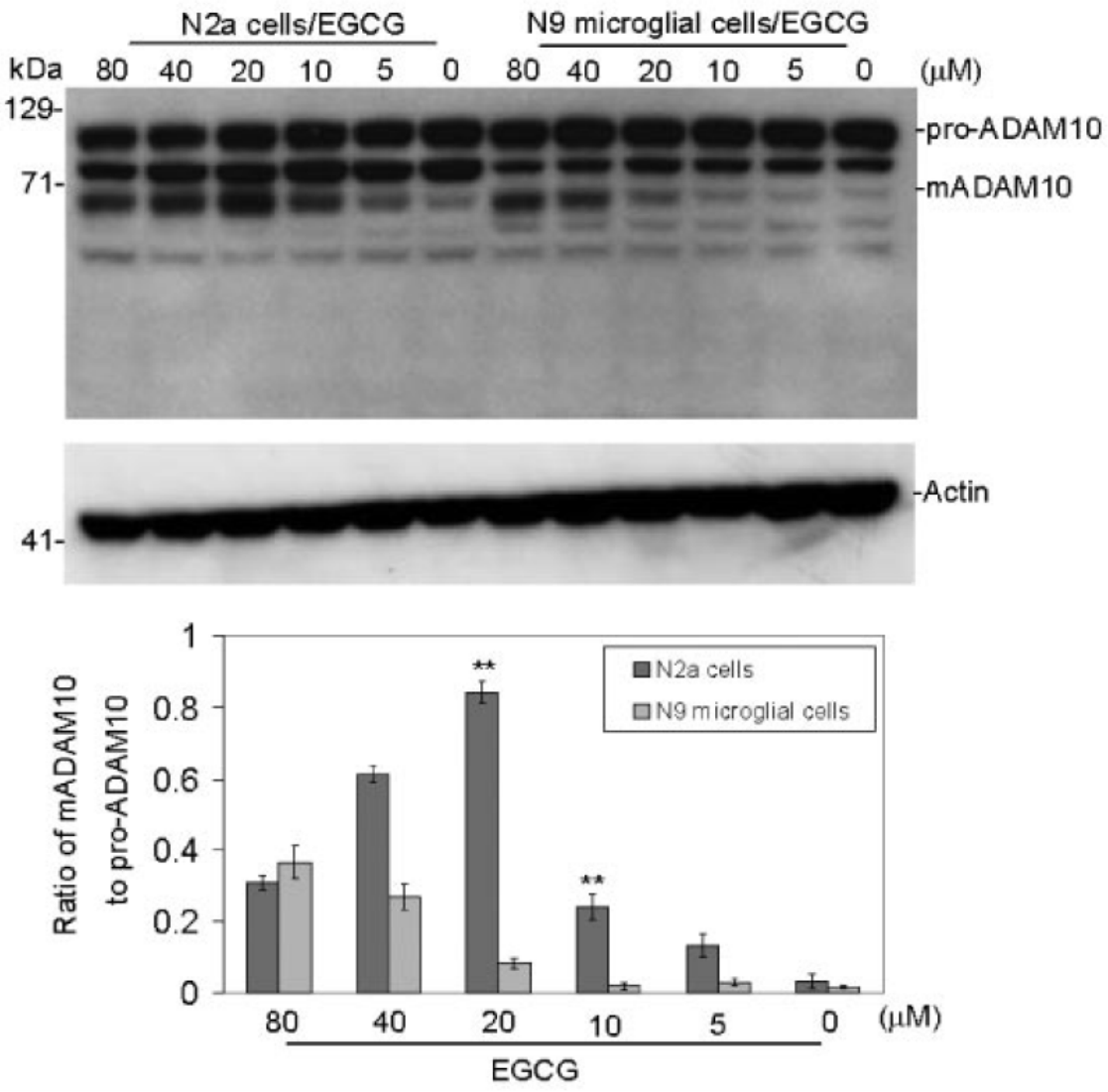

Figure 3.5a

EGCG treatment enhances ADAM10 activation in both N2a and N9 cells. Cell lysates were prepared from N2a cells or N9 microglial cells that were treated with EGCG at various concentrations indicated for 8 hours and subjected to western blot for ADAM10. Densitometric analysis reveals the band density ratio of mADAM10 to pro-ADAM10 as indicated below. One-way ANOVA followed by *post hoc* analysis revealed significant differences between N2a and N9 cells treated with EGCG at 10 and 20 μM (**, $p < 0.001$) with $n = 3$ for each condition.

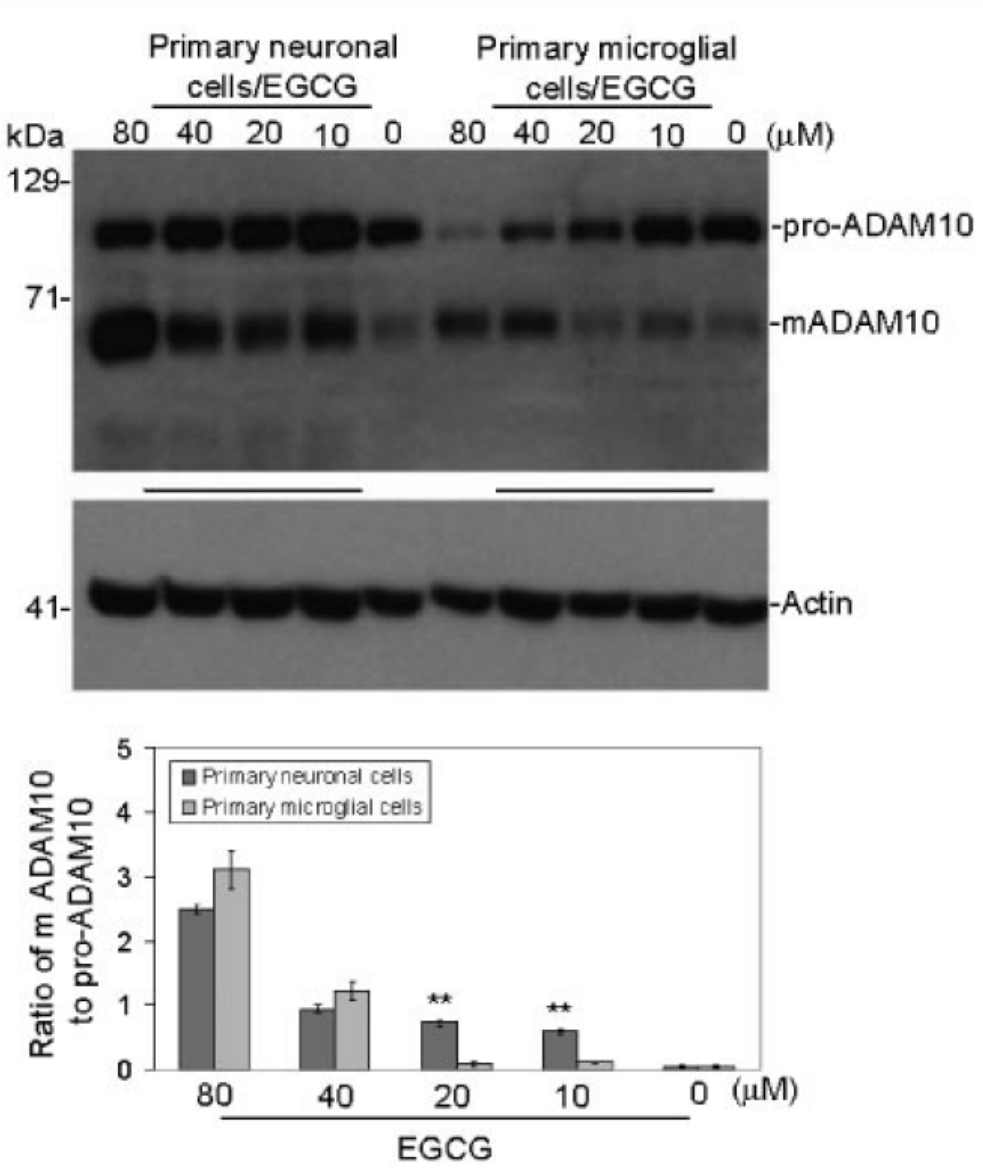

Figure 3.5b

EGCG treatment enhances ADAM10 activation in both cultured primary neuronal and microglial cells. Cell lysates were prepared wild-type mouse-derived primary neuronal or microglial cells that were treated with EGCG at various concentrations indicated for 8 hours and subjected to western blot for ADAM10. Densitometric analysis reveals the band density ratio of mADAM10 to pro-ADAM10 as indicated below. One-way ANOVA followed by *post hoc* analysis revealed significant differences between primary neuronal and microglial cells treated with EGCG at 10 and 20 μM (**, $p < 0.001$) with $n = 3$ for each condition.

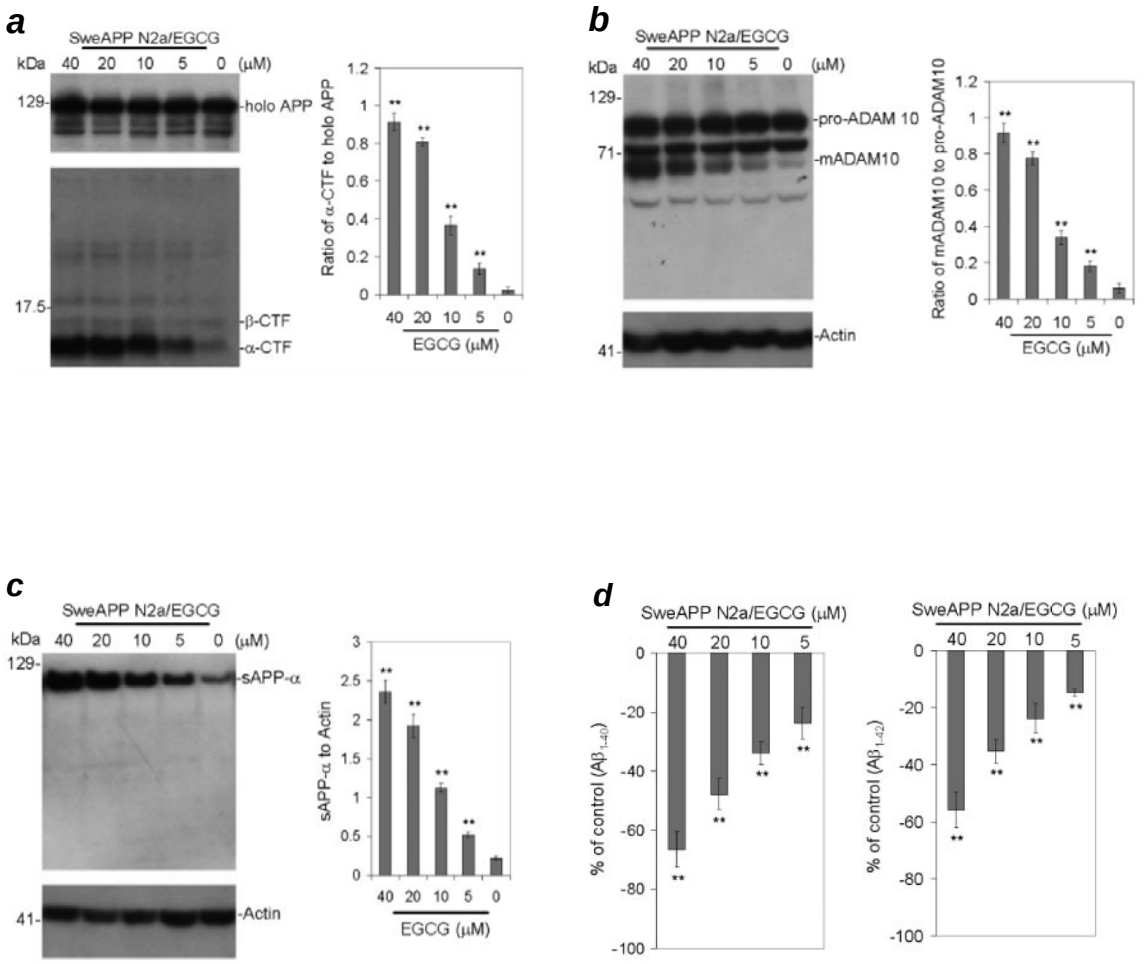

Figure 3.6a-d

EGCG-mediated maturation of ADAM10 correlates with α-secretase activity in SweAPP N2a cells. SweAPP N2a cells were treated with EGCG at concentrations indicated for 8 hours. a, b, Lysates were subject to western blot for APP CTFs and ADAM10. c, d, Cell cultured media was subjected to western blot for sAPP-α or ELISA for Aβ. As indicated in panels to the right, densitometry analysis shows the band density ratio of α-CTF to full-length APP (holo APP) (a) or mADAM10 to pro-ADAM10 (b). One-way ANOVA revealed significant EGCG concentration differences on both ratios of α-CTF to holo-APP and mADAM10 to pro-ADAM10 (**, $p < 0.001$) with n = 3 for each condition. c, d, Data are represented as % change relative to control (medium from cultured SweAPP N2a cells without any treatment). One-way ANOVA revealed significant EGCG dose differences in both ratios of sAPP-α to Actin (**, $p < 0.001$) and reduction of $A\beta_{1-40}$ and $A\beta_{1-42}$ (*, $p < 0.05$; **, $p < 0.001$) with $n = 3$ for each condition.

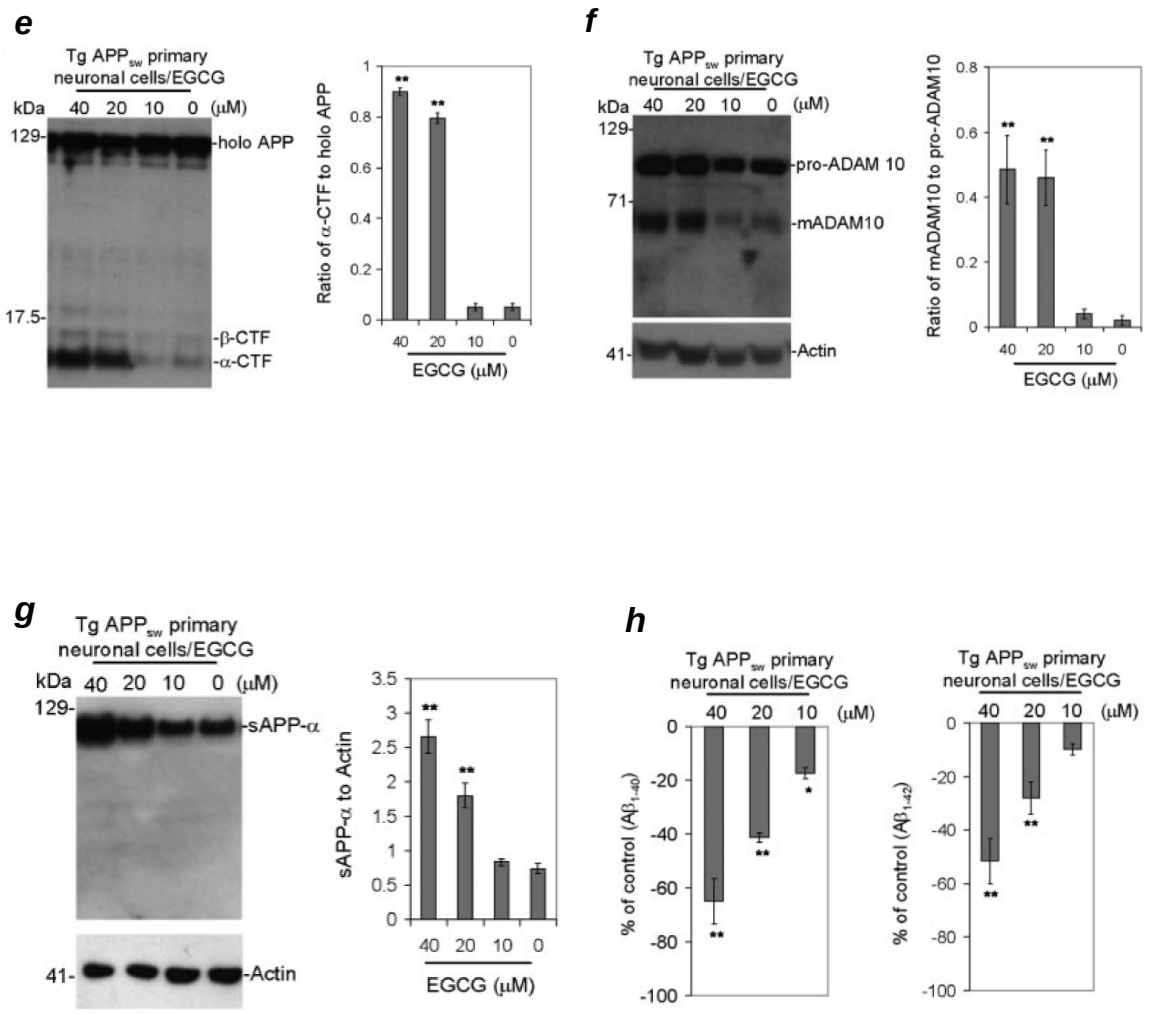

Figure 3.6e-h

EGCG-mediated maturation of ADAM10 correlates with α-secretase activity Tg APP_{sw} primary neuronal cells. Tg APP_{sw} mouse-derived primary neuronal cells were treated with EGCG at concentrations indicated for 8 hours. e, f, Lysates were subject to western blot for APP CTFs and ADAM10. g, h, Cell cultured media was subjected to western blot for sAPP-α or ELISA for Aβ. As indicated in panels to the right, densitometry analysis shows the band density ratio of α-CTF to full-length APP (holo APP) (e) or mADAM10 to pro-ADAM10 (f). One-way ANOVA revealed significant EGCG dose differences on both ratios of α-CTF to holo-APP and mADAM10 to pro-ADAM10 (**, $p < 0.001$) with n = 3 for each condition. g, h, Data are represented as % change relative to control (medium from cultured Tg APP_{sw} derived primary neuronal cells without any treatment). One-way ANOVA revealed significant EGCG dose differences in both ratios of sAPP-α to Actin (**, $p < 0.001$) and reduction of $A\beta_{1–40}$ and $A\beta_{1–42}$ (*, $p < 0.05$; **, $p < 0.001$) with $n = 3$ for each condition.

$A\beta_{1-42}$ after EGCG treatment were evident (Figure 3.6d), not only confirming that EGCG promotes non-amyloidogenic APP proteolysis, but also that this effect correlates with increased ADAM10 maturation. Accordingly, primary Tg APP_{sw}-derived neuronal cells were also analyzed for changes in APP metabolism in response to EGCG treatment. Western blot analysis again revealed EGCG-mediated the promotion of non-amyloidogenic proteolysis, as indicated by α-CTF to holo-APP ratios (Figure 3.6e). Similar to data observed in SweAPP N2a cells, α-secretase activity positively correlated with both mature ADAM10 levels and with secreted sAPP-α (Figure 3.6f,g) in these cells. Importantly, these findings were again consistent with concentration dependent reductions in Aβ levels following EGCG treatment (Figure 3.6h).

3.3.6 ADAM10 is required for EGCG-mediated non-amyloidogenic proteolysis of APP

To directly examine whether ADAM10 α-secretase activity was required for EGCG promotion of non-amyloidogenic proteolysis, siRNA knockdown experiments targeting ADAM9, -10, or -17 were conducted. First, to confirm siRNA knockdown efficiency, SweAPP N2a cells were treated with ADAM9, -10, or -17 siRNAs and subjected to western blot analysis. As shown in Figure 3.7a-c protein expression levels of ADAM10, -9, or -17 were significantly inhibited by respective ADAM-specific siRNAs. In addition, to test the specificity of siRNA against ADAM10 versus ADAM9 or -17, the expression of ADAM9 and -17 was analyzed from the cell lysates derived from siRNA knockdown for ADAM10 by western blot. Lysates revealed that ADAM10 siRNA did

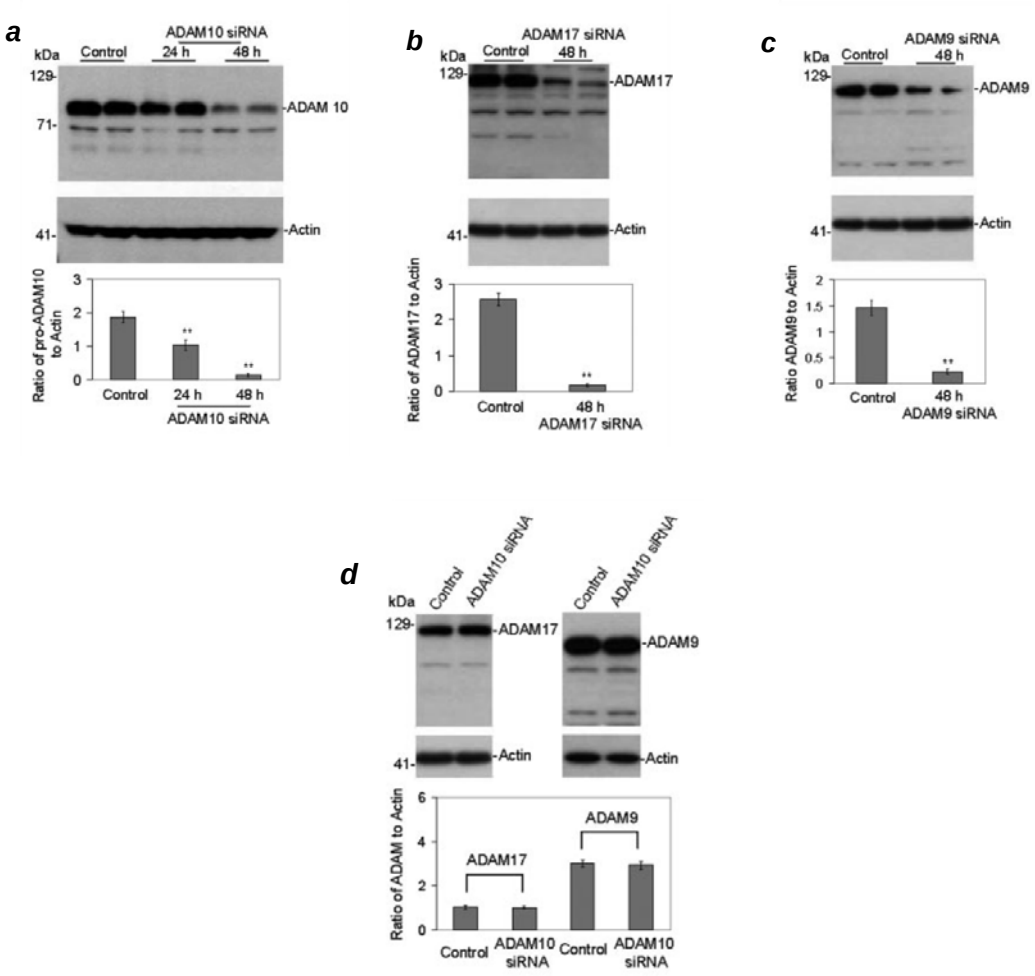

Figure 3.7

siRNA knockdown efficiency for ADAM10, -9, or -17. Expression of ADAM10 (a), -17 (b), or -9 (c) was analyzed by western blot in cell lysates from SweAPP N2a cells transfected with siRNA targeting ADAM10, -9, or -17 at 48 hours after transfection. Densitometric analysis reveals the band density ratios of pro-ADAM10, ADAM17, and ADAM9 to Actin as indicated in the panels below. One-way ANOVA revealed significant differences between siRNA-transfected cells and control cultures on the ratio of ADAMs to Actin (**, $p > 0.001$) with n = 3 for each condition. d, expression of ADAM9 or -17 was analyzed by western blot in cell lysates from SweAPP N2a cells transfected with siRNA targeting ADAM10 at 48 hours after transfection. Densitometric analysis reveals the band density ratios of pro-ADAM17 to Actin or ADAM10 to Actin as indicated in the panel below. A *t* test revealed no significant differences between siRNA-transfected cells and control cultures on the ratio of ADAM9 or ADAM17 to Actin ($p > 0.05$) with $n = 3$ for each condition.

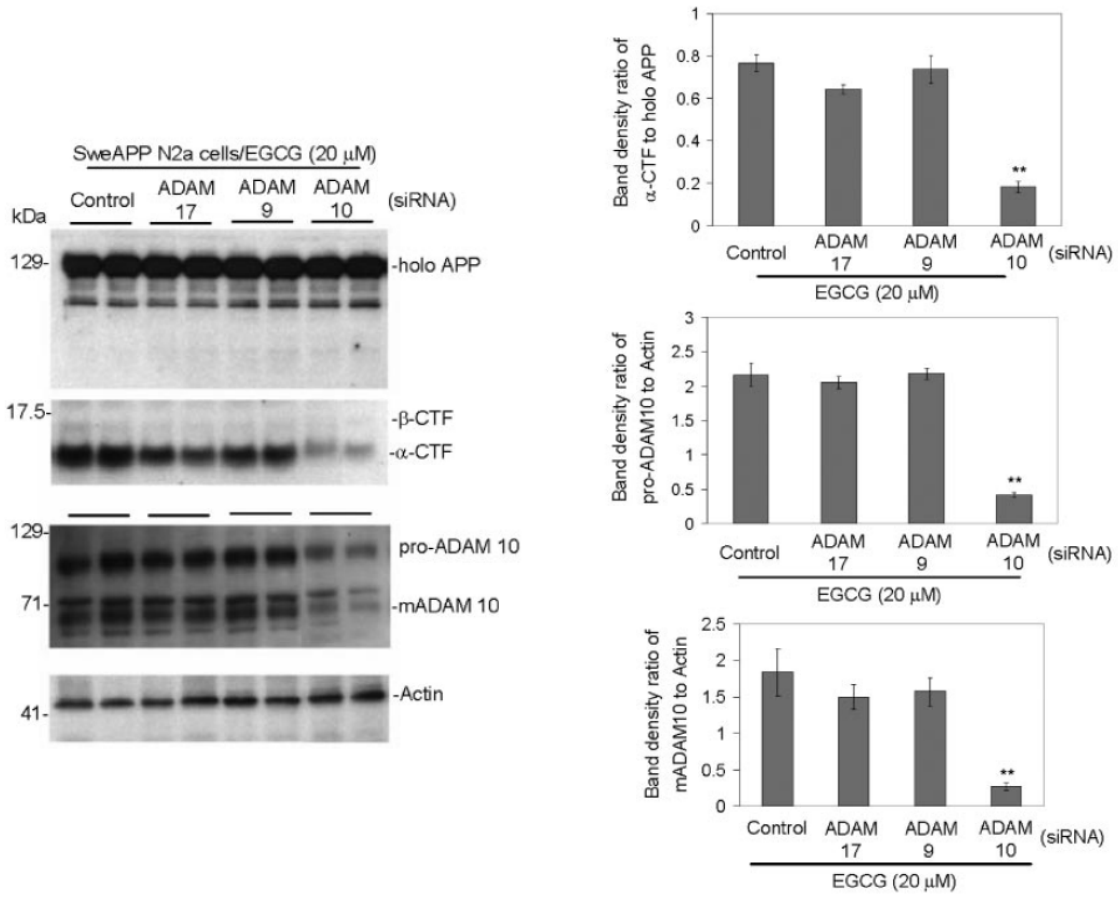

Figure 3.8a

ADAM10 is required for EGCG-mediated non-amyloidogenic proteolysis of APP. Cell lysates were prepared and collected from SweAPP N2a cells transfected with ADAM9, -10, or -17 siRNA or non-targeting siRNA control (siRNA control) for 48 hous and then treated with EGCG (20 μM) for 8 hours. Cell lysates were subjected to western blot for APP CTFs and ADAM10. Densitometric analysis reveals the band density ratios of α-CTF to holo-APP (upper right panel), pro-ADAM10 to Actin (middle right panel), or mADAM10 to Actin (lower right panel) as indicated. A *t* test revealed a significant difference between ADAM10 siRNA and ADAM9 or ADAM17 siRNA or siRNA control (**, $p < 0.001$) on the ratios of α-CTF to holo-APP, pro-ADAM10 to Actin, or mADAM10 to Actin with $n = 3$ for each condition.

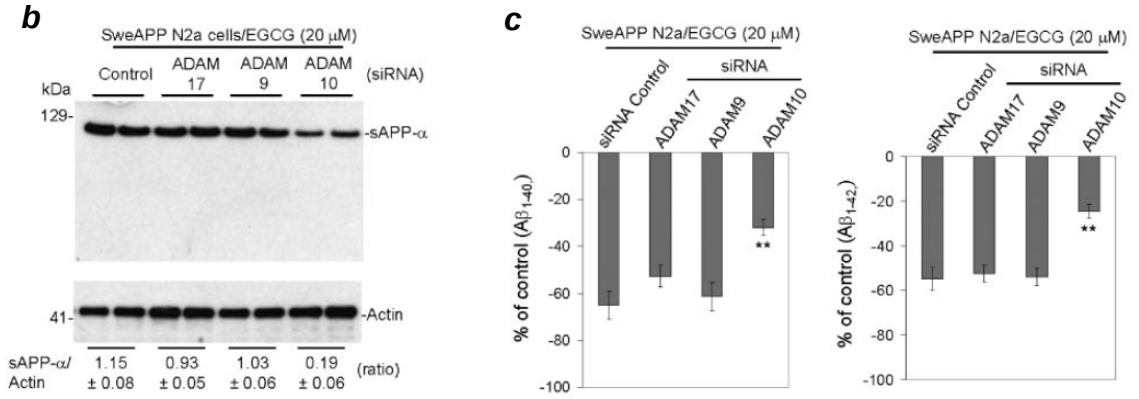

Figure 3.8b and c

ADAM10 is required for EGCG-mediated non-amyloidogenic proteolysis of APP and reduction of Aβ generation. b, c, conditioned media were prepared and collected from SweAPP N2a cells transfected with ADAM9, -10, or -17 siRNA or non-targeting siRNA control (siRNA control) for 48 h and then treated with EGCG (20 μM) for 8 hours. Cell cultured media were subjected to western blot for sAPP-α release (b) or ELISA for Aβ (c). Densitometric analysis reveals the band density ratios of sAPP-α to Actin as indicated below. A *t* test revealed a significant difference between ADAM10 siRNA and ADAM9 or ADAM17 siRNA or siRNA control (**, $p < 0.001$) on the reduction of sAPP-α and Aβ species as indicated with $n = 3$ for each condition.

not alter the expression of ADAM9 or -17 (Figure 3.7d). Subsequently, α-CTF production in APPsw N2a cells subjected to siRNA knockdown of ADAMs following treatment with EGCG (20 μM) was analyzed by western blot. As illustrated by Figure 3.8a and b, only ADAM10 siRNA was able to both clearly inhibit the expression of ADAM10 and block EGCG-induced α-CTF generation and sAPP-α release. This effect of ADAM10 siRNA on blocking EGCG-induced non-amyloidogenic APP proteolysis was further borne out by ELISA analysis, where only ADAM10 siRNA attenuated EGCG-induced reduction of $A\beta_{1-40}$ and $A\beta_{1-42}$ (Figure 3.8c). Taken together, these data demonstrate the requirement of ADAM10 for EGCG-mediated promotion of non-amyloidogenic proteolysis of APP

3.3.7 PI3K signaling is involved in EGCG-mediated α-secretase activity.

To further establish the mechanism whereby EGCG promotes ADAM10 maturation and non-amyloidogenic proteolysis of APP, a variety of signaling proteins and second messenger systems were investigated for their potential importance. SweAPP N2a cells were first co-treated with various signaling inhibitors in the presence of 20 μM EGCG for 12 hours and cultured media was subjected to ELISA analysis. In the context of EGCG (20 μM), the PI3K inhibitor wortmannin concentration dependently reduced sAPP-α release with an estimated IC_{50} of 20 μM (Figure 3.9a). To confirm this inhibition of EGCG-mediated non-amyloidogenic proteolysis, SweAPP N2a cells were again co-treated with a range of concentrations of wortamanin in presence of EGCG for 8

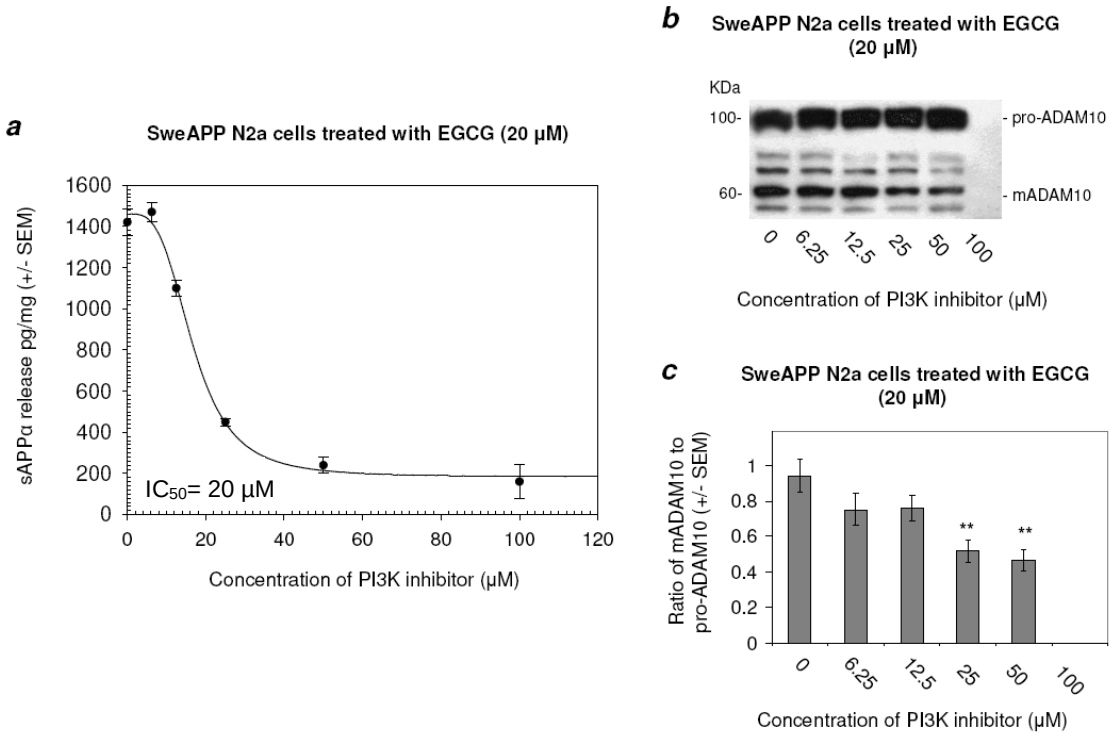

Figure 3.9a-c

PI3K signaling is involved in EGCG-mediated α-secretase activity. a, Levels of sAPP-α release were analyzed in cultured media from SweAPP N2a cells treated with EGCG (20 µM) in the presence of a PI3K inhibitor (wortmannin) at concentrations indicated for 12 hour by ELISA. b,c, ADAM10 expression was analyzed in lysates from SweAPP N2a cells treated with EGCG (20 µM) in the presence of a PI3K inhibitor (wortmannin) at concentrations indicated for 8 hours by western blot. c, Densitometric analysis shows the band density ratio of the mature (mADAM10) to the pro (pro-ADAM10) form of ADAM10. One-way ANOVA followed by *post hoc* analysis revealed significant differences between between wortmannin treated cells and control (**, $p < 0.005$) with $n = 3$ for each condition.

hours and lysates were subjected to western blot analysis. As expected, wortmannin treatment significantly inhibited EGCG-mediated ADAM10 maturation (Figure 3.9b,c). As depicted in Figure 3.9a-c, a concentration dependent trend is noticeable, even though there is obvious cellular toxicity following co-treatment at concentrations of 100 μM. Importantly, given the lack of any detectable cytotoxicity of wortmannin at concentrations below 100 μM (by protein levels and LDH release; data not shown), it may be fair to conclude that these effects are not mediated by cell death. Interestingly, following western blot analysis of lysates from SweAPP N2a cells treated with a range of concentrations of EGCG, a significant increase in phosphorylated p85 binding motifs on a high molecular weight species (~100 kDa) is evident (Figure 3.9e,d). Therefore, when considering the above data, it is apparent that ADAM10 maturation involves or even is potentially dependent upon PI3K signaling.

3.3.8 EGCG treatment enhances furin activation in SweAPP N2a cells

To determine whether EGCG modulates expression of potential proprotein convertases upstream of ADAM10, APP_{sw} N2a cells were treated with various concentrations of EGCG for 4 hours and lysates were subjected to western blot analysis. Expression of furin, but neither isoform of PC7, concentration dependently increased in response to EGCG treatment (Figure 3.10a-d). Notably, both the pro-form (~108 kDa) and mature (~96 kDa) form of furin significantly increase, which suggests that EGCG may be acting at the level of transcription. However, to rule out the role of PI3K in the

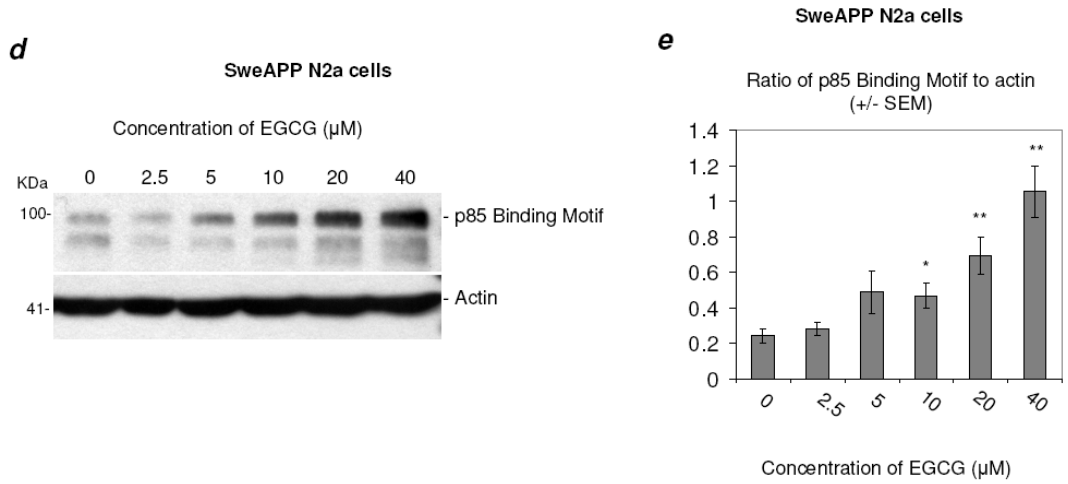

Figure 3.9d and e

EGCG enhances PI3K signaling in SweAPP N2a cells. d, Expression of phosphorylated p85 binding motifs was analyzed in lysates from SweAPP N2a cells treated with EGCG at concentrations indicated for 4 hours by western blot. e, Densitometric analysis reveals the band density ratio of p85 binding motifs to Actin. One-way ANOVA followed by *post hoc* analysis revealed significant differences between EGCG treatments and control (*, $p < 0.05$; **, $p < 0.005$) with $n = 3$ for each condition.

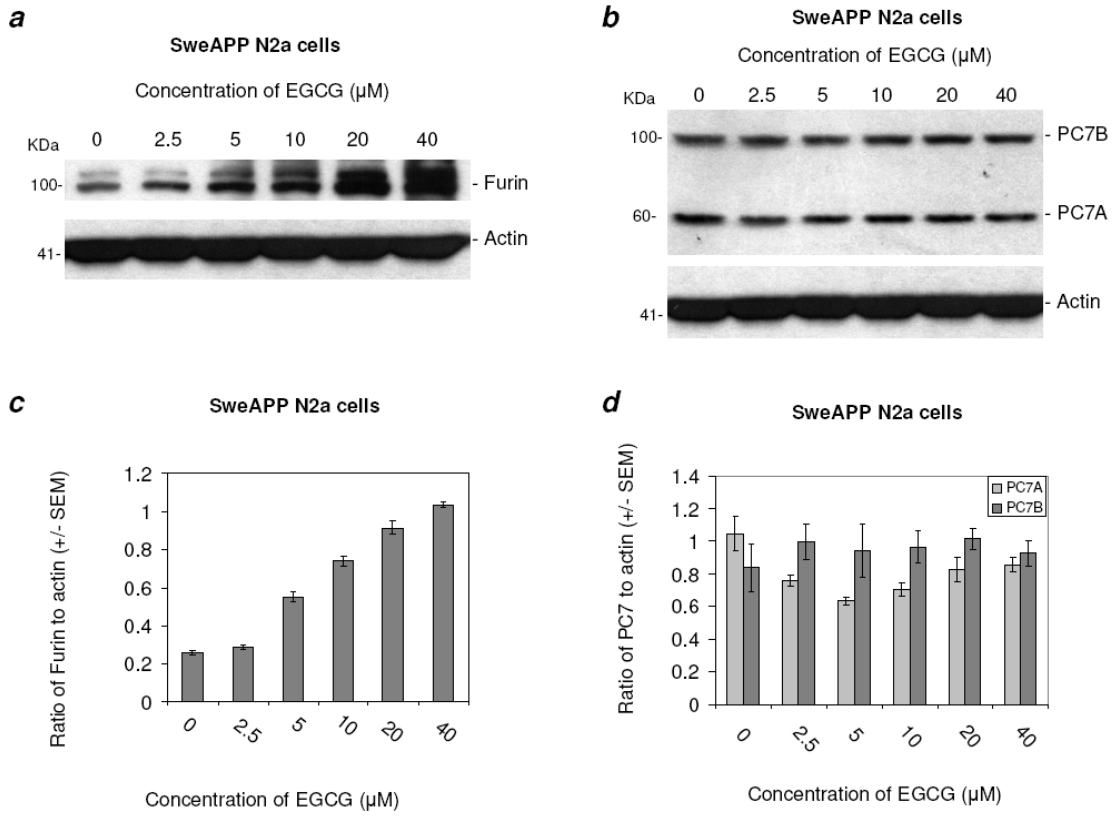

Figure 3.10a-d

EGCG treatment enhances furin activation in SweAPP N2a cells. a, b, Expression of furin and PC7 was analyzed in lysates from SweAPP N2a cells treated with EGCG at concentrations indicated for 4 hours by western blot. c, d, Densitometric analysis reveals the band density ratio of furin or PC7 isoforms to Actin. One-way ANOVA revealed significant differences between each EGCG concentration in ratios of furin to Actin ($p < 0.01$) with $n = 3$ for each condition.

.

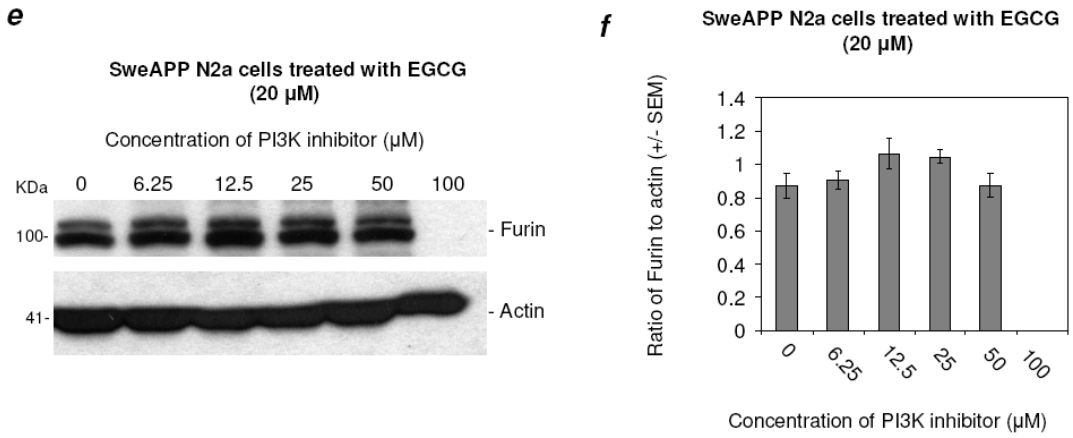

Figure 3.10e and f

PI3K inhibition does not affect EGCG-mediated furin activation in SweAPP N2a cells. e, Expression of furin was analyzed in lysates from SweAPP N2a cells treated with EGCG (20 μM) in the presence of a PI3K inhibitor (wortmannin) at concentrations indicated at concentrations indicated for 4 hours by western blot. f, Densitometric analysis reveals the band density ratio of furin or to Actin.

EGCG-mediated maturation of furin, SweAPP N2a cells were co-treated with a range of concentrations of the PI3K inhibitor wortamanin in presence of EGCG (20 μM) for 4 hours and lysates were subjected to western blot analysis. As illustrated by Figure 3.10 e and f, wortmannin treatment did not significantly affect furin expression in the context of EGCG. This phenomenon not only suggests that EGCG's signaling mechanism may branch, but also suggests that PI3K may be acting at the level of ADAM10 maturation.

3.3.9 EGCG treatment reduces Aβ pathology and promotes non-amyloidogenic proteolysis of APP in Tg APP_{sw} mice

To validate *in vivo* whether EGCG treatment could modulate APP metabolism and impact cerebral Aβ levels/plaque burden in Alzheimer transgenic mice we intraperitoneally administered EGCG to Tg APP_{sw} mice, a well-established transgenic mouse model of AD, at an age when Aβ deposits had begun to form (12 months). EGCG was administered based on a treatment schedule that produced benefit in an atherosclerosis mouse model (Chyu et al., 2004). At 12 months of age, Tg APP_{sw} mice were intraperitoneally injected with EGCG (20 mg/kg) or PBS daily for 60 days. Following treatment, ELISA analysis of brain homogenates revealed that both soluble $A\beta_{1\text{-}40}$ and $A\beta_{1\text{-}42}$ levels were reduced by 54% and 44%, respectively, in EGCG-treated Tg APP_{sw} mice. Insoluble $A\beta_{1\text{–}40}$ and $A\beta_{1\text{-}42}$ levels were also reduced by 47% and 38%, respectively, in EGCG-treated Tg APP_{sw} mice, as determined by ELISA of brain homogenates (Figure 3.11b,c). Consistent with these findings, analysis of plaque burden by 4G8 immunohistochemistry and thioflavin S staining from coronally sectioned brains

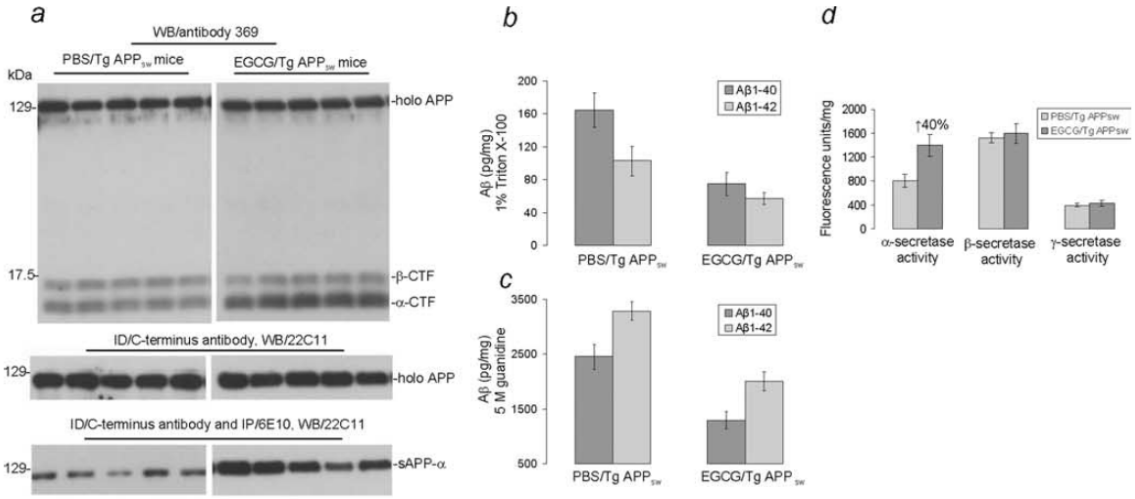

Figure 3.11a-d

EGCG treatment reduces Aβ pathology and promotes non-amyloidogenic proteolysis of APP in Tg APP_{sw} mice. Brain homogenates were prepared from female Tg APP_{sw} mice treated with EGCG (n = 5) or PBS (n = 5). a, Top panel, western blot analysis by antibody 369 shows holo APP and two bands corresponding to β-CTF and α-CTF. a, Middle and bottom panels, western blot analysis by antibody 22C11 shows holo-APP (middle; following ID/carboxyl-terminal APP antibody) and sAPP-α (bottom; following ID/C-terminal APP antibody and IP/6E10). Detergent-soluble $A\beta_{1–40,42}$ (b) and insoluble $A\beta_{1–40,42}$ prepared with 5 M guanidine (c) were analyzed by ELISA. Data are presented as mean ± 1 SEM of $A\beta_{1–40}$ or $A\beta_{1–42}$ (pg/mg protein) separately. b, c, A t test revealed a significant between-groups difference for either soluble or insoluble $A\beta_{1–40,42}$ ($p < 0.001$ for each comparison). d, α-, β-, and γ-secretase cleavage activities were analyzed by secretase cleavage activity assays. Data are presented as mean ± 1 SEM of fluorescence units/mg protein. A t test revealed a significant difference between EGCG- and PBS-treated Tg APP_{sw} mice for α-secretase activity ($p < 0.001$).

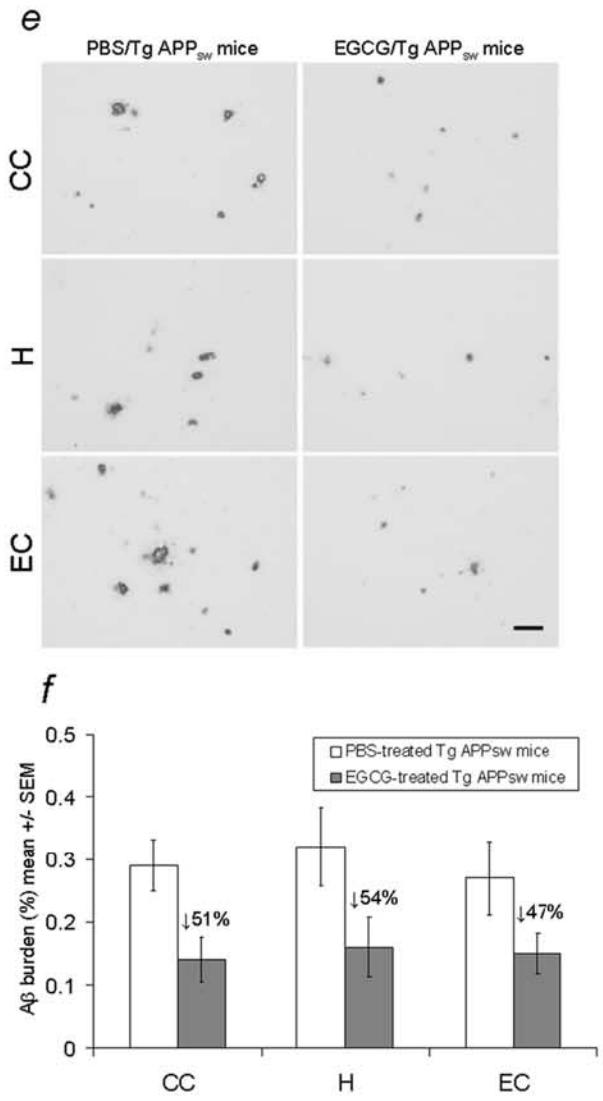

Figure 3.11e and f

EGCG treatment reduces Aβ pathology in Tg APP$_{sw}$ mice. e, Mouse brain coronal paraffin sections were stained with anti-human Aβ antibody (4G8). Left, Control PBS treated mice (n = 5). Right, EGCG treated mice (n = 5). The top panels are from the cingulate cortex (CC), the middle panels are from the hippocampus (H), and the bottom panels are from the entorhinal cortex (EC). f, Percentages of 4G8-immunoreactive Aβ plaques (mean ± 1 SEM) were calculated by quantitative image analysis, and reduction for each brain region is indicated. A t test for independent samples revealed significant differences ($p < 0.005$) between groups for each brain region examined. Scale bar, 50 μm.

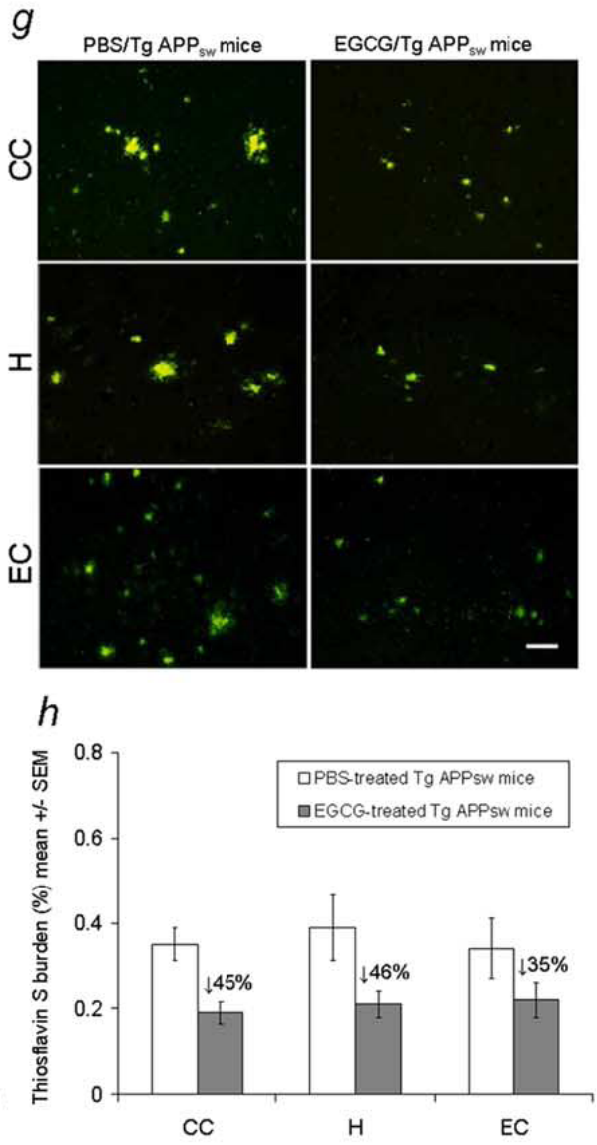

Figure 3.11g and h

EGCG treatment reduces Aβ pathology in Tg APP_{sw} mice. g, Mouse brain sections from the indicated brain regions were stained with thioflavin S. Left, Control PBS treated mice (n = 5). Right, EGCG treated mice (n = 5). h, Percentage of thioflavin S plaques (mean ± 1 SEM) were quantified by image analysis, and reduction for each brain region is indicated. A t test for independent samples revealed significant differences ($p < 0.005$) between groups for each brain region examined. Scale bar, 50 μm.

of EGCG treated Tg APP_{sw} mice showed 47–54% (Figure 3.11f) and 35–46% (Figure 3.11h) reductions in amyloid pathology across hippocampal and cortical brain regions, respectively. In addition, non-amyloidogenic APP fragments, including α-CTF and sAPP-α, were markedly increased in brain homogenates of Tg APP_{sw} mice treated with EGCG versus vehicle, as determined by western blot (Figure 3.11a). Fluorometric assay analysis also revealed a 40% increase in α-secretase activity in treatment animals (Figure 3.11d). Taken together, the above data suggest that EGCG may act as an α-secretase agonist in this transgenic mouse model of AD.

However, due to route of administration, it was unclear as to whether these EGCG-mediated effects were attributable to action of the compound in the periphery and/or the CNS. To answer this question, EGCG was administered intracerebroventricularly (0.5 mg/kg) to Tg APP_{sw} mice. Following 24 hours treatment, brain homogenates of Tg APP_{sw} mice showed significant reductions in cerebral soluble $A\beta_{1–40,42}$ levels by 39%, an effect that was associated with increased α-CTF generation, sAPP-α release, α-secretase activity (data not shown). Importantly, cerebral soluble $A\beta_{1–40,42}$ levels were reduced by a comparable magnitude as was evidenced in intraperitoneally injected Tg APP_{sw} mice, further indicating that the *in vivo* effects of EGCG are mainly owed to the action of this compound CNS. Together, the above lines of evidence confirm that EGCG promotes non-amyloidogenic proteolysis of APP and attenuates cerebral amyloidosis in this transgenic mouse model of AD.

To determine whether oral administration of EGCG could have similar anti-amyloidogenic effects using a theoretically equivalent dose to that used in the previous intraperitoneally administered EGCG study, Tg APP_{sw} mice were orally treated with

EGCG or vehicle (H_2O) starting at 8 months of age for 6 months. As shown in Figure 3.12a and c, EGCG treatment (50 mg/kg as determined by recorded daily intake and HPLC) similarly reduced cerebral amyloidosis in these mice. Image analysis of micrographs from Aβ antibody stained coronal sections revealed that plaque burdens were significantly reduced in the cingulate cortex, hippocampus, and entorhinal cortex by 54%, 43%, and 51%, respectively (Figure 3.12b). Furthermore, Congo red plaque burdens decreased significantly by 53%, 53%, and 58% respectively as well (Figure 3.12d). To verify the findings from these coronal sections, we analyzed anterior quarter brain homogenates for Aβ levels by ELISA. Again, EGCG oral treatment markedly decreased both soluble and insoluble forms of $A\beta_{1-40,\,42}$ (Figure 3.13a,b). As expected, EGCG treatment significantly increased ADAM10 maturation and resulted in an approximately 2-fold elevation in sAPP-α release, as determined by western blot and ELISA analysis (Figure 3.13c,d). Taken together, the above data confirm an oral route of administration provides effective attenuation of amyloid pathology comparable to that of intraperitoneally administered EGCG.

3.3.10 EGCG treatment modulates tau hyperphosphorylation in Tg APP_{sw} mice

To investigate the possibility that EGCG treatment may also affect tau physiology, brain homogenates from the intraperitoneally injected EGCG (20 mg/kg) treatment groups were analyzed by western blot. Figure 3.14 represents soluble and insoluble fractions of phosphorylated tau detected in the homogenates of the treatment

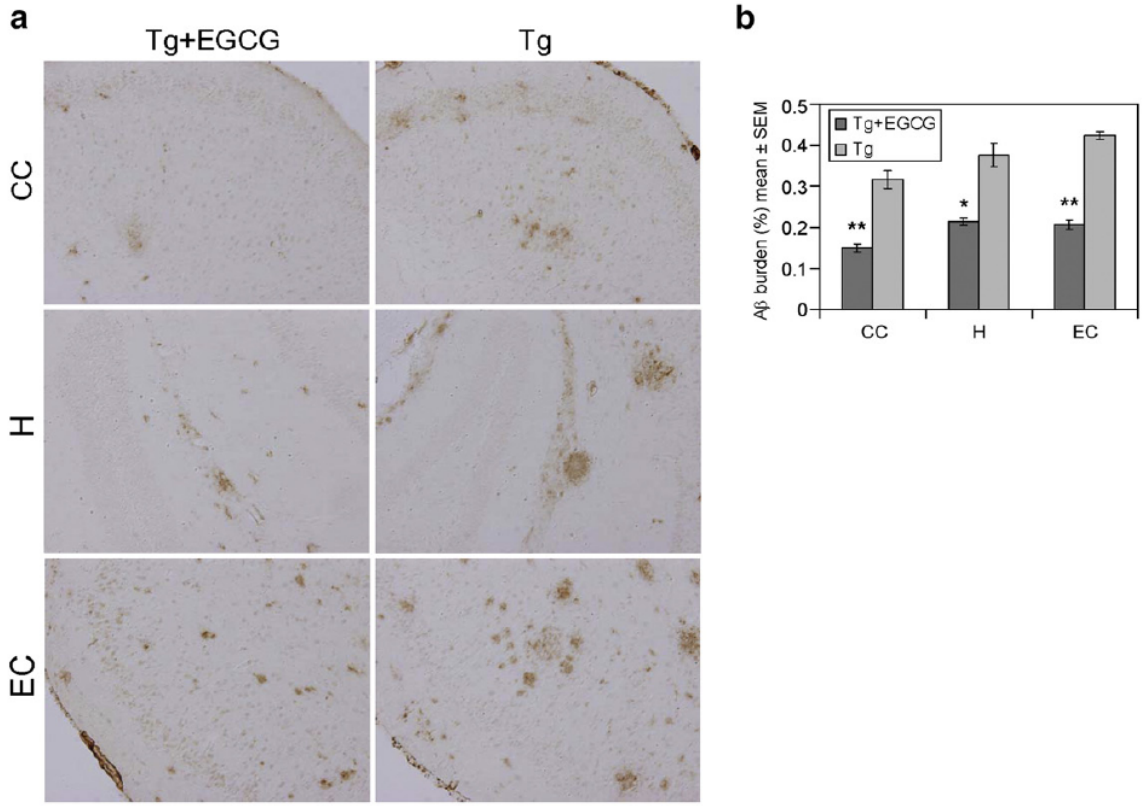

Figure 3.12a and b

Oral administration of EGCG reduces Aβ pathology in Tg APP_{sw} mice. a, Mouse brain coronal frozen sections were stained with rabbit polyclonal anti-human Aβ antibody. Left, EGCG treated Tg mice. Right, Control Tg mice. The top panels are from the cingulated cortex (CC), the middle panels are from the hippocampus (H), and bottom panels are from the entorhinal cortex (EC). b, Percentages of Aβ antibody-immunoreactive Aβ plaque (mean ± SEM) were calculated by quantitative image analysis. A *t* test for independent samples revealed significant differences (n = 10 for each condition; *p< 0.05; **p < 0.001) between groups for each brain region examined.

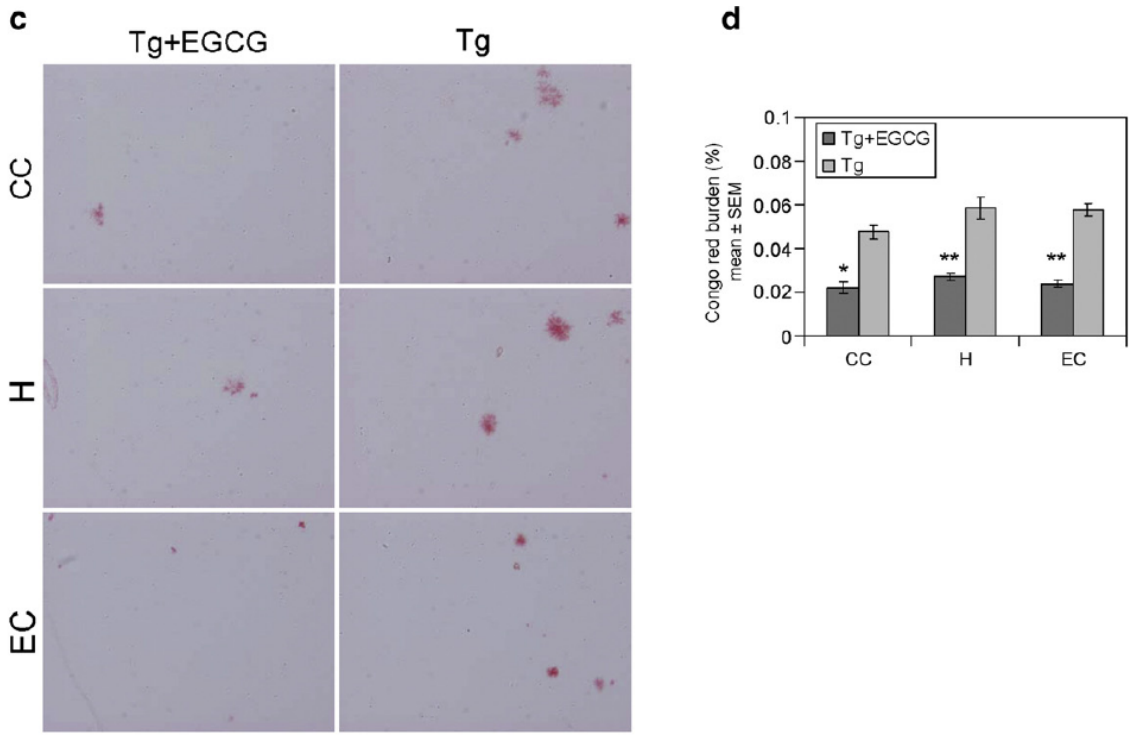

Figure 3.12c and d

Oral administration of EGCG reduces Aβ pathology in Tg APP_{sw} mice. c, Mouse brain coronal frozen sections were stained with Congo red. Left, EGCG treated Tg mice. Right, Control Tg mice. The top panels are from the cingulated cortex (CC), the middle panels are from the hippocampus (H), and bottom panels are from the entorhinal cortex (EC). d, Percentage of Congo red plaques (mean ± SEM) were quantified by image analysis. A *t* test for independent samples revealed significant differences ($n = 10$ for each condition; $*p < 0.005$; $**p < 0.001$) between groups for each brain region examined.

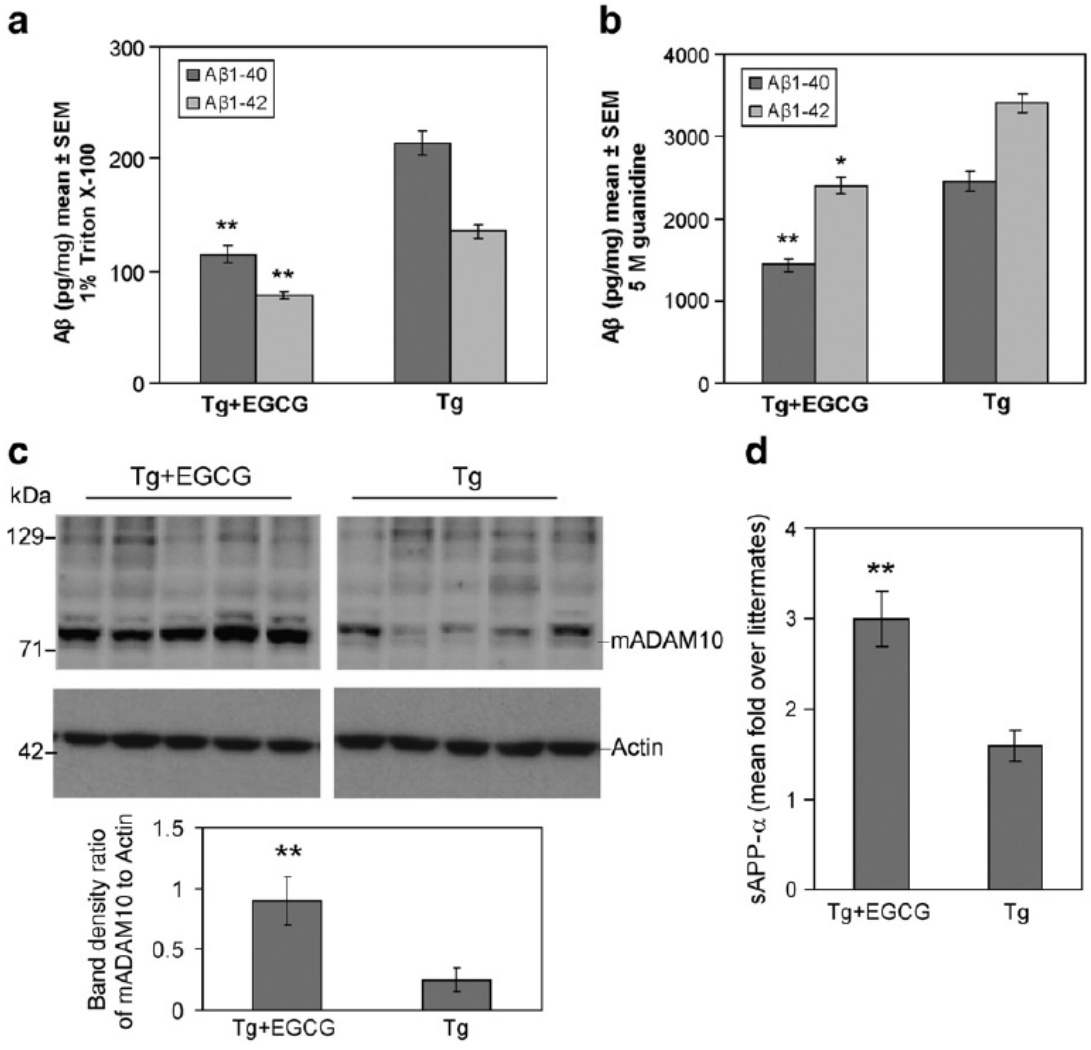

Figure 3.13

Oral administration of EGCG reduces both soluble and insoluble $A\beta_{1-40,\,42}$ levels by non-amyloidogenic APP proteolysis. Brain homogenates were prepared from Tg APP_{sw} mice treated with EGCG or H_2O. Soluble $A\beta_{1-40,\,42}$ (a) and insoluble Soluble $A\beta_{1-40,\,42}$ prepared with 5 M guanidine (b) were analyzed by ELISA. Data are presented as (pg/mg protein) of $A\beta_{1-40}$ or $A\beta_{1-42}$ separately. c, Densitometric analysis reveals the band density ratio of mADAM10 to Actin indicated below. D, ELISA for sAPP-α release in brain homogenates. Data were represented as a mean fold of sAPP-α relative to control. a, b, A *t* test revealed a significant between-groups difference for either soluble or insoluble $A\beta_{1-40,\,42}$ (*$p < 0.005$; **$p < 0.001$ for each comparison). Mean ± SEM for each group (n = 10 for each condition). c, d, A *t* test revealed a significant between-groups difference for sAPP-α generation (**$p < 0.001$). Mean ± SEM for each group ($n = 5$ for each condition).

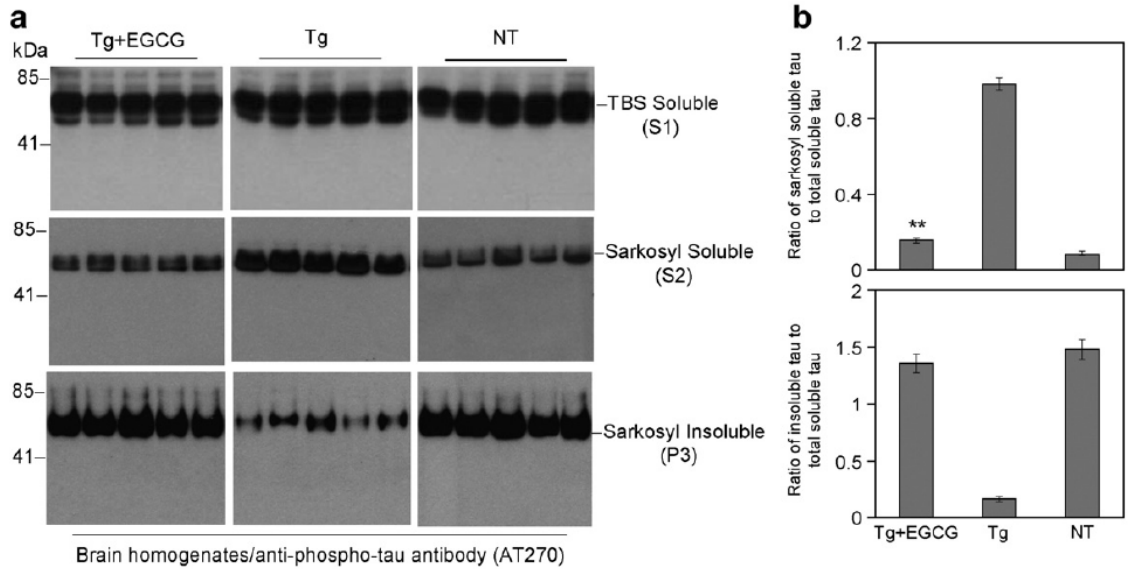

Figure 3.14

EGCG treatment modulates tau hyperphosphorylation in Tg APP_{sw} mice. Brain homogenates were prepared from Tg mice treated intraperitoneally with EGCG or PBS. a, Top, western blot analysis by antibody AT270 shows total phosphorylated tau protein. Western blot analysis by antibody AT270 shows sarkosyl-soluble phospho-tau (a, middle) and sarkosyl-insoluble phospho-tau (a, bottom). b, Densitometric analysis reveals the ratios of sarkosyl-soluble phospho-tau to total soluble tau (top) and of insoluble phospho-tau to total soluble tau (bottom). A *t* test revealed a significant difference between EGCG treatment and PBS control Tg mice (**$p < 0.001$). Mean ± SEM for each group ($n = 5$ for each condition).

groups and their control littermates by AT270 antibody. Clearly, untreated transgenic animals exhibit significantly higher amounts of sarkosyl-soluble (S2) phospho-tau and lower amounts of sarkosyl-insoluble (P3) phospho-tau when compared to EGCG-treated animals (Figure 3.14). In fact, EGCG-treated Tg APP_{sw} mice present a phospho-tau profile similar to that of the control littermates (NT, non-transgenics). In accordance with expectations, oral treatment groups also presented similar phospho-tau profiles (data not shown). Interestingly, the S2 fraction of non-treated Tg APP_{sw} mice presents the highest amount of A68 bands, which are supposedly indicative of the 60–68 kD abnormally phosphorylated, neurotoxic tau species (Brion et al., 1991; Shin et al., 1993). On the other hand, both the EGCG-treated Tg APP_{sw} mice and control littermates have markedly higher levels of insoluble A68 bands present in the P3 fraction compared to that of non-treated Tg APP_{sw} animals. Phospho-tau analysis of brain homogenates employing AT8 antibody revealed no significant differences between treatment groups; however, it is important to note that levels of tau pathology were quite low in comparison to AT270 (data not shown). Altogether, these findings not only suggest that the presence of Aβ may sustain levels of neurotoxic soluble phosphorylated tau isoforms, but also suggest that EGCG may oppose these effects.

3.3.11 EGCG provides cognitive benefit in Tg APP_{sw} mice

To determine any potential cognitive benefits afforded by EGCG administered either intraperitoneally or orally, working memory performance was evaluated using a well established radial arm water maze (RAWM) task. In Tg APP_{sw} vehicle injected mice tested at 14 months of age, a clear working memory impairment was evident in

comparison to NT controls (Figure 3.15a,c). By sharp contrast, Tg APP_{sw} mice that had been given two months of intraperitoneally injected EGCG (20 mg/kg) from 12–14 months of age had substantiallyimproved working memory performance that was comparable to that of NT control mice. Specifically, robust benefits of intraperitoneally administered EGCG were evident on Trial 5 (T5) working memory performance during the final block of RAWM testing (Figure 3.15a), as well as comparing Trial 1 (naïve trial) to Trial 5 improvement on the final day of RAWM testing (Figure 3.15c). Regarding the later, both NT controls and EGCG treated Tg APP_{sw} mice showed a marked improvement between T1 and T5, while Tg APP_{sw} control mice showed no working memory improvement. Moreover, the T5 working memory performance of Tg APP_{sw} mice treated with EGCG was dramatically better than Tg APP_{sw} controls and identical to NT controls during this last day of RAWM testing (Figure 3.15c).

In the other study, Tg APP_{sw} mice were treated with EGCG orally (50 mg/kg) in their drinking water beginning at 8 months of age and continuing through behavioral testing at 14 months. Because these mice had a more prevalent B6 background than Tg APP_{sw} mice of the intraperitoneal study, control Tg APP_{sw} mice were not substantially impaired in working memory at 14 months of age compared to NT controls (Figure 3.15b). Thus, the rather good performance of Tg APP_{sw} controls precluded significant EGCG benefit in this measure ("basement effect"), even though there was a trend for beneficial effects of oral EGCG treatment on T5 performance during the last block of testing (Figure 3.15b). This is further underscored by the T1 vs. T5 improvement present during the final day of RAWM testing (Figure 3.15d), wherein all 3 groups showed significant T1 vs. T5 improvement. However, despite the essentially

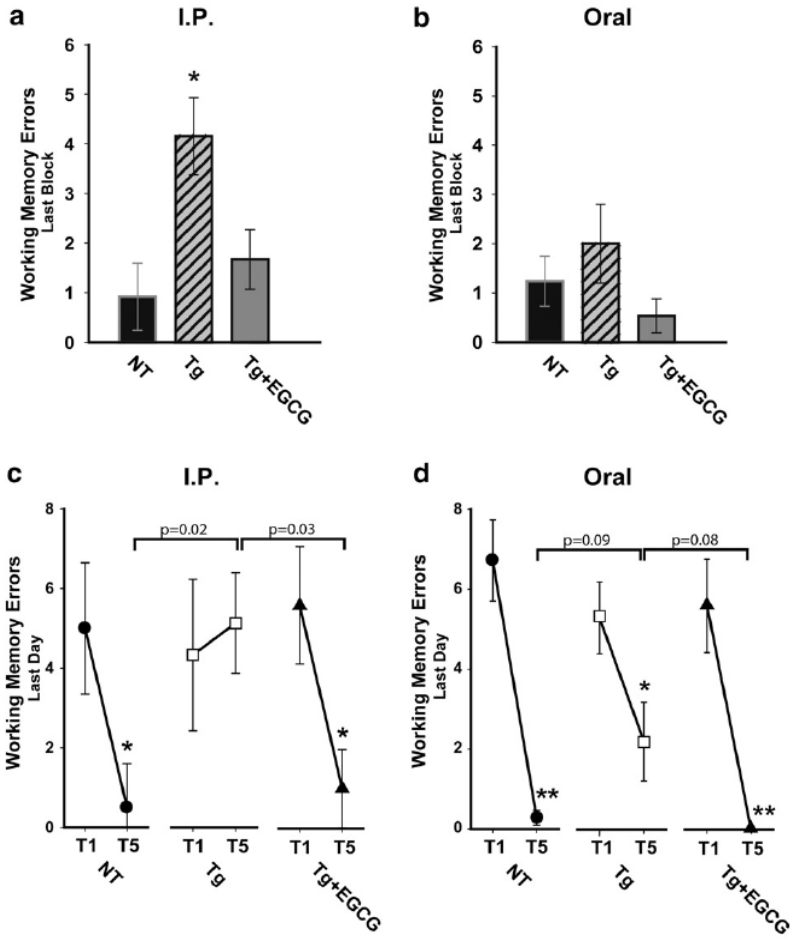

Figure 3.15

EGCG provides cognitive benefit in Tg APP_{sw} mice. a,c, Tg mice treated with intraperitoneal (I.P.) injection of EGCG (20 mg/kg; $n = 5$) or PBS ($n = 5$). Similarly-aged non-transgenic (NT) mice ($n = 5$) were concurrently given daily intraperitoneal injections of PBS. For the last block of RAWM testing (a), control Tg mice were significantly impaired versus NT controls in Trial 5 working memory errors, while Tg+EGCG mice performed significantly better than Tg controls and no different from NT controls (*$p < 0.05$). c, Only Tg+EGCG and NT controls were able to significantly decrease their working memory errors between Trial 1 (T1) and Trial 5 (T5) on the final day of testing (*$p < 0.02$ vs T1). Tg controls made substantially more T5 errors during this last day of testing compared to the other two groups. b,d, Tg mice given oral administration of EGCG (50 mg/kg; n = 10) in drinking water or normal H_2O ($n = 10$). Similarly-aged NT mice ($n = 5$) were concurrently given normal water daily. b, No statistical differences were evident in T5 performance over the last block of testing. d, Animals in all three groups were able to significantly reduce their working memory errors from T1 to T5 during the last day of testing (*$p < 0.05$; **$p < 0.002$). All group data are presented as mean ± SEM.

flawless performance of both NT and Tg APP_{sw} mice treated with EGCG during T5 on the final test day, the good performance of Tg APP_{sw} controls resulted in both of these groups barely missing statistical significance ($p < 0.08$, 0.09; Figure 3.15) when compared to Tg APP_{sw} controls. Nonetheless, the ability of oral EGCG treatment to result in perfect T5 performance during the final day of testing (vs. a 2-error average for Tg APP_{sw} controls), strongly suggests a cognitive benefit provided by oral EGCG treatment.

3.4 Conclusions

The studies detailed in this chapter qualify EGCG, the main naturally-occurring polyphenolic constituent of green tea, as an effective anti-amyloidogenic and anti-pathogenic tau agent. Treatment with EGCG reduces Aβ generation in both APP_{sw} overexpressing primary neurons and neuron-like cells. In concert with these findings, α-CTF generation and sAPP-α release increased in these cell lines. Accordingly, it was clear that EGCG accomplished Aβ reductions by promoting non-amyloidogenic proteolysis of APP. Central to this non-amyloidogenic proteolysis was α-secretase activity, which was also directly detected to increase in APP_{sw} N2a cells following EGCG treatment. While initial experiments suggested that TACE/ADAM17 may be involved, the effects of its activation were transient at best. In the following study, it became evident that EGCG elevated α-secretase activity through enhanced activation of ADAM10. In this study, maturation of ADAM10 correlated with both increased α-CTF generation and sAPP-α release in both APP_{sw} overexpressing primary neurons and

neuron-like cells. Furthermore, EGCG was also found to promote ADAM10 maturation in both primary microglial and N9 microglial lines, albeit with lower potency than evidenced in neurons and neuron-like cells. To assess the level of contribution of ADAM10 in EGCG-mediated non-amyloidogenic APP proteolysis, RNAi was performed to knock-down expression of ADAM9, 10, or 17. Results showed that ADAM10, but not ADAM9 or 17, was required. Investigating further upstream revealed the involvement of PI3K signaling and furin activity in EGCG-mediated non-amyloidogenic APP proteolysis. Interestingly, these events appear to be mutually exclusive. Therefore, it is becoming increasingly evident that EGCG possess a multifaceted cellular/molecular mechanism. Altogether, these data provide important mechanistic insight into the potential use of EGCG and/or other activators of ADAM10 as therapeutic targets to oppose cerebral amyloidosis associated with AD.

As a validation of these above findings *in vivo*, Tg APP_{sw} mice were treated with EGCG *via* intracerebroventricular, intrapertioneal, and oral routes. In all instances of treatment, Aβ levels/plaque burden decreased concurrently with increases in α-CTF generation, sAPP-α release, and α-secretase activity. While ADAM10 activation was confirmed in orally treated animals, it was also observed in both intracerebroventricular and intrapertioneal routes (data not shown). The effect of both intraperitoneally and orally treated EGCG on tau pathology and cognition was also investigated. Both intraperitoneally and orally-treated Tg APP_{sw} mice were found to have modulated tau profiles, with markedly suppressed sarkosyl-soluble phosphorylated tau isoforms. RAWM testing for working memory indicated that EGCG provided cognitive benefit to Tg APP_{sw} mice with both routes of administration, although intraperitoneally treated

animals showed a more pronounced benefit because of the greater impairment of their Tg controls at the time of testing. Taken together, these data qualify α-secretase activation as a viable anti-amyloidogenic strategy and raise the possibility that EGCG dietary supplementation may provide effective prophylaxis for AD.

CHAPTER 4

ANTI-AMYLOIDOGENIC PROPERTIES OF LUTEOLIN AND STRUCTURALLY ANALOGOUS 5,7-DIHYDROXYFLAVONES

4.1 γ-Secretase inhibition

While both β and γ-secretase cleavage events are essential to the formation of an Aβ peptide, it is the γ-secretase cleavage that determines which of the two major forms of the peptide ($A\beta_{1\text{-}40,\,42}$) will be generated and consequently both the peptide's ability to aggregate and the rate at which it is deposited (Citron et al., 1996; Evin et al., 1995). Thus, one clear potential therapeutic target for AD has been γ-secretase. Despite the potential toxicity involving possible disruption of Notch signaling and intracellular accumulation of β-CTFs, γ-secretase inhibition remains a viable anti-amyloidogenic strategy (Barten et al., 2006; Evin et al., 2006). In addition to previous reports that novel γ-secretase inhibitors (GSI) significantly reduced Aβ production both *in vitro* and *in vivo* (Dovey et al., 2001; Games et al., 1995; Higaki et al., 1995; Klafki et al., 1995), Comery and colleagues (2005) recently reported that similar GSIs may even improve cognitive functioning in a transgenic mouse model of AD (Tg2576). These finding have functioned to further the vigorous search for potential candidate GSIs.

4.1.1 Presenilin-1 (PS1)

Although γ-secretase has not been entirely characterized, it is well known that it consists of a multi-protein complex including presenilin-1 or -2 (PS1 or PS2), nicastrin, anterior pharynx-defective-1 (APH1), and presenilin enhancer-2 (PEN2) (Sato et al., 2007). PS1 or PS2 are believed to form the catalytic core of the γ-secretase complex. However, deletion of the PS1 gene in mice has been reported to markedly abolish γ-secretase activity, which would suggest that it is likely responsible for the majority of this enzyme's activity. Following endoproteolytic cleavage of PS1, the remaining dimer is consists of a large a amino-terminal fragment (NTF) and a smaller carboxyl-terminal fragment (CTF), which is believed to contain regulatory phospho-residues (Capell et al., 1998). Whether endoproteolytic cleavage of PS1 is both the seminal and final required process for γ-secretase activity remains to be determined.

4.1.2 Glycogen synthase kinase-3 (GSK-3)

Among the many promising potential candidate GSIs are the glycogen synthase kinase 3 (GSK-3) inhibitors. These compounds target this tonically active serine/threonine kinase, which has been implicated in several disorders of the CNS (Carmichael et al., 2002; Engel et al., 2006; Kozlovsky et al., 2000). With regard to AD, both isoforms of GSK-3 (α and β) have been found to directly phosphorylate tau on residues specific to hyperphosphorylated paired helical filaments (PHF) (Ishiguro et al., 1993), GSK-3β has been shown to phosphorylate APP and to contribute to Aβ mediated neurotoxicity (Aplin et al., 1996; Takashima et al., 1996) and GSK-3β has been found to phosphorylate PS1, which may act as a docking site for subsequent tau phosphorylation (Takashima et al., 1998). Therefore, GSK-3 inhibitors are especially attractive as they

may not only oppose Aβ generation but also NFT formation. Moreover, Phiel and colleages (2003) reported that inhibition of the GSK-3α isoform may regulate γ-secretase cleavage of APP in a substrate-specific manner (Phiel et al., 2003). Accordingly, this selective inhibition of GSK-3 might provide the maximal therapeutic benefit while reducing the potential for toxic side-effects.

4.2 Materials and methods

4.2.1 Reagents

Luteolin (> 95% purity by HPLC), was purchased from Sigma (St Louis, MO, USA). Diosmin (> 90% purity by HPLC), was purchased from Axxora (San Diego, CA, USA). SB-415286 was obtained from Biomol International (Plymouth Meeting, PA, USA). Calf intestine alkaline phosphatase (CIAP) was purchased from Fermentas (Hanover, Maryland). amino-terminal and carboxyl-terminal PS1 antibodies were obtained from Chemicon (Temecula, California, USA), carboxyl -terminal antibody APP 369 (1:1000; kindly provided by S. Gandy and H. Steiner), carboxyl -terminal APP antibody (1:500; Calbiochem, Temecula, CA, USA), amino-terminal APP antibody (1:1000, 22C11; Roche, Basel, Switzerland), amino-terminal Aβ antibody 6E10 (1:1000; Signet Laboratories, Dedham, MA, USA), phospho-GSK3α(pSer^{21}) (1:1000; BK202; Upstate, Lake Placid, New York, USA), antibodies against phospho-GSK3α/β (pTyr$^{279/216}$), phospho-GSK-3β (Ser^{9}), and total GSK-3α/β (1:1000; Sigma), or actin antibody (1:1500; as an internal reference control; Roche) were employed for western blot analysis as described in section 2.4. Co-immunoprecitipation was performed for

detection of APP bound to PS1 CTF by incubating 400 μg of total protein from cell lysates with PS1 CTF antibody (1:50) as decribed in section 2.5.

4.2.2 Mice

For intraperitoneal administration of luteolin, a total of 16 (8♂/8♀) Tg APP_{sw} mice were used; 8 mice received luteolin, and the other 8 received vehicle (PBS). Beginning at 8 months of age, these mice were intraperitoneally injected with luteolin (20 mg/kg) or PBS daily for 30 days based on previously described methods (chapter3). These mice were then sacrificed at 9 months of age for analyses of Aβ levels and plaque burdens according to methods described in sections 2.3 and 2.10. For oral administration of diosmin, a total of 20 (10♂/10♀) APP_{sw} mice were used; 10 mice received a diet containing 0.05% diosmin in standard mouse chow (7012; Harlan Teklad, Madison, WI, USA), and the other 10 received the standard diet alone. Beginning at 8 months of age, these mice consumed both diets *ad libitum* for 6 months. These mice were then sacrificed at 14 months of age for analyses of Aβ levels and plaque burdens according to methods described in sections 2.3 and 2.10. GSK-3α/β immunohistochemical staining was performed using anti-phospho-GSK-3/α/β ($pTyr^{279/216}$) antibody (1:50) in conjunction with the VectaStain Elite™ ABC kit (Vector Laboratories, Burlingame, CA, USA) coupled with diaminobenzidine substrate according to methods described in section 2.10.

4.3 Results

4.3.1 Luteolin inhibits $A\beta_{1\text{-}40,\,42}$ generation from SweAPP N2a cells and Tg APP_{sw} mouse-derived primary neuronal cells

To examine the effects of luteolin on APP metabolism, APP_{sw} N2a cells and primary neuronal cells derived from Tg APP_{sw} mice were treated with a wide range of concentrations of the flavonoid for 12 hours. Following a series of analyses, of which involved immunoprecipitation, western blot, and ELISA, data revealed that luteolin effectively reduced both $A\beta_{1\text{-}40,\,42}$ production in either cell line in a concentration dependent manner (Figure 4.1a,c). In fact, luteolin markedly abolished generation of both Aβ peptides with >70% and >85% reductions at treatment concentrations of 20 and 40 μM, respectively (Figure 4.1a,c). Furthermore, to determine at which level luteolin impacts APP metabolism, CTF profiles of SweAPP N2a cells and primary neuronal cells derived from Tg APP_{sw} mice were investigated following treatment. As illustrated in Figure 4.1b and d, western blot analysis shows a concentration dependent accumulation of both α and β–CTFs, approximately 2-3 fold increases in either cell line. Given the obvious implications on γ-secretase activity, SweAPP N2a cells and primary neuronal cells derived from Tg APP_{sw} mice were treated with an range of concentrations of luteolin for various periods of time and lysates were subjected to fluorometric assay for γ-cleavage. In accordance with expectations, luteolin lowered γ-secretase cleavage activity in both a concentration and time dependent fashion (Fig. 4.1e,f). More importantly, these concentration and time dependent decreases in γ-secretase cleavage activity correlate with the decreases in total Aβ generation in cultured media, as determined by ELISA

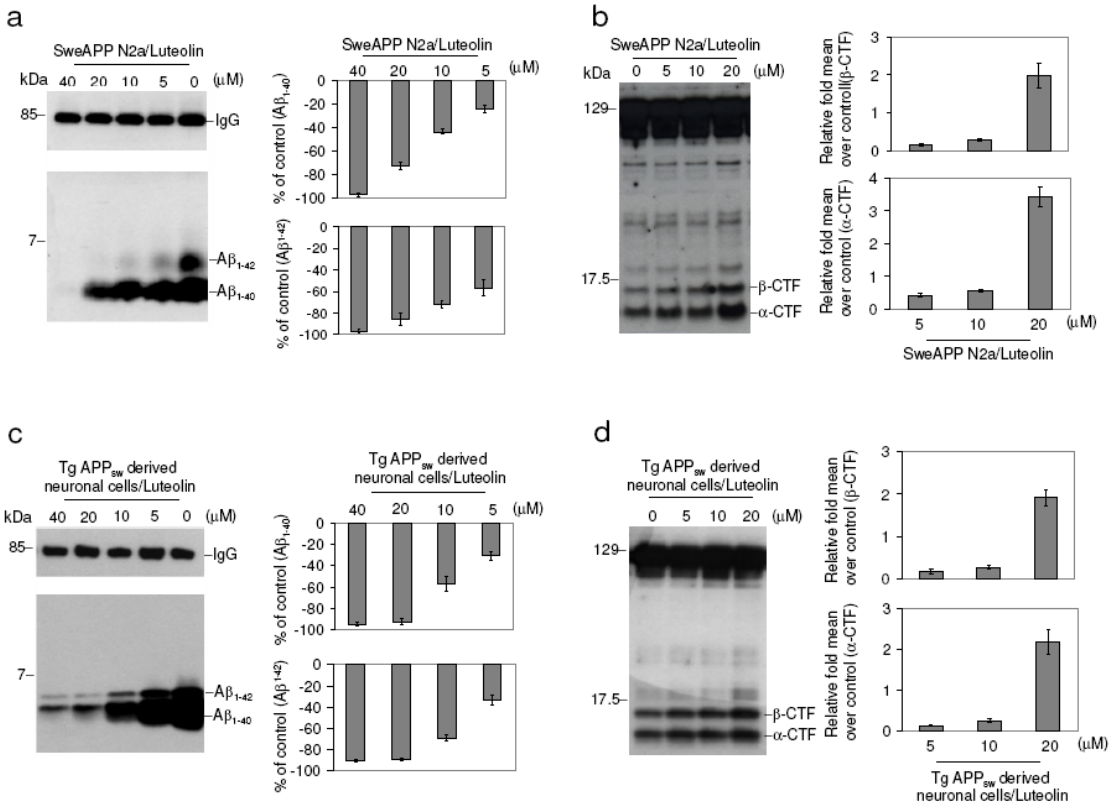

Figure 4.1a-d

Luteolin inhibits $A\beta_{1\text{-}40,\ 42}$ generation from SweAPP N2a cells and Tg APP_{sw} mouse-derived primary neuronal cells. SweAPP N2a cells (a, b) or Tg APP_{sw} mouse-derived primary neuronal cells (c, d) were treated with luteolin at various concentrations as indicated for 12 hours. a, c, Secreted $A\beta_{1\text{-}40,\ 42}$ peptides were analyzed by immunoprecipitation/Western blot (right) and ELISA (left; $n = 3$ for each condition) in cell cultured media. For Aβ ELISA, data are represented as a percentage of $A\beta_{1\text{-}40,\ 42}$ peptides secreted 12 hours after luteolin treatment relative to control (untreated). b, d, APP CTFs were analyzed by western blot (right) in cell lysates and relative fold mean over control (α, β-CTF) was calculated by densitometric analysis (left). a, b, c, d, One-way ANOVA followed by *post hoc* comparison revealed significant differences between each concentration ($p < 0.005$) except between 20 μM and 40 μM ($p > 0.05$).

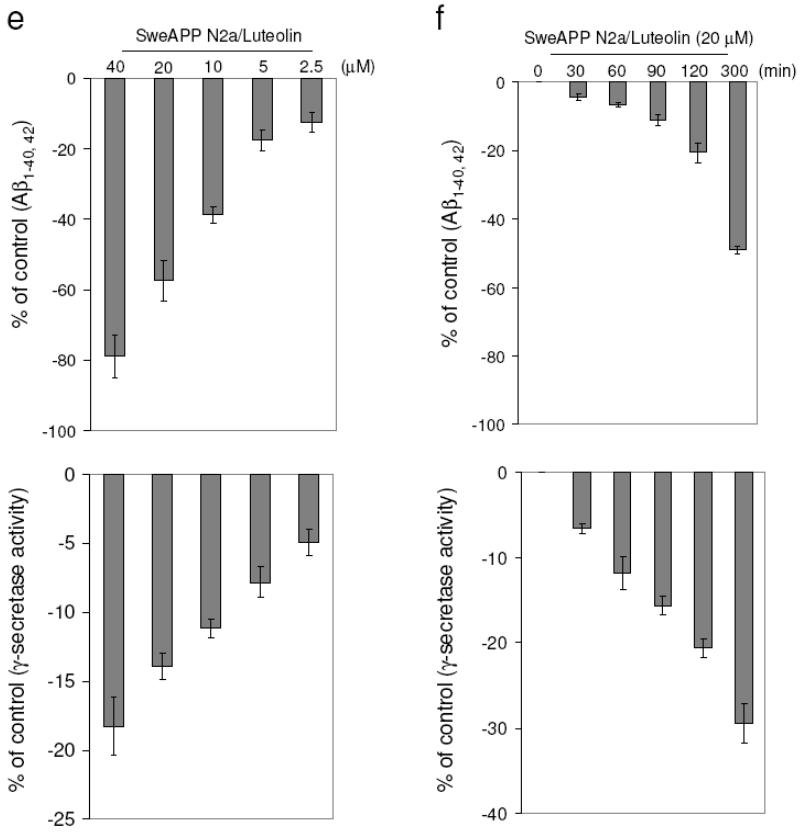

Figure 4.1e and f

Luteolin inhibits $A\beta_{1\text{-}40,\ 42}$ generation by reducing γ-secretase activity in SweAPP N2a cells. SweAPP N2a cells were treated with luteolin at a single concentration (20 μM) for various time points as indicted. e, f, Secreted $A\beta_{1\text{-}40,\ 42}$ peptides were analyzed in conditional media by ELISA following 12 hours incubation (top panel; $n = 3$ for each condition) and γ-secretase activity was analyzed in cell lysates following 90 min incubation using secretase cleavage activity assay (lower panel; $n = 3$ for each condition). e,f, Data presented as a percentage of fluorescence units/milligrams protein activated 30, 60, 90, 120, 300 minutes after luteolin treatment relative to control (untreated). e,f, One-way ANOVA followed by *post hoc* comparison revealed a significant difference between each time point examined ($p < 0.005$).

(Figure 4.1e,f). Taken together, the above data suggests that luteolin exerts its anti-amyloidogenic effects through down-regulation of γ-secretase activity.

4.3.2 Luteolin reduces GSK-3α/β activation in SweAPP N2a cells and Tg APP_{sw} mouse-derived primary neuronal cells

To establish a mechanism whereby luteolin modulates γ-secretase activity and subsequent Aβ generation, the effect this flavonoid had on a variety of proteins related to and/or required for proper functioning of the γ-secretase complex were investigated. Interestingly, treatment with an effective concentration of luteolin (20 μM) increased levels of serine 21 phosphorylated inactive GSK-3α isoforms in lysates from both SweAPP N2a cells and Tg APP_{sw} mouse-derived primary neuronal cells (Figure 4.2). However, no significant changes in overall expression of either GSK3-α or β were observed by western blot, confirming that this phenomenon most likely occurs at the post-translational or protein stage of this kinase (Figure 4.2). In addition, this increase in GSK-3α serine 21 residue phosphorylation-mediated inactivation continued through 3 hours (Figure 4.2b,e). At the same time, it is evident that levels of tyrosine 279 phosphorylated active GSK-3α isoforms decreased in a time dependent manner (Figure 4.2b,e). More to the point, these time dependent decreases in phospho-tyrosine 279 active GSK-3α are quite congruent with the increases observed with phospho-serine 21 inactive isoforms (Figure 4.2). Figure 4.2c and f clearly indicate abrupt decreases in active phosphorylated isoforms and increases in inactive phosphorylated isoforms within 60 minutes of luteolin treatment. Also notable, following 2 hours of treatment, levels of

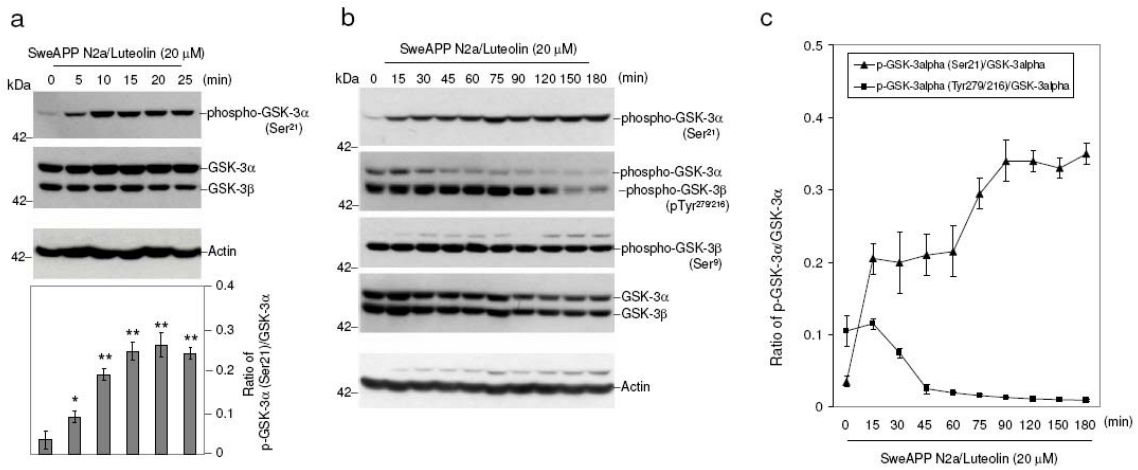

Figure 4.2a-c

Luteolin reduces GSK-3α/β activation in SweAPP N2a. SweAPP N2a cells were treated with luteolin at 20 μM for various time points as indicated. Cell lysates were prepared and subjected to western blot analysis for phosphorylated forms of GSK-3α/β. a, Western blot analysis using anti-phospho-GSK-3α (Ser^{21}) antibody shows one band (51 kDa) corresponding to phosphorylated form of GSK-3α or using anti-GSK-3 monoclonal antibody recognizes both total GSK-3α and GSK-3β, 51 and 47 kDa, respectively. Western blot analysis using anti-Actin antibody shows Actin protein (as an internal reference control). Densitometric analysis reveals the ratio of phospho-GSK-3α (Ser^{21}) to total GSK-3α as indicated below the figures (n = 3 for each condition). a, One-way ANOVA followed by *post hoc* comparison revealed a significant difference between 0 min and 5, 10, 15, 20 or 25 minutes (p< 0.001). b, Western blot analysis using anti-phospho-GSK-3α/β($Tye^{279/216}$) antibody shows two bands (51 and 47 kDa) corresponding to phosphorylated forms of GSK-3α and GSK-3β or using anti-phospho-GSK-3β (Ser^{9}) antibody recognizes phosphorylated form of GSK-3β at 47 kDa. Anti-Actin antibody was used as shows an internal reference control. Densitometric analysis reveals the ratio of phospho-GSK-3α ($Tye^{279/216}$) to total GSK-3α as indicated below the figures (n = 3 for each condition). b, One-way ANOVA followed by *post hoc* comparison significant difference was noted between 30 min and 45, 60, 75, 90, 120, 150 or 180 min (p < 0.005). For c, plots comparing ratios of phospho-GSK-3α (Ser^{21}) and phospho-GSK-3α/β($Tye^{279/216}$) to total GSK-3α from densitometric analysis of western blots over time.

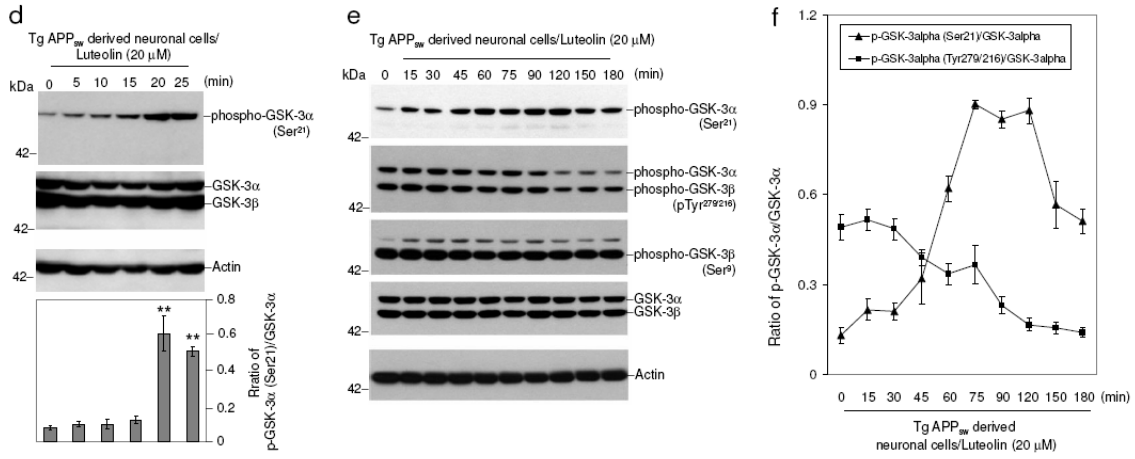

Figure 4.2d-f

Luteolin reduces GSK-3α/β activation in Tg APP_{sw} mouse-derived primary neuronal cells. Tg APP_{sw} mouse-derived primary neuronal cells were treated with luteolin at 20 μM for various time points as indicated. Cell lysates were prepared and subjected to western blot analysis for phosphorylated forms of GSK-3α/β. d, Western blot analysis using anti-phospho-GSK-3α (Ser^{21}) antibody shows one band (51 kDa) corresponding to phosphorylated form of GSK-3α or using anti-GSK-3 monoclonal antibody recognizes both total GSK-3α and GSK-3β, 51 and 47 kDa, respectively. Western blot analysis using anti-Actin antibody shows Actin protein (as an internal reference control). Densitometric analysis reveals the ratio of phospho-GSK-3α (Ser^{21}) to total GSK-3α as indicated below the figures (n = 3 for each condition). d, One-way ANOVA followed by *post hoc* comparison revealed a significant difference between 0 min and 5, 10, 15, 20 or 25 minutes (p< 0.001). e, Western blot analysis using anti-phospho-GSK-3α/β($Tye^{279/216}$) antibody shows two bands (51 and 47 kDa) corresponding to phosphorylated forms of GSK-3α and GSK-3β or using anti-phospho-GSK-3β (Ser^{9}) antibody recognizes phosphorylated form of GSK-3β at 47 kDa. Anti-Actin antibody was used as shows an internal reference control. Densitometric analysis reveals the ratio of phospho-GSK-3α ($Tye^{279/216}$) to total GSK-3α as indicated below the figures (n = 3 for each condition). e, One-way ANOVA followed by *post hoc* comparison significant difference was noted between 30 min and 45, 60, 75, 90, 120, 150 or 180 min (p < 0.005). For f, plots comparing ratios of phospho-GSK-3α (Ser^{21}) and phospho-GSK-3α/β($Tye^{279/216}$) to total GSK-3α from densitometric analysis of western blots over time.

phospho-tyrosine 216 active GSK-3β drop off, which may also explain, in part, the luteolin-mediated effects on the γ-secretase complex *via* PS1. Although luteolin clearly affects that of GSK-3α, no such significant changes in phospho-serine 9 GSK-3β inactivation were detected. Therefore, when considering the above data, it is apparent that luteolin affects GSK-3α/β signaling and confirms that this signaling is a potential upstream event required for modulation of γ-secretase activity.

4.3.3 GSK-3 inhibition alters PS1 processing/phosphorylation in SweAPP N2a cells

As indicated by panels a,b,c of Figure 4.3, western blot analysis of carboxyl-terminal portions of PS1 reveals three distinct bands. The two bands of highest molecular weight, approximately 20 kDa and 18 kDa in size, most likely represent previously reported phosphorylated PS1 CTFs with the smaller 16 kDa band representing the more common CTF product indicative of PS1 endoproteolytic cleavage. Following treatment of SweAPP N2a cells with various concentrations of luteolin, lysates revealed that PS1 CTF phosphorylation increased. Significant differences in phospho-PS1 CTF:PS1 CTF ratios with luteolin treatment were evident, both concentration and time dependently (Figure 4.3a). More to the point, these trends correlated with the concentration and time dependent decreases in $A\beta_{1\text{-}40,\,42}$ generation. To confirm that the 20 kDa and 18 kDa bands were representative of phosphorylated PS1 isoforms, APP_{sw} N2a cells were again treated with luteolin (20 μM) prior to lysis and subsequently cell lysates were incubated with calf intestine alkaline phosphatase (CIAP) to dephosphorylate any potential phosphorylated proteins, which consequently may have skewed electrophorectic mobilities. Indeed, following 30 minutes of incubation, the 20

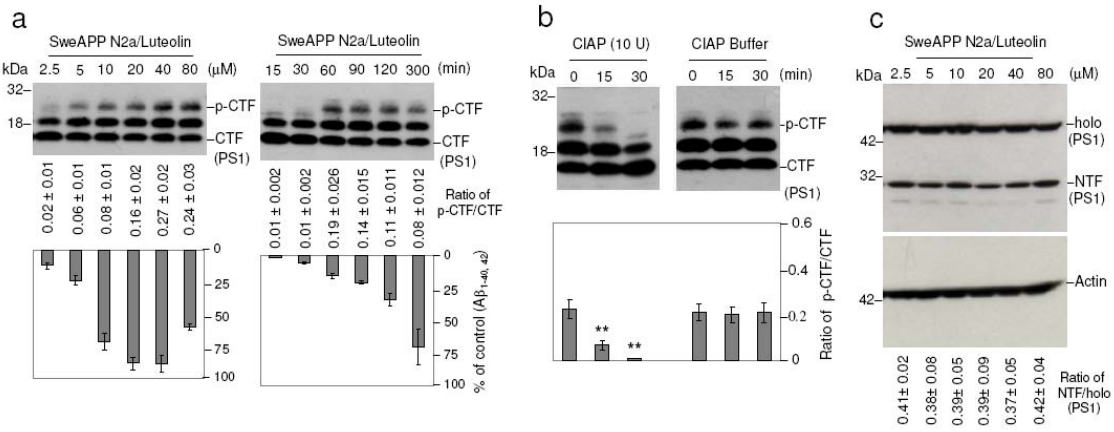

Figure 4.3

PS1 phosphorylation is associated with luteolin-mediated inhibition of Aβ generation. SweAPP N2a cells were treated with luteolin at a range of concentrations for 4 hours or at 20 μM for various time points as indicated. Cell lysates were prepared from these cells and subjected to western blot analyses of PS1 carboxyl-terminal fragments (CTFs) (a) and amino-terminal fragment (NTFs) (c). Western blot analysis by anti-PS1 CTF antibody shows two bands corresponding to phosphorylated PS1 CTF (p-CTF) and one dephosphorylated PS1 CTF (CTF). While western blot analysis by anti-PS1 CTF antibody shows tow bands corresponding to holo-PS1 and PS1 NTF. b, cell lysates from luteolin treated cells (20 μM) were incubated with calf-intestine alkaline phosphatase (CIAP) or buffer for various time points. Western blot analysis by anti-PS1 CTF antibody confirms two higher molecular weight bands corresponding to phosphorylated isoforms. Densitometric analysis reveals the ratio of PS1 p-CTF to CTF below figures. A *t* test revealed a significant deference between luteolin concentrations and time points for ratio of PS1 p-CTF to CTF ($p < 0.005$ with $n = 3$ for each condition, but not for ratio of holo-PS1 to PS1 NTF ($p > 0.05$ with $n = 3$ for each condition) at each time point examined. Cultured media were collected for Aβ ELISA. Data corresponds to percentage of $A\beta_{1\text{-}40,\ 42}$ peptides secreted 4 hours after luteolin treatment relative to control (untreated) as indicated below panel a.

kDa band is not evident in the CIAP treated lysates (Figure 4.3b). Also the 18 kDa band is clearly reduced and the endogenous CTF, 16 kDa, appears to accumulate. When compared to lysates incubated with only reaction buffer, time dependent decreases in phosphorylated residues are apparent by ratios of the 20 kDa CTF:16 kDa CTF (Figure 4.3b) While luteolin treatment influenced PS1 CTF species, this compound had no significant effect on either full-length PS1 or PS1 NTF protein levels (Figure 4.3c). Luteolin therefore appears to affect PS1 phosphorylation and may indicate a means by which γ-secretase activity may be regulated.

To determine if this phenomenon was specifically attributable to luteolin treatment or more generally in regards to GSK-3 inhibition, SweAPP N2a cells were treated with an effective concentration of GSK-3 inhibitor SB-415286 (20 μM) for various periods of time (Figure 4.4a). Again, similar decreases in $A\beta_{1\text{-}40,\ 42}$ generation (data not shown) and alterations in phospho-PS1 CTF:PS1 CTF ratios were evident following SB-415286 treatment (Figure 4.4a). Furthermore, to substantiate the role of GSK-3α in this luteolin-mediated PS1 processing, RNAi knock-down was conducted and successfully knocked-down the expression of both GSK-3α and β (>70%, data not shown) in SweAPP N2a cells. As expected, GSK-3α siRNA transfected cells exhibited significantly higher phosphorylated PS1 isoforms as compared to GSK-3β siRNA or mock transfectants (Figure 4.4b). Similar differences were observed when comparing the level of PS1 phosphorylation in luteolin treated (20 μM) cells to that of GSK-3 β siRNA or mock transfectants (Figure 4.4b). This data suggests that GSK-3α may regulate PS1 CTF phosphorylation and

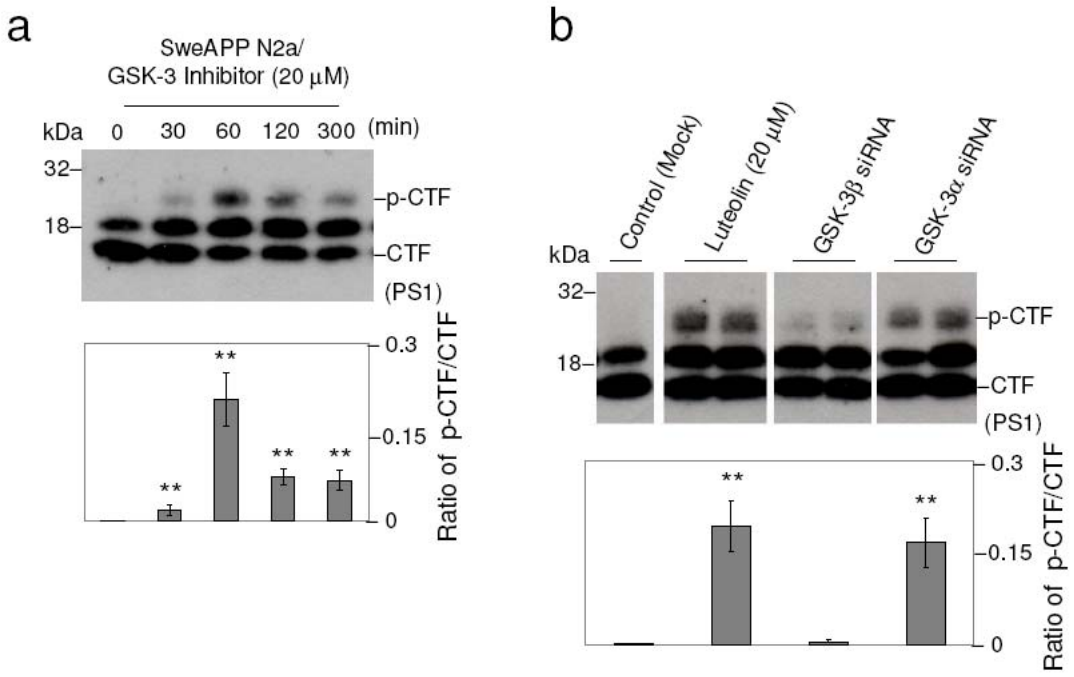

Figure 4.4

GSK-3α regulates PS1 phosphorylation. a, SweAPP N2a cells were treated with a known GSK-3 inhibitor (SB-415286) at 20 μM for various time points. Western blot analysis by anti-PS1 CTF antibody produces a similar phosphorylation profile to that of luteolin treated cells. Densitometric analysis reveals the ratio of PS1 p-CTF to CTF and ratio of holo-PS1 to Actin as indicated below the figures. A *t* test revealed significant differences between time points for the ratio of PS1 p-CTF to CTF ($p < 0.001$ with n = 3 for each condition). b, expression of PS1 CTFs was analyzed by western blot in cell lysates from SweAPP N2a cells transfected with siRNA targeting GSK-3α, β, or mock transfected 48 hours post-transfecion. Prior to experiments, siRNA knockdown efficiency >70% for GSK-3α, β was confirmed by Western blot analysis (data not shown). Densitometric analysis reveals the ratio of PS1 p-CTF to CTF as indicated below the each panel. A *t* test revealed significant differences between GSK-3α siRNA-transfected cells and GSK-3β siRNA or control (Mock transfected cells) ($p < 0.001$ with $n = 4$ for each condition) on the ratio of PS1 p-CTF to CTF. In addition, a *t* test also revealed significant differences between luteolin treated cells and GSK-3β siRNA or control (Mock transfeced cells) ($p < 0.001$ with n = 4 for each condition) on the ratio of PS1 p-CTF to CTF.

additionally that this 20 kDa phospho-PS1 CTF band may represent a less active or non-amyloidogenic form of γ-secretase.

4.3.4 GSK-3α regulates PS1-APP association in SweAPP N2a cells

Although previous study has linked GSK-3 inhibitors to reduced Aβ generation through the γ-secretase complex (Phiel et al., 2003), the manner in which this complex's activity is affected remains unclear. To clarify how phospho-PS1 CTF isoforms may regulate γ-secretase activity, cell lysates of luteolin, SB-415286, and GSK-3α siRNA treated SweAPP N2a cells were immunoprecipitated by PS1 antibody and probed for APP (Figure 4.5). As illustrated in panel a of Figure 4.5, the APP-PS1 association is significantly disrupted by not only luteolin and SB-415286 treatment, but also by GSK-3α siRNA. Moreover, this treatment mediated disruption has no correlation to full-length APP levels (Figure 4.5b). This analysis suggests that treatment has little effect on APP expression/trafficking. Thus, it is likely that GSK-3α or, more specifically, downstream phosphorylation of the PS1 CTF plays an essential role in regulating the association of γ-secretase complex with its APP substrate.

4.3.5 Luteolin treatment reduces GSK-3 activation and results in reduction of Aβ pathology in Tg APP_{sw} mice

To validate the above findings *in vivo*, 8 month-old Tg APP_{sw} mice were treated with 20 mg/kg luteolin administered by daily intraperitoneal injection for 30 days. Brain homogenates from these mice were subsequently analyzed by immunoprecipitation,

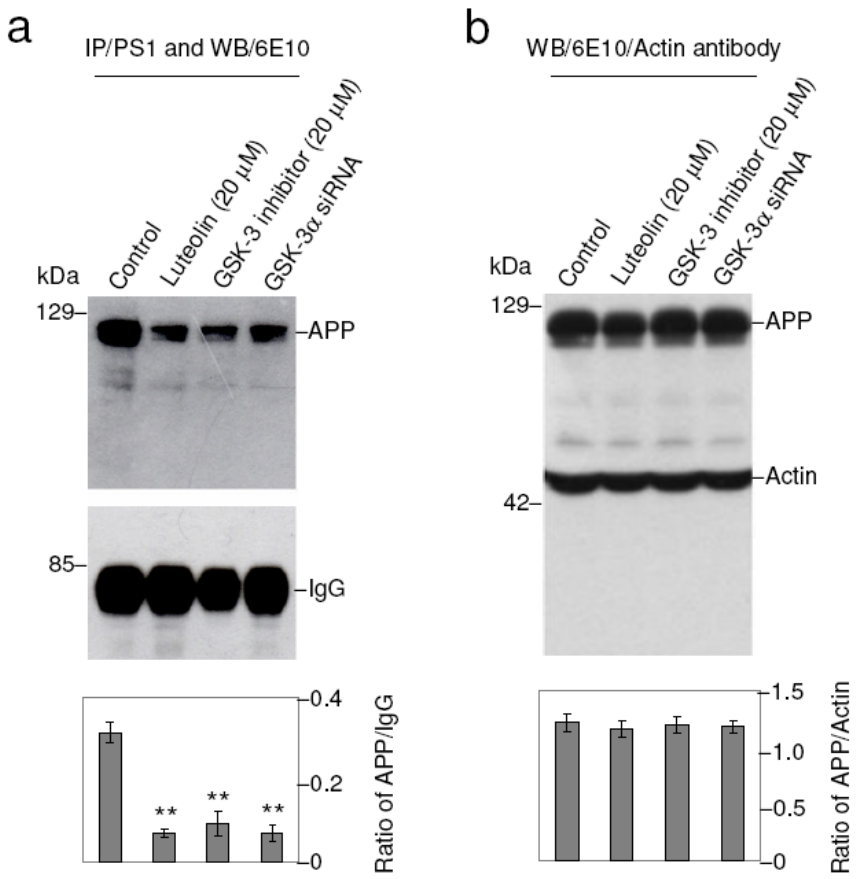

Figure 4.5

GSK-3α regulates PS1-APP association. SweAPP N2a cells were treated with either luteolin (20 μm) SB-415286 (20 μm) for 4 hours. Cell lysates from these treated cells and GSK-3α siRNA-transfected cells were subsequently analyzed by immunoprecipitation/western blot. a, lysates were immunoprecipitated by anti-PS1 CTF antibody. Densitometric analysis of western blot by 6E10 antibody reveals the ratio of APP to IgG as indicated below panel a. A *t* test revealed significant differences between all treatments and control ($p < 0.001$ with $n = 3$ for each condition). b, cell lysates were analyzed by western blot by 6E10 antibody. Densitometric analysis of western blot by anti-Actin antibody reveals no significant changes in the ratio of APP to Actin as indicated below panel b ($p > 0.05$).

western blot, and ELISA (Figure 4.6). As shown in panel a of Figure 4.6, both GSK-3α/β active isoforms from the homogenates of luteolin treated mice are reduced when compared to control. Moreover, ratios of each phosphorylated GSK-3 isoform to its respective total protein revealed a significant decrease in activation with treatment (Figure 4.6a). These decreases in activation are also apparent in the immunohistochemical analysis of GSK-3α/β activity in neurons of the CA1 region of the hippocampus and regions of the cingulate cortex (Figure 4.6c). Western blot analysis of PS1 from treated mice interestingly shows significantly lower levels of PS1 processing by CTF to Actin ratios (Figure 4.6b). To further confirm luteolin's mechanism in this model, brain homogenates were immunoprecipitated by PS1 antibody and probed for APP. As expected, luteolin treatment effectively abolished the PS1-APP association (Figure 4.6d). In addition, no significant changes in holo-APP expression following treatment were observed. Interestingly, a potential decrease in oligomeric forms of Aβ was detected as illustrated in panel e of Figure 4.6. Finally, to assess this potential decrease, ELISA of both soluble and insoluble $A\beta_{1\text{-}40,\,42}$ was conducted (Figure 4.6f). Luteolin treatment markedly reduced both soluble isoforms of Aβ by 25% and 49%, respectively (Figure 4.6f). Although no such significant reductions in insoluble Aβ isoforms were evident (Figure 4.6f), one would expect this result given the age and consequent low plaque burden of these Tg APP_{sw} mice. All together, the above lines of evidence suggest luteolin treatment can attenuate ongoing AD pathology *in vivo* and does so through GSK-3-mediated regulation of PS1/γ-secretase activity.

4.3.6 Oral administration of diosmin reduces Aβ pathology in Tg APP_{sw} mice

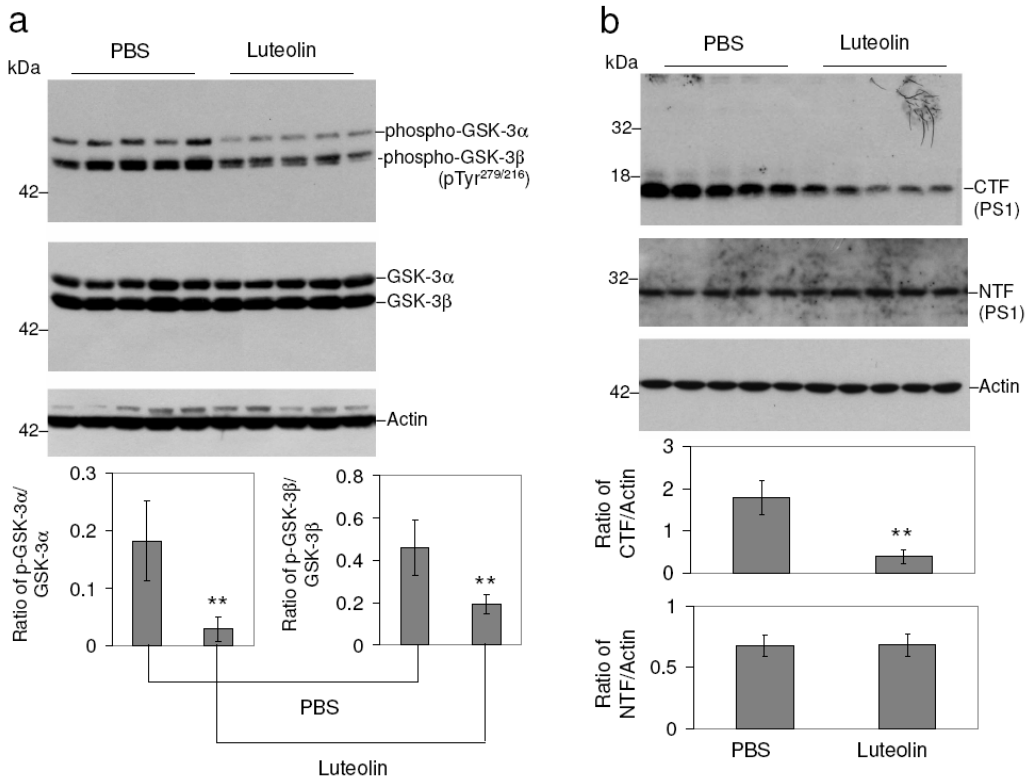

Figure 4.6a and b

Luteolin treatment reduces GSK-3 activation and PS1 CTF expression in Tg APP_{sw} mice. Brain homogenates from Tg APP_{sw} mice treated with luteolin (n = 5) or vehicle (PBS, n = 5). a, homogenates were analyzed by western blot with active and holo anti-GSK-3 antibodies with anti-Actin antibodies as an internal control. Densitometric analysis reveals the ratio of active phosphorylated GSK-3α/β to holo-GSK-3. A t test reveals significant reductions in both active GSK-3α and β isoforms from luteolin treated animals compared to control (p <0.001). b, homogenates were analyzed by western blot with anti-PS1 CTF or NTF antibody. Densitometric analysis reveals the ratio of PS1 CTF or NTF to Actin (internal control). A t test shows significant reductions in PS1 CTF levels with luteolin treatment (p <0.001), but not for PS1 NTF levels (p > 0.05).

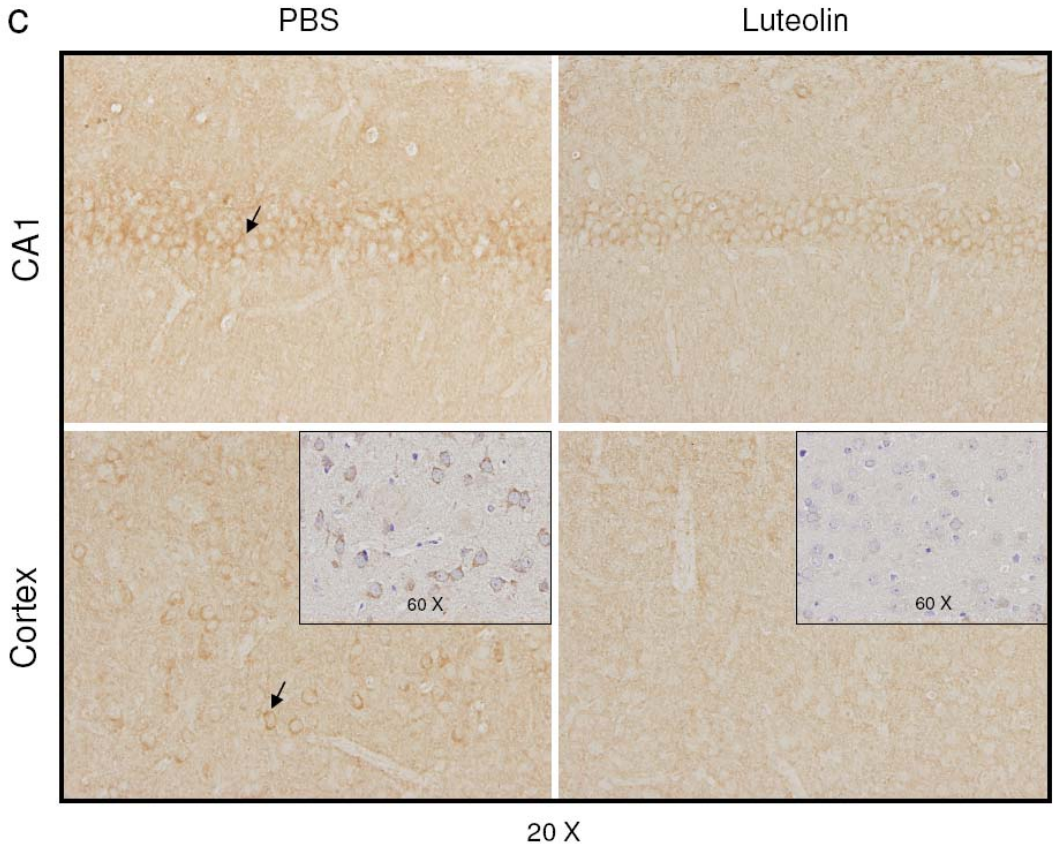

Figure 4.6c

Luteolin treatment reduces GSK-3 activation in Tg APP_{sw} mice. Brain sections from Tg APP_{sw} mice treated with luteolin (n = 5) or vehicle (PBS, *n* = 5). c, immunochemistry staining analysis for active phosphorylated GSK-3α/β.

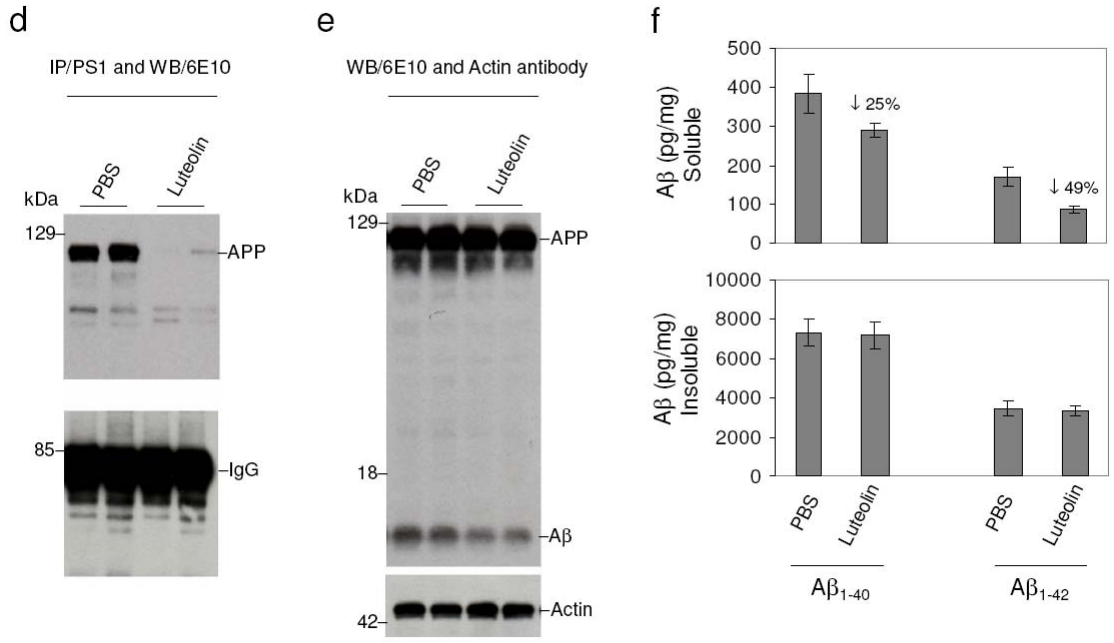

Figure 4.6d-f

Luteolin treatment inhibits PS1-APP association and results in reduction of Aβ pathology in Tg APP_{sw} mice. Brain homogenates from Tg APP_{sw} mice treated with luteolin (n = 5) or vehicle (PBS, n = 5). d, homogenates were immunoprecipitated by anti-PS1 CTF antibody. Densitometric analysis of western blot by 6E10 antibody reveals the ratio of APP to IgG. A t test revealed significant differences between luteolin treatment and control (p <0.001). e, homogenates were analyzed by western blot by 6E10 antibody. Approximately 12 kDa band may represent oligomeric form of amyloid. Densitometric analysis of western blot by anti-Actin antibody reveals no significant changes in the ratio of APP to Actin. f, soluble and insoluble $A\beta_{1\text{-}40,\ 42}$ peptides from homogenates were analyzed by ELISA. For Aβ ELISA, data are represented as picograms of peptide present in milligrams of total protein. Luteolin treatment results in markedly reduced soluble $A\beta_{1\text{-}40,\ 42}$ levels, 25% and 49%, respectively (top panel). No significant reductions in insoluble Aβ isoforms following treatment were observed (bottom panel).

Previous pharmacokinetic studies suggest luteolin has an oral bioavailability < 2% and a half-life in plasma < 4 hrs, which would make it a poor candidate compound for oral clinical trials (Shimoi et al., 1998; Wittemer et al., 2005). Taking this situation into consideration, other compounds with a 5,7-dihydroxyflavone structural backbone were screened to identify a more suitable flavonoid for oral administration (Figure 4.7). One compound, diosmetin, proved to be just as efficacious as luteolin in promoting PS1 CTF phosphorylation and consequently inhibiting γ-secretase activity in SweAPP N2a cells (data not shown). Cova and colleagues (1992) reported that the flavonoid diosmin, a well-evidenced vascular protecting agent, is rapidly transformed by intestinal flora to its aglycone form, diosmetin. Taken in this manner, diosmetin was found to be readily absorbed and rapidly distributed throughout the body with a plasma half-life > 26 hrs (Cova et al., 1992). To determine whether oral administration of diosmin, as a parent compound for diosmetin, could have similar anti-amyloidogenic effects *in vivo* as luteolin, Tg APP_{sw} mice were orally treated with 0.05% diosmin supplemented or control diet at 8 months of age for 6 months. As shown in Figure 4.8, diosmin treatment similarly reduced cerebral amyloidosis in these mice. Image analysis of micrographs from Aβ antibody (4G8) stained sections reveals that plaque burdens were significantly reduced throughout the brain (Figure 4.8a,b). To verify the findings from these coronal sections, brain homogenates for Aβ levels were analyzed by ELISA. Again, diosmin oral treatment markedly decreased both soluble and insoluble forms of $A\beta_{1\text{-}40,\,42}$ (Figure 4.8c). Taken together, the above data confirm an oral route of administration of diosmin

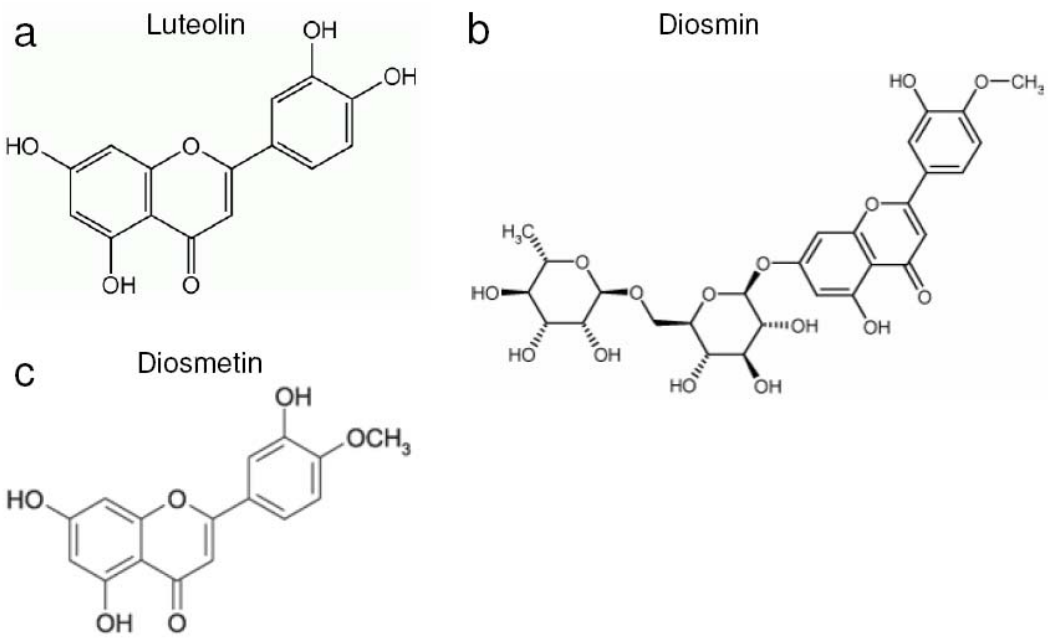

Figure 4.7

Chemical structures of the 5,7-dihydroxyflavone compounds.

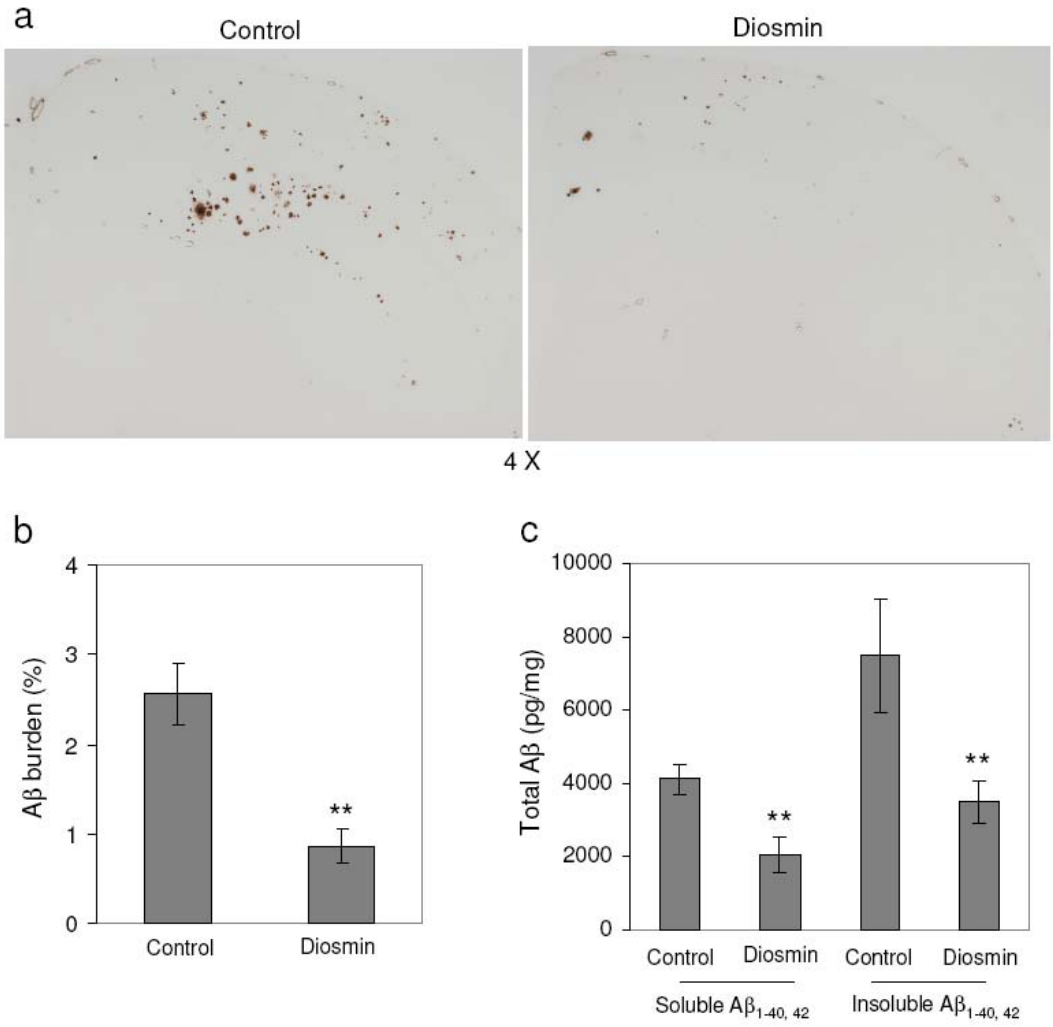

Figure 4.8

Oral administration of diosmin reduces Aβ pathology in Tg APP_{sw} mice. Brain homogenates and sections from Tg APP_{sw} mice treated with 0.05% diosmin supplemented diet (n = 10) or control diet (n = 10). a, half-brain coronal sections were analyzed by Aβ antibody, 4G8 staining. b, percentage of 4G8 positive plaques (mean ± SEM) was quantified by image analysis. A *t test* for independent samples revealed significant differences ($p < 0.001$) between groups. c, total soluble and insoluble $Aβ_{1\text{-}40,\ 42}$ peptides from homogenates were analyzed by ELISA. For Aβ ELISA, data are represented as picograms of peptide present in milligrams of total protein. Diosmin treatment results in markedly reduced total soluble and insoluble $Aβ_{1\text{-}40,\ 42}$ levels, 37% and 46%, respectively. A *t test* for independent samples revealed significant differences ($p < 0.005$) between groups.

provides effective, if not superior, attenuation of amyloid pathology comparable to that of intraperitoneal injected luteolin.

4.4 Conclusions

The studies detailed in this chapter qualify the flavonoid luteolin, and structurally similar compounds diosmetin and disomin, as effective anti-amyloidogenic agents. Treatment with luteolin reduces Aβ generation in both APP_{sw} overexpressing primary neurons and neuron-like cells. Interestingly, luteolin induces changes consistent with GSK-3 inhibition that decrease amyloidogenic γ-secretase APP proteolysis and promote PS1 CTF phosphorylation. Following investigation of the contribution of GSK-3 in this mechanism, data revealed that GSK-3α activity was essential for both PS1 CTF phosphorylation and PS1-APP interaction. As validation of these findings *in vivo*, luteolin, when applied to the APP_{sw} mouse model of AD, decreased soluble Aβ levels, reduced GSK-3 activity, and disrupted PS1-APP association. In addition, Tg APP_{sw} mice treated with diosmin, a glycoside of diosmetin, display significantly reduced Aβ pathology. Taken together, these data suggest GSK-3 inhibition is a viable therapeutic approach for AD by impacting PS1 phosphorylation-dependent regulation of amyloidogenesis.

CHAPTER 5

DISCUSSION

5.1 EGCG-mediated non-amyloidogenic APP proteolysis

Previous reports have shown that green tea components such as EGCG have neuroprotective properties; however, a clear cellular/ molecular mechanism underlying these effects has hitherto not been established (Mandel et al., 2004). The studies detailed in Chapter 3 show that EGCG promotes non-amyloidogenic APP proteolysis *in vitro* and *in vivo*, and that it accomplishes this by promoting α-secretase activity. A previous study by Jeong and colleagues (2003) suggested that EGCG might act as a β-secretase inhibitor in a cell-free system, raising the possibility that EGCG-mediated inhibition of Aβ generation may be accomplished via direct blockade of BACE activity. To address this possibility, SweAPP N2a cells were treated with the BACE inhibitor (data not shown). Importantly, treatment with an effective concentration of the inhibitor failed to mimic the increased α-CTF and sAPP-α levels observed following EGCG treatment. Rather, it appears that there may actually be a slight increase in β-secretase activity, as depicted in Figure 3.2a and c. This increase may be an indication of the extent of competition for APP between the two pathways or an effect of the underlying anti-amyloidogenic mechanism of EGCG.

While both TACE/ADAM17 and ADAM10 were implicated as the potential α-secretase affected by EGCG, the induction of TACE/ADAM17 appears to be transient. In addition, TACE/ADAM17 protein levels were not significantly altered in brain

homogenates derived from EGCG treated Tg APP_{sw} mice (data not shown). However, TAPI-1, a TACE/ADAM17 inhibitor, significantly attenuated the effect of EGCG on promoting α-secretase cleavage of APP. This inhibition may be explained by the possibility of off-target effects of TAPI-1, namely by inhibiting ADAM10. The transient role of TACE/ADAM17 may also be an effect of the underlying anti-amyloidogenic mechanism of EGCG. It is well known that TACE/ADAM17 is a multifunctional molecule that has been shown to be critically involved in TNF-α maturation associated with pro-inflammatory responses (Moro et al., 2003). Because TACE/ADAM17 has not been shown to exhibit substrate preference for TNF-α versus APP, EGCG may also transiently, via increasing TACE/ADAM17 levels, promote TNF-α maturation and release in cultured primary murine microglial cells. Interestingly, no elevation of TNF-α levels were detectable in cultured media from primary microglial cells (data not shown). This observation is consistent with other reports, in which EGCG treatment actually inhibits TNF-α expression and subsequently neuronal damage (Suganuma et al., 2000; Li et al., 2004). Because microglia must first undergo coordinated activation in response to innate immune stimuli to cleave pro-TNF-α and subsequently secrete TNF-α, a likely explanation for why EGCG does not elicit TNF-α release from murine microglia is that it does not trigger microglial activation and may in fact be immunosuppressive.

Upon further examination it was clear that EGCG treatment primarily induced increases in ADAM10 maturation. Moreover, these elevations even persisted after 18 hours (data not shown), thereby differentiating the effect of EGCG on ADAM10 from the more transient (less than 5 h) effect on TACE/ADAM17. This robust increase in mature ADAM10 agrees with studies conducted by Stoeck and colleagues (2006), suggesting

that TACE/ADAM17 displays transient "inducible" activity mediated by protein kinase C activation, whereas ADAM10 achieves inducible and "constitutive" activity for substrate processing. Indeed, EGCG induced dramatic increases in ADAM10 maturation after only 30 minutes and through to 2 hours, at which time there was a drop off in pro-ADAM10 isoforms. These data in combination with semi-quantitative RT-PCR analysis of ADAM10 RNA expression suggested that EGCG activated ADAM10 predominantly at the post-translational level, possibly through the proteolysis of this zymogen pro-form. Curiously, whereas the ~75 kDa form of ADAM10 is reduced in N9 microglia cells (Figure 3.5a) and nearly absent from primary cells (Figure 3.5b), it does not significantly change after EGCG treatment and could represent a previously reported ADAM10 non-glycosylated isoform (Chubinskaya et al., 2001; Reiss et al., 2005).

Initial data, and reports by others (Asai et al., 2003; Selkoe, 2001) suggesting that one or multiple ADAM family members play(s) dominant roles in inducible and/or constitutive methods of substrate processing, also led to the examination of which of the putative α-secretases analyzed here were required and whether inter-α-secretase modulation (Cisse et al., 2005) was involved in EGCG-mediated non-amyloidogenic APP proteolysis. As expected, siRNA knockdown of ADAM10 primarily blocked EGCG induction of APP α-secretase metabolism (Figure 3.8a,b). In addition, siRNA knock-down of TACE/ADAM17 also slightly inhibited EGCG modulation of APP metabolism (Figure 3.5a), again in accordance with the previous findings of the transient role of TACE/ADAM17. These observations, coupled with the findings that anti-ADAM10 siRNA failed to affect ADAM9 or -17 protein levels (Figure 3.7d), greatly diminishes the probability of the involvement of intermolecular regulation between ADAMs as a

contributing factor in EGCG-mediated APP metabolism. Thus, whereas ADAM9 and/or -17 may play minor or transient roles in EGCG modulation of APP metabolism, ADAM-10 appears to be the major downstream effector.

Mechanisms governing ADAM10 activation are currently not fully understood, yet studies have implicated PC family members, particularly furin and PC7 (Anders et al., 2001), as mediators of proteolytic activation of ADAM10. Additionally, maturation of various matrix metalloproteases (MMPs) has been reported to be PI3K-dependent (Zahradka et al., 2004). Accordingly, EGCG-mediated ADAM10 maturation appears to involve both furin and PI3K. These findings suggest that furin activates ADAM10 in the TGN, as PI3K inhibition may prevent appropriate vesicular trafficking. Interestingly, furin is also involved in proteolysis of the N-glycosylated zymogen/pro-form of BACE and TACE/ADAM17, which may explain the transient increases in the activity both of these enzymes following EGCG treatment (Anders et al., 2001; Annaert and De Strooper, 2002). Additionally, overexpression of full-length BACE reduces sAPP-α while driving β-CTF production, and only moderately increases Aβ formation; whereas overexpression of mature BACE results in dramatic increases in Aβ production (Benjannet et al., 2001; Bennett et al., 2000). Altogether, these data suggest an attractive notion whereby furin may be rate-limiting for the proteolytic activation of both BACE and α-secretases. Accordingly, imbalances in substrate processing by furin could represent a mechanism of disease.

Direct and/or indirect molecular interactions between EGCG and ADAM10 remain to be determined. As EGCG is an ampiphatic small molecule, it is very likely that it reaches its molecular target by passive diffusion through cell membranes. This means

of cellular uptake may explain the rapid onset of ADAM10 maturation observed following EGCG treatment (Figure 3.4c) and suggests an intracellular molecular target, such as PI3K. On the other hand, cell surface receptor interactions have also been suggested (Fujimura et al., 2005; Rodriguez et al., 2006) and may also involve PI3K signaling. However, as both furin activity and PI3K signaling appear to be mutually exclusive it is likely that EGCG may affect multiple cellular targets, likely owing this phenomenon to its pleiotropic nature. Future studies will be needed to further establish the molecular mechanism(s) whereby furin and PI3K regulate EGCG-mediated ADAM10 maturation and enhancement of non-amyloidogenic APP proteolysis.

5.2 5,7-Dihydroxyflavone-mediated PS1 CTF phosphorylation

Although previous reports have substantiated the therapeutic potential of GSK-3 inhibitors in AD (Engel et al., 2006; Hong et al., 1997; Munoz-Montano et al., 1997; Phiel et al., 2003) the underlying anti-amyloidogenic mechanisms have hitherto not been established. Through the studies detailed in Chapter 4 a mechanism is elucidated whereby these GSK-3 inhibitors may reduce amyloidosis. It is apparent that reductions in GSK-3α activation, whether achieved by pharmacological means or by genetic silencing, promoted the phosphorylation of the CTF of PS1, which subsequently disrupted the enzyme-substrate association with APP. As *in vitro* validation, significant increases in PS1 CTF phosphorylation (20 kDa isoforms) were observed following luteolin, SB-415286, and GSK-3α RNAi treatment, which act with similar potentcy (luteolin and SB-415286) and efficacy (Fig. 4.4). Moreover, both *in vitro* and *in vivo* analysis revealed significant reductions in APP co-immunoprecipitated with PS1

following treatment (Figure 4.5a,b and Figure 4.6d,e). Accordingly, it is fair to expect the concentration and time dependent reductions in $A\beta_{1\text{-}40,\,42}$ generation following treatment that were observed in Figure 4.1e and f. Even though it is apparent that γ-secretase activity also concentration and time dependently decreased (Figure 4.1e,f), it is unclear how this protein complex is affected. GSK-3α inhibition may potentially affect complex formation; however, no changes in the expression of PS1, nicastrin, PEN2, or APH-1 were observed following treatment (data not shown). Furthermore, GSK-3α inhibition did not appear to phosphorylate full-length PS1 and did not affect endoproteolytic cleavage based on PS1 NTF analysis (Figure 4.3c). Although no phospho-PS1 CTFs species were detected *in vivo*, there were clear reductions in the 16 kDa PS1 CTF bands (Figure 4.6b), which are presumably indicative of a more highly active, amyloidogenic γ-secretase complex. Therefore, it is likely that these compounds affect γ-secretase at the level of the CTF of PS1. However, it remains to be seen if phosphorylation of the CTF of PS1 is a required step for γ-secretase inhibition/Aβ reduction mediated by luteolin. There are some obvious complexities to the mechanism of dimerization of PS1 along with subsequent association with other essential γ-secretase components such as nicastrin, which recent studies suggest may function as the γ-secretase substrate receptor (Shah et al., 2005). Accordingly, it will now be important to determine at what residue(s) this 20 kDa phospho-PS1 CTF is phosphorylated and subsequently how it interacts with PS1 NTFs or nicastrin.

Some of the earliest work investigating the activity of PS1 endoproteolytic fragments and the oligomerization of the γ-secretase complex has already identified two

human phosphorylated PS1 CTFs (Seeger et al., 1997; Walter et al., 1997). What is more, the presence of these aforementioned phosphorylated PS1 CTFs corresponded with both reduction of Aβ generation and accumulation of the β-CTF of APP (Buxbaum et al., 1990; Seeger et al., 1997; Walter et al., 1997), which is evidenced following luteolin treatment (Fig. 1). It is also important to note that the accumulation β-CTFs following luteolin treatment is a mere fraction of that seen when compared to the use of a direct γ-secretase inhibitor (data not shown). In view of this finding, it becomes increasingly evident that selective GSK-3 inactivation may be a less toxic, more regulative, substrate-specific mode of γ-secretase inhibition. Given the fact that the above earlier studies routinely employed the use of phorbol-12,13-dibutyrate (PDBu), a potent PKC activator, as their phosphorylating agent (Buxbaum et al., 1990; Seeger et al., 1997; Walter et al., 1997) it was possible that luteolin was similarly acting as a PKC activator, rather than a GSK-3 inhibitor. Co-treatment of SweAPP N2a cells with luteolin or SB-415286 and the PKC inhibitor GF109203X had no effect on GSK-3 inhibition (data not shown). However, minor decreases in both 20 kDa and 18 kDa phospho-PS1 CTF isoforms following GF109203X treatment were observed, indicating that PKC may play a part either in the downstream signaling mechanism or by directly phosphorylating the PS1 CTF (data not shown). Additionally, there were no indications that GSK-3α inhibition affected non-amyloidogenic proteolysis of APP as luteolin, SB-415286, and GSK-3α RNAi treatment had no effect on the maturation of TACE/ADAM17, ADAM10, or sAPP-α release (data not shown), which are all strongly associated with PKC activation (Buxbaum et al., 1998; Checler, 1995; Hung et al., 1993; Lopez-Perez et al., 2001).

Collectively, these data suggest that GSK-3α may be an upstream regulator of PS1 CTF phosphorylation and consequently of γ-secretase activity.

However, it must be noted that although changes consistent with GSK-3 inhibition following luteolin treatment were observed, it remains unclear whether or not this flavonoid is a direct inhibitor of this kinase. What seems to be evident, and a point at which it potentially differs from direct GSK-3 inhibitors (including SB-415286), is that luteolin treatment appears to preferentially inactivate GSK-3α isoforms over β isoforms (Figure 4.2). That is to say, luteolin treatment did appear to reduce active GSK-3β isoforms expressed at about 2 hours (Figure 4.2b,e), as compared to control (data not shown), but expression of active GSK-3α isoforms was more timely and effectively reduced (Figure 4.2b,e). Remarkably, β-catenin remained unaffected by luteolin treatment, which may imply that this selective GSK-3 inactivation can circumvent the potential toxicity of more general GSK-3 inhibitors, which may inhibit Notch cleavage (data not shown). Furthermore, there was a clear correlation between increases in inactive and decreases in active GSK-3α (Figure 4.2c,f) following treatment, which suggests that luteolin may affect the positive feedback loop of GSK-3 activation by inactivating the PP1 phosphatase (Hirano et al., 2004). The direct targeting of this feedback loop as a means to reduce GSK-3 activation seems highly probable in light of the fact that calyculin A, a PP1 inhibitor, treatment has previously been found to increase PS1 CTF phosphorylation (Buxbaum et al., 1990). Future studies will be needed to further establish the molecular mechanism(s) whereby luteolin and diosmetin regulate GSK-3 activity and consequently γ-secretase APP proteolysis.

5.3 Potential of flavonoids as therapeutic interventions for AD

5.3.1 EGCG

Green tea contains numerous flavonoids and studies that have shown therapeutic benefits of green tea generally do not identify the active component(s) responsible. While EGCG promoted non-amyloidogenic proteolysis of APP, other flavonoids, including GC and C, actually opposed this effect (Figure 3.1c and Figure 3.2f). This finding suggests that the mixture of these flavonoids as found in whole green tea may actually prevent or mask the beneficial properties of EGCG and may explain why research involving green tea extracts or combinations of flavonoids results with such variable findings (Chung et al., 2003). Furthermore, these findings may lead to the generation of "optimized" green tea extracts, which yield the greatest therapeutic benefit for AD. However, it may remain that a purified nutraceutical-grade formulation of EGCG possesses the most efficacious anti-amyloidogenic properties.

While studies described in Chapter 3 confirm the promotion of non-amyloidogenic APP proteolysis and the consequent reductions in cerebral amyloidosis in intracerebroventricular, intraperitoneal, and orally EGCG treated Tg APP_{sw} mice, they also suggest another potential means of neuroprotection afforded by EGCG treatment, a reduction of potentially toxic sarkosyl-soluble phospho-tau isoforms. Despite the lack of evidence for tangle formation and neuronal loss as mediators of cognitive impairment in Tg APP_{sw} mice, this AD model remains a useful tool in understanding the basis of tau hyperphosphorylation. Furthermore, it is probable that soluble hyperphosphorylated isoforms are ultimately the neurotoxic species of tau (Dickey et al., 2007; Kosik and

Shimura, 2005). Results clearly validate this possibility when comparing the high soluble tau profiles of non-treated Tg APP_{sw} mice to the much lower profiles of treated Tg APP_{sw} mice, which were nearly identical to the NT animals. It may also be likely that the P3 insoluble bands are comprised of less toxic ubiquinated phospho-tau isoforms, as ubiquination has been previously found to shift soluble phosphorylated tau to insoluble fractions (Kosik and Shimura, 2005). This shift may explain the elevated levels of insoluble phospho-tau present in EGCG-treated and NT animals in relation to non-treated Tg animals, as well as represent the basis of a biological means of compensating for an abundance of toxic soluble phospho-tau isoforms (Figure 3.14). In a recent study by Dickey and colleagues (2007), heat shock protein 90 (HSP90) inhibitors were found to reduce levels of soluble phospho-tau isoforms by promoting turnover through an increased rate of ubiquination and degradation via carboxy terminus of Hsp70-interacting protein (CHIP). Interestingly, EGCG has been found to inhibit the activity of HSP90 by directly binding to this chaperone protein (Palermo et al., 2005). For these reasons, it may now be important to investigate CHIP-mediated ubiquination and HSP90 inhibition as the means whereby EGCG modulates neurotoxic phospho-tau isoforms.

In addition to demonstrating the ability of chronic EGCG administration to decrease brain levels of soluble hyperphosphorylated tau, these were the first studies demonstrating that EGCG can have marked cognitive benefits in a transgenic model for AD. Consistent with the findings detailed here, Haque and colleagues (2006) have reported that rats given drinking water high in green tea catechins (mostly EGCG) for 5 months showed less memory impairment following intracerebroventricular injection of $A\beta_{1-40}$ compared to those given normal drinking water. Here, in a similar 6 month oral

administration of EGCG to Tg APP_{sw} mice not only reduced both cerebral amyloidosis in cognitively-important brain areas, but also improved working memory performance to a flawless/errorless level by the end of testing. Since prior studies have clearly shown a strong and presumably causative relationship between brain Aβ levels and impaired memory in the RAWM task (Arendash et al., 2001; Leighty et al., 2004), the ability of orally administered EGCG to improve upon the already good RAWM performance of Tg APP_{sw} is most probably related in part to the anti-amyloidogenic effect of this treatment through enhancement of α-secretase activity.

Indeed, the presently reported decreases in cerebral amyloidosis mediated by chronic oral administration of EGCG are comparable to those induced by intraperitoneal administration. Yet, the cognitive benefits of intraperitoneal EGCG administration were more profound than those provided by oral EGCG administration, despite Tg animals in both treatment paradigms being testing at the same 14 month age. This is most likely due to the greater cognitive impairment manifested by the inbred Tg APP_{sw} mice on a mixed C57/B6/SJL/SW background (given intraperitoneal injected EGCG) compared to the Tg2576/Taconic mice on a B6/SJL background (given orally administered EGCG). Even in advanced age, mice primarily bearing a B6 background are unusually capable performers in spatial tasks (King and Arendash, 2002). Thus, the mutant APP_{sw} transgene had not fully penetrated this B6 background by 14 months of age, resulting in maintained RAWM performance in Tg controls. By contrast, it has been previously reported that the inbred Tg APP_{sw} mice exhibit cognitive impairment by 6–8 months of age, before Aβ deposition is even evident (Arendash et al., 2004, 2006). In the intraperitoneal study, inbred Tg APP_{sw} mice began treatment at 12 months of age, long

after they typically display cognitive impairment. Therefore, the substantial cognitive benefits seen after 2 months of treatment suggest that EGCG could be an effective treatment for established Alzheimer's disease cases. Importantly and consequently, both intraperitoneal and oral administration of EGCG provided cognitive benefit to AD transgenic mice, suggesting oral EGCG treatment as a viable therapeutic approach against AD pathology and associated cognitive impairment.

Major difficulties in preparing an effective therapeutic formulation of EGCG for clinical trial stem from both the inherent differences in its metabolism between rodents and humans as well as its poor oral bioavailability. For example, in one study that was employed to formulate the concentration of EGCG in the drinking water, Lambert and colleagues (2003) reported the oral bioavailability of free/unconjugated EGCG in mice < 1% for a singly gavaged dose of 75 mg/kg. Furthermore, they found a large part (50–90%) of orally administered EGCG became rapidly conjugated due to its exposure to respective enzymes in the liver and small intestine (Lambert et al., 2003). In an earlier study by Suganuma and colleagues (1998), EGCG was found to be primarily composed of free/unconjugated EGCG in various tissues (including the brain) following gavage, whereas the blood/plasma was composed of mostly conjugated forms. This study also confirmed the blood - brain barrier permeability of EGCG. Conjugation of EGCG, which includes methylation, glucuronidation, and sulfation, unfortunately reduces its half-life from 18 hours down to < 4 hours. This conjugation is a limiting factor in both mice and rats. On the other hand, human patients orally treated with EGCG present primarily free EGCG (unconjugated ~77-100%), but still evidence its poor oral bioavailability (< 1%)

(Lee et al., 2002). The potential effects of metabolites aside, the animal studies conducted may be quite reflective and relevant to the human condition.

Importantly, the administration of EGCG in drinking water, wherein Tg APP_{sw} mice were continuously taking in EGCG, would appear to have circumvented its poor oral bioavailability, as these mice evidenced both reduced cerebral amyloidosis and cognitive benefit. However, Tg APP_{sw} mice treated via intraperitoneal injection presumably distribute free/unconjugated EGCG into the brain, where its direct action occurs, more efficiently than oral administration because this route avoids first pass metabolism. Whether this potential difference between intraperitoneal and oral administration in the levels of free/unconjugated EGCG truly affects cognitive benefit remains to be determined. Taking the aforementioned studies into account, along with the fact that orally treated Tg APP_{sw} mice received a dose spread throughout the daily consumption of their drinking water, it is obvious that single-dose administration of EGCG (gavaged or injected) would yield higher effective concentrations in these animals. Therefore, when considering application in human clinical trials, a single oral bolus of EGCG may be an effective dosing paradigm. Based on the faster metabolic rate of mice, the doses employed in both the intraperitoneal and oral studies would be equivalent to a ~ 1500 mg of EGCG daily intake in humans. Although not administered on a chronic basis, oral doses of similar magnitudes have been used in clinical trial (Ullmann et al., 2003). Taken together, these data prompt the need for future clinical trials with a purified nutraceutical grade-EGCG or its structural analogs, which may demonstrate more effective anti-amyloidogenic properties or possess better bioavailabilities.

5.3.2 5,7-Dihydroxyflavones

Although luteolin treatment markedly reduced both soluble $A\beta_{1\text{-}40,\ 42}$ isoforms *in vivo* (Figure 4.6f), its poor bioavailability makes it less attractive as a potential nutraceutical for opposing AD pathogenesis. Like many aglycone forms of flavonoids, luteolin potentially reaches its molecular target by passive diffusion through cell membranes. This means of cellular uptake may explain the rapid onset of GSK-3α inactivation as observed following luteolin treatment (Figure 4.2a,d) and, along with findings in Figure 4.6, may indicate favorable blood - brain barrier permeability. It would also appear that diosmetin, via its parent compound diosmin, may possess favorable blood - brain barrier permeability as Aβ pathology is markedly reduced in treated Tg APP_{sw} mice (Figure 4.8). A micronized nutraceutical formulation of diosmin, under the trade name Daflon, has been both safely and effectively used to treat chronic venous disease and hemorrhoids for over a decade in Europe. Recently, improved formulations of diosmin have been marketed in both Europe and the United States for treatment of varicose and spider veins. However, these newer formulations may not actually improve efficacy of diosmin, as diosmetin is likely the active compound responsible for this nutraceutical's therapeutic attributes. At the same time, clinical study evaluating diosmin and its various formulations has already laid the groundwork for future AD clinical trial. Based on the faster metabolic rate of the Tg APP_{sw} mice, the dose employed in the oral study would be equivalent to a ~1000 mg of diosmin daily intake in humans. Future pre-clinical studies may be warranted, though, to assess any cognitive benefits afforded by disomin/diosmetin treatment.

5.4 Conclusions

Currently there are few treatment options for AD. Furthermore, those that have been approved focus on the management of symptoms rather than the underlying pathological mechanisms of the disease. While attempts at rational drug design against amyloid pathology have appeared promising in pre-clinical studies, they have often fallen short in clinical trials. Accordingly, natural compounds, which have been proven in traditional medicine systems, are just beginning to be investigated as therapeutic interventions for AD. The studies contained herein demonstrate that such natural compounds can provide both neuropathologic, neurochemical, and cognitive benefits in AD transgenic mice. These findings strongly argue for their continued investigation as a safe and effective therapeutics against AD. Moreover, these flavonoids also proved to be invaluable tools for studying the cellular and molecular mechanisms of AD. If Aβ pathology in APP_{sw} models is representative of disease pathology in the clinical syndrome, then flavonoid administration to AD patients may be an effective prophylactic strategy for reduction of both cerebral amyloidosis and tau pathology. Ultimately, the identification of compounds that target multiple pathologies is essential for the formulation of effective therapeutic interventions. For these reasons, EGCG, luteolin, and diosmin/diosmetin may prove to be such effective compounds.

REFERENCES

Ahmed S, Rahman A, Hasnain A, Lalonde M, Goldberg VM, Haqqi TM (2002) Green tea polyphenol epigallocatechin-3-gallate inhibits the IL-1 beta-induced activity and expression of cyclooxygenase-2 and nitric oxide synthase-2 in human chondrocytes. Free Radic Biol Med 33:1097-1105.

Akiyama H, Barger S, Barnum S, Bradt B, Bauer J, Cole GM, Cooper NR, Eikelenboom P, Emmerling M, Fiebich BL, Finch CE, Frautschy S, Griffin WS, Hampel H, Hull M, Landreth G, Lue L, Mrak R, Mackenzie IR, McGeer PL, O'Banion MK, Pachter J, Pasinetti G, Plata-Salaman C, Rogers J, Rydel R, Shen Y, Streit W, Strohmeyer R, Tooyoma I, Van Muiswinkel FL, Veerhuis R, Walker D, Webster S, Wegrzyniak B, Wenk G, Wyss-Coray T (2000) Inflammation and Alzheimer's disease. Neurobiol Aging 21:383-421.

Aktas O, Prozorovski T, Smorodchenko A, Savaskan NE, Lauster R, Kloetzel PM, Infante-Duarte C, Brocke S, Zipp F (2004) Green tea epigallocatechin-3-gallate mediates T cellular NF-kappa B inhibition and exerts neuroprotection in autoimmune encephalomyelitis. J Immunol 173:5794-5800.

Allinson TM, Parkin ET, Turner AJ, Hooper NM (2003) ADAMs family members as amyloid precursor protein alpha-secretases. J Neurosci Res 74:342-352.

Alvarez G, Munoz-Montano JR, Satrustegui J, Avila J, Bogonez E, Diaz-Nido J (1999) Lithium protects cultured neurons against beta-amyloid-induced neurodegeneration. FEBS Lett 453:260-264.

Anders A, Gilbert S, Garten W, Postina R, Fahrenholz F (2001) Regulation of the alpha-secretase ADAM10 by its prodomain and proprotein convertases. Faseb J 15:1837-1839.

Anders L, Mertins P, Lammich S, Murgia M, Hartmann D, Saftig P, Haass C, Ullrich A (2006) Furin-, ADAM 10-, and gamma-secretase-mediated cleavage of a receptor tyrosine phosphatase and regulation of beta-catenin's transcriptional activity. Mol Cell Biol 26:3917-3934.

Annaert W, De Strooper B (2002) A cell biological perspective on Alzheimer's disease. Annu Rev Cell Dev Biol 18:25-51.

Aplin AE, Gibb GM, Jacobsen JS, Gallo JM, Anderton BH (1996) In vitro phosphorylation of the cytoplasmic domain of the amyloid precursor protein by glycogen synthase kinase-3beta. J Neurochem 67:699-707.

Arendash GW, Gordon MN, Diamond DM, Austin LA, Hatcher JM, Jantzen P, DiCarlo G, Wilcock D, Morgan D (2001) Behavioral assessment of Alzheimer's transgenic mice following long-term Abeta vaccination: task specificity and correlations between Abeta deposition and spatial memory. DNA Cell Biol 20:737-744.

Arendash GW, Lewis J, Leighty RE, McGowan E, Cracchiolo JR, Hutton M, Garcia MF (2004) Multi-metric behavioral comparison of APPsw and P301L models for Alzheimer's disease: linkage of poorer cognitive performance to tau pathology in forebrain. Brain Res 1012:29-41.

Arendash GW, Schleif W, Rezai-Zadeh K, Jackson EK, Zacharia LC, Cracchiolo JR, Shippy D, Tan J (2006) Caffeine protects Alzheimer's mice against cognitive impairment and reduces brain beta-amyloid production. Neuroscience 142:941-952.

Arendt T, Holzer M, Fruth R, Bruckner MK, Gartner U (1998) Phosphorylation of tau, Abeta-formation, and apoptosis after in vivo inhibition of PP-1 and PP-2A. Neurobiol Aging 19:3-13.

Asai M, Hattori C, Szabo B, Sasagawa N, Maruyama K, Tanuma S, Ishiura S (2003) Putative function of ADAM9, ADAM10, and ADAM17 as APP alpha-secretase. Biochem Biophys Res Commun 301:231-235.

Awasthi A, Matsunaga Y, Yamada T (2005) Amyloid-beta causes apoptosis of neuronal cells via caspase cascade, which can be prevented by amyloid-beta-derived short peptides. Exp Neurol 196:282-289.

Bae JH, Mun KC, Park WK, Lee SR, Suh SI, Baek WK, Yim MB, Kwon TK, Song DK (2002) EGCG attenuates AMPA-induced intracellular calcium increase in hippocampal neurons. Biochem Biophys Res Commun 290:1506-1512.

Barten DM, Meredith JE, Jr., Zaczek R, Houston JG, Albright CF (2006) Gamma-secretase inhibitors for Alzheimer's disease: balancing efficacy and toxicity. Drugs R D 7:87-97.

Bastianetto S (2002) Red wine consumption and brain aging. Nutrition 18:432-433.

Benjannet S, Elagoz A, Wickham L, Mamarbachi M, Munzer JS, Basak A, Lazure C, Cromlish JA, Sisodia S, Checler F, Chretien M, Seidah NG (2001) Post-translational processing of beta-secretase (beta-amyloid-converting enzyme) and its ectodomain shedding. The pro- and transmembrane/cytosolic domains affect its cellular activity and amyloid-beta production. J Biol Chem 276:10879-10887.

Bennett BD, Denis P, Haniu M, Teplow DB, Kahn S, Louis JC, Citron M, Vassar R (2000) A furin-like convertase mediates propeptide cleavage of BACE, the Alzheimer's beta -secretase. J Biol Chem 275:37712-37717.

Bernstein HG, Bukowska A, Krell D, Bogerts B, Ansorge S, Lendeckel U (2003) Comparative localization of ADAMs 10 and 15 in human cerebral cortex normal aging, Alzheimer disease and Down syndrome. J Neurocytol 32:153-160.

Brion JP, Anderton BH, Authelet M, Dayanandan R, Leroy K, Lovestone S, Octave JN, Pradier L, Touchet N, Tremp G (2001) Neurofibrillary tangles and tau phosphorylation. Biochem Soc Symp:81-88.

Busciglio J, Lorenzo A, Yeh J, Yankner BA (1995) beta-amyloid fibrils induce tau phosphorylation and loss of microtubule binding. Neuron 14:879-888.

Butterfield DA (2002) Amyloid beta-peptide (1-42)-induced oxidative stress and neurotoxicity: implications for neurodegeneration in Alzheimer's disease brain. A review. Free Radic Res 36:1307-1313.

Buxbaum JD, Gandy SE, Cicchetti P, Ehrlich ME, Czernik AJ, Fracasso RP, Ramabhadran TV, Unterbeck AJ, Greengard P (1990) Processing of Alzheimer beta/A4 amyloid precursor protein: modulation by agents that regulate protein phosphorylation. Proc Natl Acad Sci U S A 87:6003-6006.

Buxbaum JD, Thinakaran G, Koliatsos V, O'Callahan J, Slunt HH, Price DL, Sisodia SS (1998) Alzheimer amyloid protein precursor in the rat hippocampus: transport and processing through the perforant path. J Neurosci 18:9629-9637.

Calhoun ME, Wiederhold KH, Abramowski D, Phinney AL, Probst A, Sturchler-Pierrat C, Staufenbiel M, Sommer B, Jucker M (1998) Neuron loss in APP transgenic mice. Nature 395:755-756.

Camden JM, Schrader AM, Camden RE, Gonzalez FA, Erb L, Seye CI, Weisman GA (2005) P2Y2 nucleotide receptors enhance alpha-secretase-dependent amyloid precursor protein processing. J Biol Chem 280:18696-18702.

Capell A, Grunberg J, Pesold B, Diehlmann A, Citron M, Nixon R, Beyreuther K, Selkoe DJ, Haass C (1998) The proteolytic fragments of the Alzheimer's disease-associated presenilin-1 form heterodimers and occur as a 100-150-kDa molecular mass complex. J Biol Chem 273:3205-3211.

Carmichael J, Sugars KL, Bao YP, Rubinsztein DC (2002) Glycogen synthase kinase-3beta inhibitors prevent cellular polyglutamine toxicity caused by the Huntington's disease mutation. J Biol Chem 277:33791-33798.

Cataldo AM, Barnett JL, Berman SA, Li J, Quarless S, Bursztajn S, Lippa C, Nixon RA (1995) Gene expression and cellular content of cathepsin D in Alzheimer's disease

brain: evidence for early up-regulation of the endosomal-lysosomal system. Neuron 14:671-680.

Checler F (1995) Processing of the beta-amyloid precursor protein and its regulation in Alzheimer's disease. J Neurochem 65:1431-1444.

Chubinskaya S, Mikhail R, Deutsch A, Tindal MH (2001) ADAM-10 protein is present in human articular cartilage primarily in the membrane-bound form and is upregulated in osteoarthritis and in response to IL-1alpha in bovine nasal cartilage. J Histochem Cytochem 49:1165-1176.

Chung JH, Han JH, Hwang EJ, Seo JY, Cho KH, Kim KH, Youn JI, Eun HC (2003) Dual mechanisms of green tea extract (EGCG)-induced cell survival in human epidermal keratinocytes. Faseb J 17:1913-1915.

Chyu KY, Babbidge SM, Zhao X, Dandillaya R, Rietveld AG, Yano J, Dimayuga P, Cercek B, Shah PK (2004) Differential effects of green tea-derived catechin on developing versus established atherosclerosis in apolipoprotein E-null mice. Circulation 109:2448-2453.

Cirrito JR, May PC, O'Dell MA, Taylor JW, Parsadanian M, Cramer JW, Audia JE, Nissen JS, Bales KR, Paul SM, DeMattos RB, Holtzman DM (2003) In vivo

assessment of brain interstitial fluid with microdialysis reveals plaque-associated changes in amyloid-beta metabolism and half-life. J Neurosci 23:8844-8853.

Cisse MA, Sunyach C, Lefranc-Jullien S, Postina R, Vincent B, Checler F (2005) The disintegrin ADAM9 indirectly contributes to the physiological processing of cellular prion by modulating ADAM10 activity. J Biol Chem 280:40624-40631.

Citron M, Diehl TS, Gordon G, Biere AL, Seubert P, Selkoe DJ (1996) Evidence that the 42- and 40-amino acid forms of amyloid beta protein are generated from the beta-amyloid precursor protein by different protease activities. Proc Natl Acad Sci U S A 93:13170-13175.

Cleary JP, Walsh DM, Hofmeister JJ, Shankar GM, Kuskowski MA, Selkoe DJ, Ashe KH (2005) Natural oligomers of the amyloid-beta protein specifically disrupt cognitive function. Nat Neurosci 8:79-84.

Colciaghi F, Marcello E, Borroni B, Zimmermann M, Caltagirone C, Cattabeni F, Padovani A, Di Luca M (2004) Platelet APP, ADAM 10 and BACE alterations in the early stages of Alzheimer disease. Neurology 62:498-501.

Comery TA, Martone RL, Aschmies S, Atchison KP, Diamantidis G, Gong X, Zhou H, Kreft AF, Pangalos MN, Sonnenberg-Reines J, Jacobsen JS, Marquis KL (2005)

Acute gamma-secretase inhibition improves contextual fear conditioning in the Tg2576 mouse model of Alzheimer's disease. J Neurosci 25:8898-8902.

Cova D, De Angelis L, Giavarini F, Palladini G, Perego R (1992) Pharmacokinetics and metabolism of oral diosmin in healthy volunteers. Int J Clin Pharmacol Ther Toxicol 30:29-33.

Dai Q, Borenstein AR, Wu Y, Jackson JC, Larson EB (2006) Fruit and vegetable juices and Alzheimer's disease: the Kame Project. Am J Med 119:751-759.

De Felice FG, Velasco PT, Lambert MP, Viola K, Fernandez SJ, Ferreira ST, Klein WL (2007) Abeta oligomers induce neuronal oxidative stress through an N-methyl-D-aspartate receptor-dependent mechanism that is blocked by the Alzheimer drug memantine. J Biol Chem 282:11590-11601.

De Strooper B, Saftig P, Craessaerts K, Vanderstichele H, Guhde G, Annaert W, Von Figura K, Van Leuven F (1998) Deficiency of presenilin-1 inhibits the normal cleavage of amyloid precursor protein. Nature 391:387-390.

Deane R, Wu Z, Sagare A, Davis J, Du Yan S, Hamm K, Xu F, Parisi M, LaRue B, Hu HW, Spijkers P, Guo H, Song X, Lenting PJ, Van Nostrand WE, Zlokovic BV (2004) LRP/amyloid beta-peptide interaction mediates differential brain efflux of Abeta isoforms. Neuron 43:333-344.

Dickey CA, Kamal A, Lundgren K, Klosak N, Bailey RM, Dunmore J, Ash P, Shoraka S, Zlatkovic J, Eckman CB, Patterson C, Dickson DW, Nahman NS, Jr., Hutton M, Burrows F, Petrucelli L (2007) The high-affinity HSP90-CHIP complex recognizes and selectively degrades phosphorylated tau client proteins. J Clin Invest 117:648-658.

Doraiswamy PM (2003) Alzheimer's disease and the glutamate NMDA receptor. Psychopharmacol Bull 37:41-49.

Dovey HF, John V, Anderson JP, Chen LZ, de Saint Andrieu P, Fang LY, Freedman SB, Folmer B, Goldbach E, Holsztynska EJ, Hu KL, Johnson-Wood KL, Kennedy SL, Kholodenko D, Knops JE, Latimer LH, Lee M, Liao Z, Lieberburg IM, Motter RN, Mutter LC, Nietz J, Quinn KP, Sacchi KL, Seubert PA, Shopp GM, Thorsett ED, Tung JS, Wu J, Yang S, Yin CT, Schenk DB, May PC, Altstiel LD, Bender MH, Boggs LN, Britton TC, Clemens JC, Czilli DL, Dieckman-McGinty DK, Droste JJ, Fuson KS, Gitter BD, Hyslop PA, Johnstone EM, Li WY, Little SP, Mabry TE, Miller FD, Audia JE (2001) Functional gamma-secretase inhibitors reduce beta-amyloid peptide levels in brain. J Neurochem 76:173-181.

Ehrhart J, Obregon D, Mori T, Hou H, Sun N, Bai Y, Klein T, Fernandez F, Tan J, Shytle RD (2005) Stimulation of cannabinoid receptor 2 (CB2) suppresses microglial activation. J Neuroinflammation 2:29.

Eisdorfer C, Cohen D, Paveza GJ, Ashford JW, Luchins DJ, Gorelick PB, Hirschman RS, Freels SA, Levy PS, Semla TP, et al. (1992) An empirical evaluation of the Global Deterioration Scale for staging Alzheimer's disease. Am J Psychiatry 149:190-194.

Engel T, Hernandez F, Avila J, Lucas JJ (2006) Full reversal of Alzheimer's disease-like phenotype in a mouse model with conditional overexpression of glycogen synthase kinase-3. J Neurosci 26:5083-5090.

Evin G, Cappai R, Li QX, Culvenor JG, Small DH, Beyreuther K, Masters CL (1995) Candidate gamma-secretases in the generation of the carboxyl terminus of the Alzheimer's disease beta A4 amyloid: possible involvement of cathepsin D. Biochemistry 34:14185-14192.

Evin G, Sernee MF, Masters CL (2006) Inhibition of gamma-secretase as a therapeutic intervention for Alzheimer's disease: prospects, limitations and strategies. CNS Drugs 20:351-372.

Friedland RP, Budinger TF, Ganz E, Yano Y, Mathis CA, Koss B, Ober BA, Huesman RH, Derenzo SE (1983) Regional cerebral metabolic alterations in dementia of the Alzheimer type: positron emission tomography with [18F]fluorodeoxyglucose. J Comput Assist Tomogr 7:590-598.

Fujimura Y, Yamada K, Tachibana H (2005) A lipid raft-associated 67kDa laminin receptor mediates suppressive effect of epigallocatechin-3-O-gallate on FcepsilonRI expression. Biochem Biophys Res Commun 336:674-681.

Funamoto S, Morishima-Kawashima M, Tanimura Y, Hirotani N, Saido TC, Ihara Y (2004) Truncated carboxyl-terminal fragments of beta-amyloid precursor protein are processed to amyloid beta-proteins 40 and 42. Biochemistry 43:13532-13540.

Furukawa K, Sopher BL, Rydel RE, Begley JG, Pham DG, Martin GM, Fox M, Mattson MP (1996) Increased activity-regulating and neuroprotective efficacy of alpha-secretase-derived secreted amyloid precursor protein conferred by a C-terminal heparin-binding domain. J Neurochem 67:1882-1896.

Games D, Adams D, Alessandrini R, Barbour R, Berthelette P, Blackwell C, Carr T, Clemens J, Donaldson T, Gillespie F, et al. (1995) Alzheimer-type neuropathology in transgenic mice overexpressing V717F beta-amyloid precursor protein. Nature 373:523-527.

Gandhi S, Refolo LM, Sambamurti K (2004) Amyloid precursor protein compartmentalization restricts beta-amyloid production: therapeutic targets based on BACE compartmentalization. J Mol Neurosci 24:137-143.

Genkinger JM, Platz EA, Hoffman SC, Comstock GW, Helzlsouer KJ (2004) Fruit, vegetable, and antioxidant intake and all-cause, cancer, and cardiovascular disease mortality in a community-dwelling population in Washington County, Maryland. Am J Epidemiol 160:1223-1233.

Glenner GG, Wong CW (1984) Alzheimer's disease: initial report of the purification and characterization of a novel cerebrovascular amyloid protein. Biochem Biophys Res Commun 120:885-890.

Goate A, Chartier-Harlin MC, Mullan M, Brown J, Crawford F, Fidani L, Giuffra L, Haynes A, Irving N, James L, et al. (1991) Segregation of a missense mutation in the amyloid precursor protein gene with familial Alzheimer's disease. Nature 349:704-706.

Golde TE, Eckman CB, Younkin SG (2000) Biochemical detection of Abeta isoforms: implications for pathogenesis, diagnosis, and treatment of Alzheimer's disease. Biochim Biophys Acta 1502:172-187.

Gong Y, Chang L, Viola KL, Lacor PN, Lambert MP, Finch CE, Krafft GA, Klein WL (2003) Alzheimer's disease-affected brain: presence of oligomeric A beta ligands (ADDLs) suggests a molecular basis for reversible memory loss. Proc Natl Acad Sci U S A 100:10417-10422.

Greenberg SG, Davies P (1990) A preparation of Alzheimer paired helical filaments that displays distinct tau proteins by polyacrylamide gel electrophoresis. Proc Natl Acad Sci U S A 87:5827-5831.

Greenberg SM, Kosik KS (1995) Secreted beta-APP stimulates MAP kinase and phosphorylation of tau in neurons. Neurobiol Aging 16:403-407; discussion 407-408.

Han MK (2003) Epigallocatechin gallate, a constituent of green tea, suppresses cytokine-induced pancreatic beta-cell damage. Exp Mol Med 35:136-139.

Haque AM, Hashimoto M, Katakura M, Tanabe Y, Hara Y, Shido O (2006) Long-term administration of green tea catechins improves spatial cognition learning ability in rats. J Nutr 136:1043-1047.

Harada J, Sugimoto M (1999) Activation of caspase-3 in beta-amyloid-induced apoptosis of cultured rat cortical neurons. Brain Res 842:311-323.

Hardy J, Allsop D (1991) Amyloid deposition as the central event in the aetiology of Alzheimer's disease. Trends Pharmacol Sci 12:383-388.

Hardy J, Selkoe DJ (2002) The amyloid hypothesis of Alzheimer's disease: progress and problems on the road to therapeutics. Science 297:353-356.

Harper JD, Wong SS, Lieber CM, Lansbury PT (1997) Observation of metastable Abeta amyloid protofibrils by atomic force microscopy. Chem Biol 4:119-125.

Hebert LE, Scherr PA, Bienias JL, Bennett DA, Evans DA (2003) Alzheimer disease in the US population: prevalence estimates using the 2000 census. Arch Neurol 60:1119-1122.

Higaki J, Quon D, Zhong Z, Cordell B (1995) Inhibition of beta-amyloid formation identifies proteolytic precursors and subcellular site of catabolism. Neuron 14:651-659.

Hirano T, Higa S, Arimitsu J, Naka T, Shima Y, Ohshima S, Fujimoto M, Yamadori T, Kawase I, Tanaka T (2004) Flavonoids such as luteolin, fisetin and apigenin are inhibitors of interleukin-4 and interleukin-13 production by activated human basophils. Int Arch Allergy Immunol 134:135-140.

Hong M, Chen DC, Klein PS, Lee VM (1997) Lithium reduces tau phosphorylation by inhibition of glycogen synthase kinase-3. J Biol Chem 272:25326-25332.

Hooper NM, Turner AJ (2002) The search for alpha-secretase and its potential as a therapeutic approach to Alzheimer s disease. Curr Med Chem 9:1107-1119.

Horvathova K, Novotny L, Tothova D, Vachalkova A (2004) Determination of free radical scavenging activity of quercetin, rutin, luteolin and apigenin in H2O2-treated human ML cells K562. Neoplasma 51:395-399.

Hsiao K, Chapman P, Nilsen S, Eckman C, Harigaya Y, Younkin S, Yang F, Cole G (1996) Correlative memory deficits, Abeta elevation, and amyloid plaques in transgenic mice. Science 274:99-102.

Hung AY, Haass C, Nitsch RM, Qiu WQ, Citron M, Wurtman RJ, Growdon JH, Selkoe DJ (1993) Activation of protein kinase C inhibits cellular production of the amyloid beta-protein. J Biol Chem 268:22959-22962.

Hwang EM, Kim SK, Sohn JH, Lee JY, Kim Y, Kim YS, Mook-Jung I (2006) Furin is an endogenous regulator of alpha-secretase associated APP processing. Biochem Biophys Res Commun 349:654-659.

Ishiguro K, Shiratsuchi A, Sato S, Omori A, Arioka M, Kobayashi S, Uchida T, Imahori K (1993) Glycogen synthase kinase 3 beta is identical to tau protein kinase I generating several epitopes of paired helical filaments. FEBS Lett 325:167-172.

Iwata N, Tsubuki S, Takaki Y, Watanabe K, Sekiguchi M, Hosoki E, Kawashima-Morishima M, Lee HJ, Hama E, Sekine-Aizawa Y, Saido TC (2000) Identification of the major Abeta1-42-degrading catabolic pathway in brain

parenchyma: suppression leads to biochemical and pathological deposition. Nat Med 6:143-150.

Jeong JH, Kim HJ, Lee TJ, Kim MK, Park ES, Choi BS (2004) Epigallocatechin 3-gallate attenuates neuronal damage induced by 3-hydroxykynurenine. Toxicology 195:53-60.

Johnson-Wood K, Lee M, Motter R, Hu K, Gordon G, Barbour R, Khan K, Gordon M, Tan H, Games D, Lieberburg I, Schenk D, Seubert P, McConlogue L (1997) Amyloid precursor protein processing and A beta42 deposition in a transgenic mouse model of Alzheimer disease. Proc Natl Acad Sci U S A 94:1550-1555.

Kandaswami C, Lee LT, Lee PP, Hwang JJ, Ke FC, Huang YT, Lee MT (2005) The antitumor activities of flavonoids. In Vivo 19:895-909.

Kang DE, Pietrzik CU, Baum L, Chevallier N, Merriam DE, Kounnas MZ, Wagner SL, Troncoso JC, Kawas CH, Katzman R, Koo EH (2000) Modulation of amyloid beta-protein clearance and Alzheimer's disease susceptibility by the LDL receptor-related protein pathway. J Clin Invest 106:1159-1166.

Kimata M, Shichijo M, Miura T, Serizawa I, Inagaki N, Nagai H (2000) Effects of luteolin, quercetin and baicalein on immunoglobulin E-mediated mediator release from human cultured mast cells. Clin Exp Allergy 30:501-508.

King DL, Arendash GW (2002) Behavioral characterization of the Tg2576 transgenic model of Alzheimer's disease through 19 months. Physiol Behav 75:627-642.

Klafki HW, Paganetti PA, Sommer B, Staufenbiel M (1995) Calpain inhibitor I decreases beta A4 secretion from human embryonal kidney cells expressing beta-amyloid precursor protein carrying the APP670/671 double mutation. Neurosci Lett 201:29-32.

Klein WL (2002) ADDLs & protofibrils--the missing links? Neurobiol Aging 23:231-235.

Klyubin I, Walsh DM, Lemere CA, Cullen WK, Shankar GM, Betts V, Spooner ET, Jiang L, Anwyl R, Selkoe DJ, Rowan MJ (2005) Amyloid beta protein immunotherapy neutralizes Abeta oligomers that disrupt synaptic plasticity in vivo. Nat Med 11:556-561.

Kosik KS, Shimura H (2005) Phosphorylated tau and the neurodegenerative foldopathies. Biochim Biophys Acta 1739:298-310.

Kozlovsky N, Belmaker RH, Agam G (2000) Low GSK-3beta immunoreactivity in postmortem frontal cortex of schizophrenic patients. Am J Psychiatry 157:831-833.

Kurochkin IV, Goto S (1994) Alzheimer's beta-amyloid peptide specifically interacts with and is degraded by insulin degrading enzyme. FEBS Lett 345:33-37.

Lambert JD, Lee MJ, Lu H, Meng X, Hong JJ, Seril DN, Sturgill MG, Yang CS (2003) Epigallocatechin-3-gallate is absorbed but extensively glucuronidated following oral administration to mice. J Nutr 133:4172-4177.

Lammich S, Kojro E, Postina R, Gilbert S, Pfeiffer R, Jasionowski M, Haass C, Fahrenholz F (1999) Constitutive and regulated alpha-secretase cleavage of Alzheimer's amyloid precursor protein by a disintegrin metalloprotease. Proc Natl Acad Sci U S A 96:3922-3927.

Lannfelt L, Basun H, Wahlund LO, Rowe BA, Wagner SL (1995) Decreased alpha-secretase-cleaved amyloid precursor protein as a diagnostic marker for Alzheimer's disease. Nat Med 1:829-832.

Laurin D, Masaki KH, Foley DJ, White LR, Launer LJ (2004) Midlife dietary intake of antioxidants and risk of late-life incident dementia: the Honolulu-Asia Aging Study. Am J Epidemiol 159:959-967.

LeBlanc AC, Xue R, Gambetti P (1996) Amyloid precursor protein metabolism in primary cell cultures of neurons, astrocytes, and microglia. J Neurochem 66:2300-2310.

Lee MS, Kwon YT, Li M, Peng J, Friedlander RM, Tsai LH (2000) Neurotoxicity induces cleavage of p35 to p25 by calpain. Nature 405:360-364.

Lee MJ, Maliakal P, Chen L, Meng X, Bondoc FY, Prabhu S, Lambert G, Mohr S, Yang CS (2002) Pharmacokinetics of tea catechins after ingestion of green tea and (-)-epigallocatechin-3-gallate by humans: formation of different metabolites and individual variability. Cancer Epidemiol Biomarkers Prev 11:1025-1032.

Lee JH, Song DK, Jung CH, Shin DH, Park J, Kwon TK, Jang BC, Mun KC, Kim SP, Suh SI, Bae JH (2004) (-)-Epigallocatechin gallate attenuates glutamate-induced cytotoxicity via intracellular Ca modulation in PC12 cells. Clin Exp Pharmacol Physiol 31:530-536.

Leighty RE, Nilsson LN, Potter H, Costa DA, Low MA, Bales KR, Paul SM, Arendash GW (2004) Use of multimetric statistical analysis to characterize and discriminate between the performance of four Alzheimer's transgenic mouse lines differing in Abeta deposition. Behav Brain Res 153:107-121.

Levites Y, Amit T, Youdim MB, Mandel S (2002) Involvement of protein kinase C activation and cell survival/ cell cycle genes in green tea polyphenol (-)-epigallocatechin 3-gallate neuroprotective action. J Biol Chem 277:30574-30580.

Levites Y, Amit T, Mandel S, Youdim MB (2003) Neuroprotection and neurorescue against Abeta toxicity and PKC-dependent release of nonamyloidogenic soluble precursor protein by green tea polyphenol (-)-epigallocatechin-3-gallate. Faseb J 17:952-954.

Levy-Lahad E, Wijsman EM, Nemens E, Anderson L, Goddard KA, Weber JL, Bird TD, Schellenberg GD (1995) A familial Alzheimer's disease locus on chromosome 1. Science 269:970-973.

Li R, Huang YG, Fang D, Le WD (2004) (-)-Epigallocatechin gallate inhibits lipopolysaccharide-induced microglial activation and protects against inflammation-mediated dopaminergic neuronal injury. J Neurosci Res 78:723-731.

Lin JK, Liang YC (2000) Cancer chemoprevention by tea polyphenols. Proc Natl Sci Counc Repub China B 24:1-13.

Lin CL, Lin JK (2008) Epigallocatechin gallate (EGCG) attenuates high glucose-induced insulin signaling blockade in human hepG2 hepatoma cells. Mol Nutr Food Res.

Loewenstein DA, Rubert MP, Arguelles T, Duara R (1995) Neuropsychological test performance and prediction of functional capacities among Spanish-speaking and English-speaking patients with dementia. Arch Clin Neuropsychol 10:75-88.

Loo DT, Copani A, Pike CJ, Whittemore ER, Walencewicz AJ, Cotman CW (1993) Apoptosis is induced by beta-amyloid in cultured central nervous system neurons. Proc Natl Acad Sci U S A 90:7951-7955.

Lopez-Perez E, Zhang Y, Frank SJ, Creemers J, Seidah N, Checler F (2001) Constitutive alpha-secretase cleavage of the beta-amyloid precursor protein in the furin-deficient LoVo cell line: involvement of the pro-hormone convertase 7 and the disintegrin metalloprotease ADAM10. J Neurochem 76:1532-1539.

Lorenz M, Wessler S, Follmann E, Michaelis W, Dusterhoft T, Baumann G, Stangl K, Stangl V (2004) A constituent of green tea, epigallocatechin-3-gallate, activates endothelial nitric oxide synthase by a phosphatidylinositol-3-OH-kinase-, cAMP-dependent protein kinase-, and Akt-dependent pathway and leads to endothelial-dependent vasorelaxation. J Biol Chem 279:6190-6195.

Lorenzo A, Yankner BA (1994) Beta-amyloid neurotoxicity requires fibril formation and is inhibited by congo red. Proc Natl Acad Sci U S A 91:12243-12247.

Mandel S, Weinreb O, Amit T, Youdim MB (2004) Cell signaling pathways in the neuroprotective actions of the green tea polyphenol (-)-epigallocatechin-3-gallate: implications for neurodegenerative diseases. J Neurochem 88:1555-1569.

Marambaud P, Zhao H, Davies P (2005) Resveratrol promotes clearance of Alzheimer's disease amyloid-beta peptides. J Biol Chem 280:37377-37382.

Masters CL, Simms G, Weinman NA, Multhaup G, McDonald BL, Beyreuther K (1985) Amyloid plaque core protein in Alzheimer disease and Down syndrome. Proc Natl Acad Sci U S A 82:4245-4249.

Matsuyama S, Teraoka R, Mori H, Tomiyama T (2007) Inverse correlation between amyloid precursor protein and synaptic plasticity in transgenic mice. Neuroreport 18:1083-1087.

Mattson MP, Barger SW, Furukawa K, Bruce AJ, Wyss-Coray T, Mark RJ, Mucke L (1997) Cellular signaling roles of TGF beta, TNF alpha and beta APP in brain injury responses and Alzheimer's disease. Brain Res Brain Res Rev 23:47-61.

Mattson MP (1999) Impairment of membrane transport and signal transduction systems by amyloidogenic proteins. Methods Enzymol 309:733-746.

Mattson MP, Chan SL (2003) Neuronal and glial calcium signaling in Alzheimer's disease. Cell Calcium 34:385-397.

Middleton E, Jr. (1998) Effect of plant flavonoids on immune and inflammatory cell function. Adv Exp Med Biol 439:175-182.

Milton NG (2004) Role of hydrogen peroxide in the aetiology of Alzheimer's disease: implications for treatment. Drugs Aging 21:81-100.

Minoshima S, Giordani B, Berent S, Frey KA, Foster NL, Kuhl DE (1997) Metabolic reduction in the posterior cingulate cortex in very early Alzheimer's disease. Ann Neurol 42:85-94.

Moro MA, Hurtado O, Cardenas A, Romera C, Madrigal JL, Fernandez-Tome P, Leza JC, Lorenzo P, Lizasoain I (2003) Expression and function of tumour necrosis factor-alpha-converting enzyme in the central nervous system. Neurosignals 12:53-58.

Moyers SB, Kumar NB (2004) Green tea polyphenols and cancer chemoprevention: multiple mechanisms and endpoints for phase II trials. Nutr Rev 62:204-211.

Mullan M, Crawford F, Axelman K, Houlden H, Lilius L, Winblad B, Lannfelt L (1992) A pathogenic mutation for probable Alzheimer's disease in the APP gene at the N-terminus of beta-amyloid. Nat Genet 1:345-347.

Munoz-Montano JR, Moreno FJ, Avila J, Diaz-Nido J (1997) Lithium inhibits Alzheimer's disease-like tau protein phosphorylation in neurons. FEBS Lett 411:183-188.

Nielsen SE, Young JF, Daneshvar B, Lauridsen ST, Knuthsen P, Sandstrom B, Dragsted LO (1999) Effect of parsley (Petroselinum crispum) intake on urinary apigenin excretion, blood antioxidant enzymes and biomarkers for oxidative stress in human subjects. Br J Nutr 81:447-455.

Nijveldt RJ, van Nood E, van Hoorn DE, Boelens PG, van Norren K, van Leeuwen PA (2001) Flavonoids: a review of probable mechanisms of action and potential applications. Am J Clin Nutr 74:418-425.

Nixon RA, Cataldo AM, Mathews PM (2000) The endosomal-lysosomal system of neurons in Alzheimer's disease pathogenesis: a review. Neurochem Res 25:1161-1172.

Odontuya G, Hoult JR, Houghton PJ (2005) Structure-activity relationship for antiinflammatory effect of luteolin and its derived glycosides. Phytother Res 19:782-786.

Olsson A, Hoglund K, Sjogren M, Andreasen N, Minthon L, Lannfelt L, Buerger K, Moller HJ, Hampel H, Davidsson P, Blennow K (2003) Measurement of alpha- and beta-secretase cleaved amyloid precursor protein in cerebrospinal fluid from Alzheimer patients. Exp Neurol 183:74-80.

Opazo C, Huang X, Cherny RA, Moir RD, Roher AE, White AR, Cappai R, Masters CL, Tanzi RE, Inestrosa NC, Bush AI (2002) Metalloenzyme-like activity of Alzheimer's disease beta-amyloid. Cu-dependent catalytic conversion of dopamine, cholesterol, and biological reducing agents to neurotoxic H(2)O(2). J Biol Chem 277:40302-40308.

Palermo CM, Westlake CA, Gasiewicz TA (2005) Epigallocatechin gallate inhibits aryl hydrocarbon receptor gene transcription through an indirect mechanism involving binding to a 90 kDa heat shock protein. Biochemistry 44:5041-5052.

Park JW, Choi YJ, Suh SI, Kwon TK (2001) Involvement of ERK and protein tyrosine phosphatase signaling pathways in EGCG-induced cyclooxygenase-2 expression in Raw 264.7 cells. Biochem Biophys Res Commun 286:721-725.

Pelzer LE, Guardia T, Osvaldo Juarez A, Guerreiro E (1998) Acute and chronic antiinflammatory effects of plant flavonoids. Farmaco 53:421-424.

Petanceska SS, Gandy S (1999) The phosphatidylinositol 3-kinase inhibitor wortmannin alters the metabolism of the Alzheimer's amyloid precursor protein. J Neurochem 73:2316-2320.

Petersen RC (2000) Mild cognitive impairment: transition between aging and Alzheimer's disease. Neurologia 15:93-101.

Phiel CJ, Wilson CA, Lee VM, Klein PS (2003) GSK-3alpha regulates production of Alzheimer's disease amyloid-beta peptides. Nature 423:435-439.

Phinney AL, Calhoun ME, Wolfer DP, Lipp HP, Zheng H, Jucker M (1999) No hippocampal neuron or synaptic bouton loss in learning-impaired aged beta-amyloid precursor protein-null mice. Neuroscience 90:1207-1216.

Plassman BL, Langa KM, Fisher GG, Heeringa SG, Weir DR, Ofstedal MB, Burke JR, Hurd MD, Potter GG, Rodgers WL, Steffens DC, Willis RJ, Wallace RB (2007) Prevalence of dementia in the United States: the aging, demographics, and memory study. Neuroepidemiology 29:125-132.

Postina R, Schroeder A, Dewachter I, Bohl J, Schmitt U, Kojro E, Prinzen C, Endres K, Hiemke C, Blessing M, Flamez P, Dequenne A, Godaux E, van Leuven F, Fahrenholz F (2004) A disintegrin-metalloproteinase prevents amyloid plaque formation and hippocampal defects in an Alzheimer disease mouse model. J Clin Invest 113:1456-1464.

Potenza MA, Marasciulo FL, Tarquinio M, Tiravanti E, Colantuono G, Federici A, Kim JA, Quon MJ, Montagnani M (2007) EGCG, a green tea polyphenol, improves endothelial function and insulin sensitivity, reduces blood pressure, and protects against myocardial I/R injury in SHR. Am J Physiol Endocrinol Metab 292:E1378-1387.

Priller C, Bauer T, Mitteregger G, Krebs B, Kretzschmar HA, Herms J (2006) Synapse formation and function is modulated by the amyloid precursor protein. J Neurosci 26:7212-7221.

Qiu Z, Strickland DK, Hyman BT, Rebeck GW (1999) Alpha2-macroglobulin enhances the clearance of endogenous soluble beta-amyloid peptide via low-density lipoprotein receptor-related protein in cortical neurons. J Neurochem 73:1393-1398.

Reddy SV, Tiwari AK, Kumar US, Rao RJ, Rao JM (2005) Free radical scavenging, enzyme inhibitory constituents from antidiabetic Ayurvedic medicinal plant Hydnocarpus wightiana Blume. Phytother Res 19:277-281.

Rego AC, Oliveira CR (2003) Mitochondrial dysfunction and reactive oxygen species in excitotoxicity and apoptosis: implications for the pathogenesis of neurodegenerative diseases. Neurochem Res 28:1563-1574.

Reiss K, Maretzky T, Ludwig A, Tousseyn T, de Strooper B, Hartmann D, Saftig P (2005) ADAM10 cleavage of N-cadherin and regulation of cell-cell adhesion and beta-catenin nuclear signalling. Embo J 24:742-752.

Ren W, Qiao Z, Wang H, Zhu L, Zhang L (2003) Flavonoids: promising anticancer agents. Med Res Rev 23:519-534.

Rocchi A, Pellegrini S, Siciliano G, Murri L (2003) Causative and susceptibility genes for Alzheimer's disease: a review. Brain Res Bull 61:1-24.

Rodriguez SK, Guo W, Liu L, Band MA, Paulson EK, Meydani M (2006) Green tea catechin, epigallocatechin-3-gallate, inhibits vascular endothelial growth factor angiogenic signaling by disrupting the formation of a receptor complex. Int J Cancer 118:1635-1644.

Roher AE, Lowenson JD, Clarke S, Woods AS, Cotter RJ, Gowing E, Ball MJ (1993) beta-Amyloid-(1-42) is a major component of cerebrovascular amyloid deposits: implications for the pathology of Alzheimer disease. Proc Natl Acad Sci U S A 90:10836-10840.

Saija A, Scalese M, Lanza M, Marzullo D, Bonina F, Castelli F (1995) Flavonoids as antioxidant agents: importance of their interaction with biomembranes. Free Radic Biol Med 19:481-486.

Sambamurti K, Greig NH, Lahiri DK (2002) Advances in the cellular and molecular biology of the beta-amyloid protein in Alzheimer's disease. Neuromolecular Med 1:1-31.

Sampson L, Rimm E, Hollman PC, de Vries JH, Katan MB (2002) Flavonol and flavone intakes in US health professionals. J Am Diet Assoc 102:1414-1420.

Sato T, Diehl TS, Narayanan S, Funamoto S, Ihara Y, De Strooper B, Steiner H, Haass C, Wolfe MS (2007) Active gamma-secretase complexes contain only one of each component. J Biol Chem 282:33985-33993.

Schubert D (2005) Glucose metabolism and Alzheimer's disease. Ageing Res Rev 4:240-257.

Seeger M, Nordstedt C, Petanceska S, Kovacs DM, Gouras GK, Hahne S, Fraser P, Levesque L, Czernik AJ, George-Hyslop PS, Sisodia SS, Thinakaran G, Tanzi RE, Greengard P, Gandy S (1997) Evidence for phosphorylation and oligomeric assembly of presenilin 1. Proc Natl Acad Sci U S A 94:5090-5094.

Selkoe DJ (2001) Alzheimer's disease: genes, proteins, and therapy. Physiol Rev 81:741-766.

Sennvik K, Fastbom J, Blomberg M, Wahlund LO, Winblad B, Benedikz E (2000) Levels of alpha- and beta-secretase cleaved amyloid precursor protein in the cerebrospinal fluid of Alzheimer's disease patients. Neurosci Lett 278:169-172.

Shah S, Lee SF, Tabuchi K, Hao YH, Yu C, LaPlant Q, Ball H, Dann CE, 3rd, Sudhof T, Yu G (2005) Nicastrin functions as a gamma-secretase-substrate receptor. Cell 122:435-447.

Shankar GM, Bloodgood BL, Townsend M, Walsh DM, Selkoe DJ, Sabatini BL (2007) Natural oligomers of the Alzheimer amyloid-beta protein induce reversible synapse loss by modulating an NMDA-type glutamate receptor-dependent signaling pathway. J Neurosci 27:2866-2875.

Shearman MS, Ragan CI, Iversen LL (1994) Inhibition of PC12 cell redox activity is a specific, early indicator of the mechanism of beta-amyloid-mediated cell death. Proc Natl Acad Sci U S A 91:1470-1474.

Shepherd PR, Withers DJ, Siddle K (1998) Phosphoinositide 3-kinase: the key switch mechanism in insulin signalling. Biochem J 333 (Pt 3):471-490.

Shimoi K, Okada H, Furugori M, Goda T, Takase S, Suzuki M, Hara Y, Yamamoto H, Kinae N (1998) Intestinal absorption of luteolin and luteolin 7-O-beta-glucoside in rats and humans. FEBS Lett 438:220-224.

Shin RW, Bramblett GT, Lee VM, Trojanowski JQ (1993) Alzheimer disease A68 proteins injected into rat brain induce codeposits of beta-amyloid, ubiquitin, and alpha 1-antichymotrypsin. Proc Natl Acad Sci U S A 90:6825-6828.

Sinha S, Lieberburg I (1999) Cellular mechanisms of beta-amyloid production and secretion. Proc Natl Acad Sci U S A 96:11049-11053.

Sipe JD, Cohen AS (2000) Review: history of the amyloid fibril. J Struct Biol 130:88-98.

Skovronsky DM, Moore DB, Milla ME, Doms RW, Lee VM (2000) Protein kinase C-dependent alpha-secretase competes with beta-secretase for cleavage of amyloid-beta precursor protein in the trans-golgi network. J Biol Chem 275:2568-2575.

Slack BE, Ma LK, Seah CC (2001) Constitutive shedding of the amyloid precursor protein ectodomain is up-regulated by tumour necrosis factor-alpha converting enzyme. Biochem J 357:787-794.

Soto C, Castano EM, Kumar RA, Beavis RC, Frangione B (1995) Fibrillogenesis of synthetic amyloid-beta peptides is dependent on their initial secondary structure. Neurosci Lett 200:105-108.

Soucek T, Cumming R, Dargusch R, Maher P, Schubert D (2003) The regulation of glucose metabolism by HIF-1 mediates a neuroprotective response to amyloid beta peptide. Neuron 39:43-56.

Stein TD, Anders NJ, DeCarli C, Chan SL, Mattson MP, Johnson JA (2004) Neutralization of transthyretin reverses the neuroprotective effects of secreted amyloid precursor protein (APP) in APPSW mice resulting in tau phosphorylation and loss of hippocampal neurons: support for the amyloid hypothesis. J Neurosci 24:7707-7717.

Steiner H, Duff K, Capell A, Romig H, Grim MG, Lincoln S, Hardy J, Yu X, Picciano M, Fechteler K, Citron M, Kopan R, Pesold B, Keck S, Baader M, Tomita T, Iwatsubo T, Baumeister R, Haass C (1999) A loss of function mutation of

presenilin-2 interferes with amyloid beta-peptide production and notch signaling. J Biol Chem 274:28669-28673.

Stoeck A, Keller S, Riedle S, Sanderson MP, Runz S, Le Naour F, Gutwein P, Ludwig A, Rubinstein E, Altevogt P (2006) A role for exosomes in the constitutive and stimulus-induced ectodomain cleavage of L1 and CD44. Biochem J 393:609-618.

Streit WJ (2005) Microglia and neuroprotection: implications for Alzheimer's disease. Brain Res Brain Res Rev 48:234-239.

Strittmatter WJ, Saunders AM, Schmechel D, Pericak-Vance M, Enghild J, Salvesen GS, Roses AD (1993) Apolipoprotein E: high-avidity binding to beta-amyloid and increased frequency of type 4 allele in late-onset familial Alzheimer disease. Proc Natl Acad Sci U S A 90:1977-1981.

Suganuma M, Okabe S, Oniyama M, Tada Y, Ito H, Fujiki H (1998) Wide distribution of [3H](-)-epigallocatechin gallate, a cancer preventive tea polyphenol, in mouse tissue. Carcinogenesis 19:1771-1776.

Suganuma M, Sueoka E, Sueoka N, Okabe S, Fujiki H (2000) Mechanisms of cancer prevention by tea polyphenols based on inhibition of TNF-alpha expression. Biofactors 13:67-72.

Sun AY, Simonyi A, Sun GY (2002) The "French Paradox" and beyond: neuroprotective effects of polyphenols. Free Radic Biol Med 32:314-318.

Swerdlow R, Marcus DL, Landman J, Kooby D, Frey W, 2nd, Freedman ML (1994) Brain glucose metabolism in Alzheimer's disease. Am J Med Sci 308:141-144.

Takashima A, Noguchi K, Michel G, Mercken M, Hoshi M, Ishiguro K, Imahori K (1996) Exposure of rat hippocampal neurons to amyloid beta peptide (25-35) induces the inactivation of phosphatidyl inositol-3 kinase and the activation of tau protein kinase I/glycogen synthase kinase-3 beta. Neurosci Lett 203:33-36.

Takashima A, Murayama M, Murayama O, Kohno T, Honda T, Yasutake K, Nihonmatsu N, Mercken M, Yamaguchi H, Sugihara S, Wolozin B (1998) Presenilin 1 associates with glycogen synthase kinase-3beta and its substrate tau. Proc Natl Acad Sci U S A 95:9637-9641.

Tan J, Town T, Mori T, Wu Y, Saxe M, Crawford F, Mullan M (2000) CD45 opposes beta-amyloid peptide-induced microglial activation via inhibition of p44/42 mitogen-activated protein kinase. J Neurosci 20:7587-7594.

Tan J, Town T, Crawford F, Mori T, DelleDonne A, Crescentini R, Obregon D, Flavell RA, Mullan MJ (2002) Role of CD40 ligand in amyloidosis in transgenic Alzheimer's mice. Nat Neurosci 5:1288-1293.

Tanzi RE (2000) Alzheimer's disease and related dementias: the road to intervention. Exp Gerontol 35:433-437.

Teplow DB (1998) Structural and kinetic features of amyloid beta-protein fibrillogenesis. Amyloid 5:121-142.

Terauchi Y, Tsuji Y, Satoh S, Minoura H, Murakami K, Okuno A, Inukai K, Asano T, Kaburagi Y, Ueki K, Nakajima H, Hanafusa T, Matsuzawa Y, Sekihara H, Yin Y, Barrett JC, Oda H, Ishikawa T, Akanuma Y, Komuro I, Suzuki M, Yamamura K, Kodama T, Suzuki H, Yamamura K, Kodama T, Suzuki H, Koyasu S, Aizawa S, Tobe K, Fukui Y, Yazaki Y, Kadowaki T (1999) Increased insulin sensitivity and hypoglycaemia in mice lacking the p85 alpha subunit of phosphoinositide 3-kinase. Nat Genet 21:230-235.

Turner PR, O'Connor K, Tate WP, Abraham WC (2003) Roles of amyloid precursor protein and its fragments in regulating neural activity, plasticity and memory. Prog Neurobiol 70:1-32.

Ueda H, Yamazaki C, Yamazaki M (2002) Luteolin as an anti-inflammatory and anti-allergic constituent of Perilla frutescens. Biol Pharm Bull 25:1197-1202.

Ullmann U, Haller J, Decourt JP, Girault N, Girault J, Richard-Caudron AS, Pineau B, Weber P (2003) A single ascending dose study of epigallocatechin gallate in healthy volunteers. J Int Med Res 31:88-101.

van Acker SA, van den Berg DJ, Tromp MN, Griffioen DH, van Bennekom WP, van der Vijgh WJ, Bast A (1996) Structural aspects of antioxidant activity of flavonoids. Free Radic Biol Med 20:331-342.

Walter J, Grunberg J, Capell A, Pesold B, Schindzielorz A, Citron M, Mendla K, George-Hyslop PS, Multhaup G, Selkoe DJ, Haass C (1997) Proteolytic processing of the Alzheimer disease-associated presenilin-1 generates an in vivo substrate for protein kinase C. Proc Natl Acad Sci U S A 94:5349-5354.

Wang JZ, Wu Q, Smith A, Grundke-Iqbal I, Iqbal K (1998) Tau is phosphorylated by GSK-3 at several sites found in Alzheimer disease and its biological activity markedly inhibited only after it is prephosphorylated by A-kinase. FEBS Lett 436:28-34.

Wisniewski KE, Dalton AJ, McLachlan C, Wen GY, Wisniewski HM (1985) Alzheimer's disease in Down's syndrome: clinicopathologic studies. Neurology 35:957-961.

Wittemer SM, Ploch M, Windeck T, Muller SC, Drewelow B, Derendorf H, Veit M (2005) Bioavailability and pharmacokinetics of caffeoylquinic acids and

flavonoids after oral administration of Artichoke leaf extracts in humans. Phytomedicine 12:28-38.

Xie L, Helmerhorst E, Taddei K, Plewright B, Van Bronswijk W, Martins R (2002) Alzheimer's beta-amyloid peptides compete for insulin binding to the insulin receptor. J Neurosci 22:RC221.

Yamamoto H, Yamauchi E, Taniguchi H, Ono T, Miyamoto E (2002) Phosphorylation of microtubule-associated protein tau by Ca2+/calmodulin-dependent protein kinase II in its tubulin binding sites. Arch Biochem Biophys 408:255-262.

Yan R, Bienkowski MJ, Shuck ME, Miao H, Tory MC, Pauley AM, Brashier JR, Stratman NC, Mathews WR, Buhl AE, Carter DB, Tomasselli AG, Parodi LA, Heinrikson RL, Gurney ME (1999) Membrane-anchored aspartyl protease with Alzheimer's disease beta-secretase activity. Nature 402:533-537.

Yang F, Lim GP, Begum AN, Ubeda OJ, Simmons MR, Ambegaokar SS, Chen PP, Kayed R, Glabe CG, Frautschy SA, Cole GM (2005) Curcumin inhibits formation of amyloid beta oligomers and fibrils, binds plaques, and reduces amyloid in vivo. J Biol Chem 280:5892-5901.

Zahradka P, Harding G, Litchie B, Thomas S, Werner JP, Wilson DP, Yurkova N (2004) Activation of MMP-2 in response to vascular injury is mediated by

phosphatidylinositol 3-kinase-dependent expression of MT1-MMP. Am J Physiol Heart Circ Physiol 287:H2861-2870.

Zarzuelo A, Jimenez I, Gamez MJ, Utrilla P, Fernadez I, Torres MI, Osuna I (1996) Effects of luteolin 5-O-beta-rutinoside in streptozotocin-induced diabetic rats. Life Sci 58:2311-2316.

Zheng H, Koo EH (2006) The amyloid precursor protein: beyond amyloid. Mol Neurodegener 1:5.

APPENDIX 1

PUBLICATIONS CONTRIBUTING TO THE DISSERTATION

Obregon DF, Rezai-Zadeh K, Bai Y, Sun N, Hou H, Ehrhart J, Zeng J, Mori T, Arendash GW, Shytle D, Town T, Tan J (2006) ADAM10 activation is required for green tea (-)-epigallocatechin-3-gallate-induced alpha-secretase cleavage of amyloid precursor protein. J Biol Chem 281:16419-16427. [Figures 3.4-3.8]

Rezai-Zadeh K, Shytle D, Sun N, Mori T, Hou H, Jeanniton D, Ehrhart J, Townsend K, Zeng J, Morgan D, Hardy J, Town T, Tan J (2005) Green tea epigallocatechin-3-gallate (EGCG) modulates amyloid precursor protein cleavage and reduces cerebral amyloidosis in Alzheimer transgenic mice. J Neurosci 25:8807-8814. [Figures 3.12-3.15]

Rezai-Zadeh K, Arendash GW, Hou H, Fernandez F, Jensen M, Runfeldt M, Shytle RD, Tan J (2008) Green tea epigallocatechin-3-gallate (EGCG) reduces beta-amyloid mediated cognitive impairment and modulates tau pathology in Alzheimer transgenic mice. Brain Res 1214:177-187. [Figures 3.1-3.3, 3.11]

Rezai-Zadeh K, Shytle RD, Bai Y, Tian J, Hou H, Mori T, Zeng J, Obregon D, Town T, Tan J (2008) Flavonoid-mediated presenilin-1 phosphorylation reduces Alzheimer's disease beta-amyloid production. J Cell Mol Med. [Figures 4.1-4.8]

ABOUT THE AUTHOR

Kavon P. Rezai-Zadeh has been involved with Alzheimer disease research since late 2002. As an undergraduate at the University of South Florida (USF), Kavon began his foray into basic research volunteering at the Roskamp Institute. Upon receiving his B.S. in biology, Kavon continued his research aspirations by pursuing a doctorate in medical sciences at USF. During his graduate studies Kavon authored research articles that were picked up by the Reuters newswire and published or broadcast by more than 40 media outlets worldwide, including BBC News and CNN News. The outcomes of his various translational studies have also lead to the filing of numerous patent applications.